

## ABSTRACT

Title of Document: VISIBLE LIGHT PHOTORELEASE OF  
CARBOXYLATE ANIONS BY MEDIATED  
PHOTOINDUCED ELECTRON TRANSFER  
TO PYRIDINIUM-BASED PROTECTING  
GROUPS

John Brian Borak, Doctor of Philosophy, 2009

Directed By: Professor Daniel E. Falvey, Department of  
Chemistry and Biochemistry

The use of sensitized photoinduced electron transfer (PET) to trigger release of redox-active photoremovable protecting groups (PRPGs) allows a broad range of chromophores to be selected that absorb in difference wavelength ranges. Mediated electron transfer (MET) is particularly advantageous as sub-stoichiometric amounts of the often costly sensitizer (relative to the amount of protected substrate) can be combined with an excess amount of an inexpensive electron donor. Thus, the sensitizer acts as an electron shuttle between the donor and the protecting group to initiate release. The development of improved MET release systems using visible light as the trigger is the focus of the current work.

The *N*-alkylpicolinium (NAP) group has demonstrated its utility as an aqueous-compatible PET-based PRPG, releasing protected substrates upon one electron reduction.

Adaptation of MET PRPG release to visible light absorbing mediators began with employing ketocoumarin dyes that primarily form excited triplet states. These chromophores demonstrated high rates of release of NAP-protected carboxylates using sub-stoichiometric concentrations of mediator. Subsequently, nanomolar concentrations of gold nanoparticles were used to mediate electron transfer to NAP-protected compounds. This system exhibited rapid deprotection with very high release quantum efficiencies.

In an effort to use highly stable visible-light-absorbing metal-centered dyes with modest redox properties, the NAP group has been synthetically modified to adjust its reduction potential to more positive values. Photolysis of solutions containing the protected substrate, a large excess of an electron donor, and substoichiometric amounts of the dye tris(bipyridyl)ruthenium(II) released the free carboxylates in high yields while photodegradation of the chromophore was minimal.

To demonstrate the utility of the NAP group, a quasi-reversible photorheological fluid has been developed based on the formation and disruption of aqueous micelles. In solutions containing the surfactant cetyltrimethylammonium bromide, visible light photorelease of a carboxylate additive from the NAP-ester derivative induces a  $10^5$  increase in solution viscosity due to the formation of an interpenetrating micelle network. Subsequent irradiation of the viscoelastic fluid with UV light induces a *cis-trans* isomerization within the released carboxylate thereby disrupting the micelle network and decreasing solution viscosity by  $10^{2.5}$ .

VISIBLE LIGHT PHOTORELEASE OF CARBOXYLATE ANIONS BY  
MEDIATED PHOTOINDUCED ELECTRON TRANSFER TO  
PYRIDINIUM-BASED PROTECTING GROUPS

By

John Brian Borak

Dissertation submitted to the Faculty of the Graduate School of the  
University of Maryland, College Park, in partial fulfillment  
of the requirements for the degree of  
Doctor of Philosophy  
2009

Advisory Committee:  
Professor Daniel E. Falvey, Chair  
Professor Philip DeShong  
Professor Jeffery Davis  
Professor Steven Rokita  
Professor Srinivasa Raghavan

© Copyright by  
John Brian Borak  
2009



## **Dedication**

This work is dedicated to my family- John, Anita, and Mark Borak, and my grandparents, John and Theresa Borak, and Constance Vanderschaaf, for their love and support throughout all the years of my education.

## Acknowledgements

I would like to thank Dr. Dan Falvey for all of his support throughout my graduate career- for all that I have learned from him, for fostering a learning environment to help me grow, and for funding over the years.

I am grateful also to my committee, Dr. Philip DeShong, Dr. Jeffery Davis, Dr. Steven Rokita, and Dr. Srinivasa Raghavan for their sage advice and guidance in my pursuits. The lessons that I have learned will continue to support me throughout my career. I am thankful also to other faculty members in the department, especially Dr. Bonnie Dixon and Dr. Michael Montague-Smith for mentoring me during my teaching career at Maryland. I would also like to thank Dr. Mike Doyle for his kind advice, his support for the growth of the Chemistry and Biochemistry Graduate Student Organization, and for his help in my career pursuits.

I am also indebted to my current and former group members of the Falvey Lab for all of their help and for creating a fun environment in which to work. I owe a great deal of thanks to Dr. Becky Vieira for all of her help- for teaching me all of the great photochemistry that you know and love and for helping me troubleshoot through synthetic and other problems, for all of the proofreading of manuscripts and this dissertation, and especially for your sarcastic, brutal honesty throughout the years. Dr. Art Winter, Dr. Selina Thomas, Dr. Andy Kung, Romina Heymann, Raffaele Perrotta, George Mann- thank you all for your support and the great times over the years.

Thanks to everyone in the analytical services in the Chemistry Department, especially Dr. Yiu-Fai Lam, Dr. Yinde Wang, and Dr. Yue Li for their help and for keeping the NMR and mass spectrometry facilities in peak operating condition.

I would like to acknowledge the United States Department of Education for my GAANN fellowship as well as the National Science Foundation for their financial support.

A special thanks to all of the current and former graduate students from my entering class. Thanks for all of the talks you have listened to and all the support you have given me. Despite the challenges, we had a lot of fun in and outside the lab and I'll always remember the great times we had.

Finally, I would like to thank all my friends and family who have supported me during my time at Maryland. I'm so grateful to have such wonderful people around me. Laura, thank you especially for all of your support and patience during the final push...and for all the banana and pumpkin bread.

# Table of Contents

Dedication .....	ii
Acknowledgements .....	iii
Table of Contents .....	v
List of Tables .....	viii
List of Figures .....	x
List of Schemes .....	xiii
List of Abbreviations .....	xv
General Abstract .....	xviii
1 Photoremovable Protecting Groups .....	1
1.1 Introduction .....	1
1.2 Direct deprotection PRPGs .....	4
1.2.1 The <i>o</i> -nitrobenzyl group .....	5
1.2.2 The benzoin (desyl) group .....	11
1.2.3 The phenacyl group .....	15
1.2.4 The coumarinyl group .....	18
1.2.5 Wavelength-orthogonal systems .....	23
1.3 Conclusions .....	27
2 Photoinduced Electron Transfer (PET) Based PRPGs .....	30
2.1 Introduction .....	30
2.2 Photoinduced electron transfer .....	30
2.3 Design of PET-based PRPGs .....	35
2.3.1 Direct electron transfer .....	36
2.3.2 Mediated electron transfer (MET) .....	43
2.4 The N-alkylpicolinium group as a PET-PRPG .....	45
2.5 Conclusions .....	51
3 Ketocoumarin Dyes for Visible Light MET Photolysis .....	53
3.1 Introduction .....	53
3.2 System design .....	54
3.3 Deprotection photolysis .....	57

3.4	Mechanistic studies .....	59
3.5	Conclusions .....	62
4	Gold Nanoparticles as Aqueous Visible Light Mediators .....	64
4.1	Introduction .....	64
4.2	Preparation of gold nanoparticles .....	64
4.3	Deprotection photolysis .....	69
4.3.1	Citrate-stabilized gold nanoparticles .....	69
4.3.2	Tryptophan-stabilized gold nanoparticles .....	71
4.4	Quantum yields .....	73
4.5	Conclusions .....	73
5	Metal-Centered Complexes as Mediators for Visible Light MET Photorelease ..	75
5.1	Introduction .....	75
5.2	Modification of the NAP group .....	78
5.3	Deprotection photolysis .....	82
5.4	Mechanistic studies .....	88
5.5	Conclusions .....	92
6	A Quasi-Reversible Photorheological Fluid Based on Photorelease and Photoisomerization .....	93
6.1	Introduction .....	93
6.2	Photorheological fluid design .....	101
6.3	Photorelease and photoisomerization .....	104
6.4	Rheology .....	108
6.5	Mechanistic studies .....	110
6.6	Conclusions .....	112
7	Conclusions .....	114
8	Experimental Section .....	118
8.1	General procedures .....	118
8.2	Cyclic voltammetry experiments .....	118
8.3	Luminescence quenching .....	119
8.4	Laser flash photolysis .....	119
8.4.1	Ketocoumarin dyes .....	120

8.4.2	mPCN-esters .....	120
8.4.3	Photorheological fluid.....	120
8.5	Deprotection photolysis .....	120
8.5.1	Ketocoumarin dye photolysis .....	120
8.5.2	Gold nanoparticle photolysis .....	121
8.5.3	mPCN photolysis .....	122
8.6	Photorheological fluid photolysis .....	123
8.7	Quantum yield determination .....	124
8.8	Synthesis .....	125
8.8.1	NAP-Esters .....	125
8.8.2	CBDAC.....	125
8.8.3	TRP-AuNP .....	125
8.8.4	mPCN-Esters.....	127
8.8.5	<i>N</i> -Methylpicolinium <i>trans</i> -cinnamate bromide (NAP-tCA).....	136
Appendix A:	Improvements for Substituted NAP Systems.....	138
Appendix B:	Alternatives for Light-induced Viscosity Changes .....	140
	Linked Surfactant-NAP-Additive .....	140
	Nanoparticle-supported Gelation Additive Release.....	141
Appendix C:	Cyclic Voltammetry Data Acquisition Labview Program .....	144
References	.....	154

## List of Tables

Table 1-1: Comparison of photolytic efficacy of various PRPGs for the release of glutamate (GLU) from $\gamma$ -carboxylate-protected glutamic acid <sup>8</sup> .....	28
Table 2-1: Comparison of quantum yields of release ( $\Phi_{rel}$ ) and photolytic efficacies ( $\Phi_{rel}E_{\lambda}$ ) for NAP-release by DET and MET <sup>110,112,117</sup> .....	51
Table 3-1: Photophysical and electrochemical data and electron transfer calculations for DEATC and CBDAC ketocoumarin dyes.....	56
Table 3-2: Deprotection photolysis data for release of carboxylates from NAP-esters with DEATC in MeCN .....	58
Table 3-3: Deprotection photolysis data for release of carboxylates from NAP-esters with CBDAC in MeCN.....	59
Table 3-4: Quantum yields and photolytic efficacies determined for release of PAA from NAP-ester <i>1</i> with DEATC or CBDAC in MeCN .....	62
Table 4-1: Deprotection photolysis data for release of PAA from NAP-ester <i>1</i> with cit-AuNP .....	70
Table 4-2: Deprotection photolysis data for release of PAA from NAP-ester <i>1</i> with TRP-AuNP .....	72
Table 5-1: Electrochemical data and electron transfer calculations for sensitizer/ascorbic acid/NAP-ester system .....	77
Table 5-2: Electrochemical data and electron transfer calculations for sensitizer/ascorbic acid/cyano-substituted NAP system.....	79
Table 5-3: First reduction potentials of prepared mPCN-esters .....	81
Table 5-4: Deprotection photolysis data for release of carboxylates from mPCN-esters by DET from Rubpy .....	83
Table 5-5: Deprotection photolysis data for release of carboxylates from mPCN-esters by MET from various donors through Rubpy.....	84
Table 5-6: Observed quenching constants, quantum yields of photorelease, and photolytic efficacies for mPCN-ester release .....	89
Table 6-1: Deprotection photolysis and photoisomerization data for NAP-tCA/Rubpy/ASC PR fluid (all samples 50 mM CTAB, 30 mM ASC) .....	106

Table 6-2: Concentration changes and ratios for NAP-tCA/Rubpy/ASC PR fluid photolysis (determined from values in Table 6-1).....	106
Table 7-1: Comparison of photolytic efficiencies and efficacies of studied MET PET- PRPG deprotection reactions .....	116



## List of Figures

Figure 1-1: ONB-Caged ATP .....	10
Figure 1-2: Substrate patterning by deprotection through a lithographic mask.....	11
Figure 1-3: Model benzoin derivative.....	12
Figure 1-4: Model <i>p</i> -hydroxyphenacyl protecting group.....	15
Figure 1-5: 7-Substituted coumarin derivative as a PRPG .....	18
Figure 1-6: Coumarin-based PRPG designed with improved aqueous compatibility for prodrug release .....	22
Figure 2-1: Dependence of $k_{ET}$ on $\Delta G_{ET}$ as described by Marcus.....	34
Figure 2-2: DMA (left) & anthracene (right) linked donor-acceptor phenacyl release systems.....	42
Figure 2-3: Model NAP-protected carboxylate .....	45
Figure 2-4: (a) Carbazole-NAP linked system (b) benzophenone-NAP linked system .....	50
Figure 3-1: Ketocoumarin dyes: (a) 3-arylcoumarins (b) carbonylbiscoumarins....	55
Figure 3-2: Ketocoumarin dyes studied for triplet MET deprotection .....	56
Figure 3-3: NAP-esters used in deprotection photolysis experiments.....	57
Figure 3-4: 355 nm pulsed laser photolysis of DEATC and DMA (MeCN).....	60
Figure 3-5: Time-dependent traces after pulsed 355 nm laser excitation of DEATC + DMA + varying concentrations of NAP-ester 3, monitored at 510 nm.....	60
Figure 3-6: 355 nm pulsed laser photolysis of CBDAC+DMA (MeCN).....	61
Figure 4-1: Model representation of ligand-stabilized gold nanoparticles .....	65
Figure 4-2: Absorption spectrum of aqueous 16 nm cit-AuNPs and aggregating cit- AuNP .....	66
Figure 4-3: UV-VIS spectra of cit-AuNP and TRP-AuNP.....	68
Figure 4-4: UV-VIS spectra of cit-AuNP with varying concentration of NAP-ester 1 .....	69
Figure 5-1: Metal-centered complexes ruthenium(II) tris(bipyridyl) (Rubpy) and zinc(II) tetraphenylporphyrin (ZnTPP).....	75

Figure 5-2: UV-VIS spectrum of Rubpy in H <sub>2</sub> O .....	78
Figure 5-3: Cyano-substituted NAP model compound.....	79
Figure 5-4: Cyclic voltammograms of <i>I</i> and <i>4BF4</i> , referenced to ferrocene/ferrocenium couple in MeCN .....	81
Figure 5-5: UV-VIS spectrum of <i>5OTf</i> in MeCN/MeOH over time .....	86
Figure 5-6: UV-VIS spectrum of <i>5BF4</i> in MeCN/MeOH after addition of base (NEt <sub>3</sub> ) and acid (H <sub>2</sub> SO <sub>4</sub> ).....	87
Figure 5-7: Luminescence quenching of Rubpy by <i>5OTf</i> .....	88
Figure 5-8: Stern-Volmer analysis of Rubpy luminescence quenching by <i>5OTf</i> .....	89
Figure 5-9: Time-dependent absorption traces from 532 nm pulsed laser photolysis of Rubpy, ASC, and varying [ <i>5OTf</i> ], monitored at 510 nm.....	90
Figure 5-10: Determination of $k_{obs}$ for quenching of Rubpy <sup>1+</sup> by <i>5OTf</i> .....	91
Figure 6-1: Cetyltrimethylammonium bromide (CTAB) surfactant and surfactant model representation .....	94
Figure 6-2: Critical packing parameters and their relationship to expected packing of surfactant molecules and larger micelle structure.....	96
Figure 6-3: Model representation of spherical (left) and cylindrical (right) micelle structures in solution .....	96
Figure 6-4: Additives known to induce wormlike micelle formation in aqueous CTAB <sup>168,170</sup> .....	98
Figure 6-5: Azobenzene surfactant derivative prepared by Sakai et al. ....	99
Figure 6-6: 50 mM CTAB in H <sub>2</sub> O with varying concentrations of tCA, 0-50 mM tCA in 10 mM increments from left to right (Rubpy added for contrast) .....	101
Figure 6-7: Normalized UV-VIS spectra of tCA and Rubpy .....	103
Figure 6-8: Photoinduced viscosity changes; (a) starting solution, (b) after 1 h VIS irradiation, (c) after 2 h UV irradiation.....	106
Figure 6-9: Expected surfactant packing before and after conversion of tCA to the <i>cis</i> isomer.....	107
Figure 6-10: Steady-shear rheology of a solution from Entry 4, Table 6-1 .....	108
Figure 6-11: Steady-shear rheology of a solution from Entry 4, Table 6-1 with additional VIS irradiation .....	110

Figure 6-12: Time-dependent absorption traces from 532 nm pulsed laser photolysis of Rubpy, ASC, and varying concentrations of (LEFT) NAP-tCA or (RIGHT) tCA, monitored at 510 nm .....	111
Figure 6-13: $k_I$ versus (LEFT) [NAP-tCA] or (RIGHT) [tCA] for LFP of Rubpy + ASC + quencher, monitored at 510 nm .....	111
Figure B-1: TRP-AuNP prepared in 50 mM aqueous CTAB/tCA (1/1) .....	142

## List of Schemes

Scheme 1-1: Use of a protecting group to prevent transformation of a functional group .....	1
Scheme 1-2: Photolytic release of glycine from <i>N</i> -benzyloxycarboamoyl glycine.....	5
Scheme 1-3: Photolytic ONB carboxylate release and NBOC amine release .....	6
Scheme 1-4: ONB alcohol release .....	7
Scheme 1-5: ONB derivatives as PRPGs.....	8
Scheme 1-6: Release of Ca <sup>2+</sup> from an ONB-based cage.....	10
Scheme 1-7: Deprotection of unsubstituted benzoin PRPG .....	12
Scheme 1-8: 3',5'-dimethoxybenzoin (DMB) deprotection .....	13
Scheme 1-9: Release from pHP in aqueous solution .....	17
Scheme 1-10: 7-acyloxycoumarins for improved membrane permeability.....	19
Scheme 1-11: Release from Coumarin Derivatives.....	20
Scheme 1-12: Release of aldehydes/ketones and diols from coumarin derivatives ...	21
Scheme 1-13: Wavelength-orthogonal deprotection of PRPGs.....	23
Scheme 1-14: Wavelength-orthogonal photorelease utilizing ONB and benzoin PRPGs .....	25
Scheme 1-15: Improved wavelength-orthogonal photorelease by spectroscopic and kinetic parameter optimization .....	26
Scheme 2-1: Schematic representation of PET.....	31
Scheme 2-2: Competitive processes in PET .....	32
Scheme 2-3: Direct and mediated photoinduced electron transfer mechanisms .....	36
Scheme 2-4: Photolytic tosyl amide deprotection .....	38
Scheme 2-5: Sensitized deprotection of phenacyl esters .....	41
Scheme 2-6: Photolytic release of alcohols from phenacyl carbonates.....	42
Scheme 2-7: Synthesis of NAP-protected carboxylates .....	46
Scheme 2-8: Proposed release of carboxylate anions from NAP-esters.....	47
Scheme 2-9: MET photolysis of DMA, benzophenone and a NAP-ester .....	49
Scheme 3-1: Mediated electron transfer deprotection .....	54

Scheme 4-1: Preparation of tryptophan-conjugate AuNPs (TRP-AuNP).....	68
Scheme 5-1: Mechanistic pathways for MET deprotection with MCCs .....	77
Scheme 5-2: Synthesis of cyano-substituted 4-pyridylcarbinol and mPCN-ester synthesis .....	80
Scheme 5-3: Photolytic release of carboxylates from mPCN-esters by DET from Rubpy .....	82
Scheme 5-4: Photolytic release of carboxylates from mPCN-esters by MET from DMA or ASC through Rubpy .....	84
Scheme 5-5: Acid/base equilibrium and side reaction with mPCN-esters .....	87
Scheme 6-1: Photoisomerization of <i>trans</i> -orthomethoxycinnamic acid (OMCA) ...	100

## List of Abbreviations

9-MC	9-methyl carbazole
ATP	adenosine triphosphate
ASC	ascorbic acid
AuNP	gold nanoparticle
BET	back electron transfer
CBDAC	3,3'-carbonylbis(7-diethylaminocoumarin)
CHD	1,4-cyclohexadiene
CIP	contact ion pair
cit-AuNP	citrate-stabilized gold nanoparticle
CMC	critical micelle concentration
CPP	critical packing parameter
CTAB	cetyltrimethylammonium bromide
CV	cyclic voltammetry
DABCO	1,4-diazabicyclo[2.2.2]octane
DCC	dicyclohexylcarbodiimide
DEA	<i>N,N</i> -diethylaniline
DEATC	7-diethylamino-3-thenoylcoumarin
DET	direct electron transfer
DMA	<i>N,N</i> -dimethylaniline
DMB	3',5'-dimethoxybenzoin
DTT	DL-dithiothreitol
EDTA	ethylenediaminetetraacetic acid

EPR	electron pair resonance
EtOH	ethanol
GABA	$\gamma$ -aminobutyric acid
HOMO	highest occupied molecular orbital
ISC	intersystem crossing
KIE	kinetic isotope effect
LFP	laser flash photolysis
LUMO	lowest unoccupied molecular orbital
MCC	metal-centered complex
MeCN	acetonitrile
MeNPOC	5'-( $\alpha$ -methyl-2-nitropiperonyl)oxycarbonyl
MeOH	methanol
MET	mediated electron transfer
MLCT	metal-to-ligand charge transfer
mPCN	cyano-substituted <i>N</i> -methylpicolinium
NBOC	<i>ortho</i> -nitrobenzyloxycarbonyl
NPE	<i>ortho</i> -nitrophenethyl
NPPOC	[2-(2-nitrophenyl)propoxy]carbonyl
NVOC	6-nitroveratroyloxycarbonyl
OMCA	<i>ortho</i> -methoxycinnamic acid
ONB	<i>ortho</i> -nitrobenzyl
Nd:YAG	neodymium-doped yttrium aluminum garnet; Nd:Y <sub>3</sub> Al <sub>5</sub> O <sub>12</sub>
NAP	<i>N</i> -alkylpicolinium

NMR	nuclear magnetic resonance
PAA	phenylacetic acid
pHP	<i>para</i> -hydroxyphenacyl
PET	photoinduced electron transfer
PG	protecting group
PRB	plasmon resonance band
PRPG	photoremovable protecting group
Rubpy	tris(2,2'-bipyridyl)ruthenium(II)
SCE	standard calomel electrode
SPR	surface plasmon resonance
TBDMS	<i>tert</i> -butyldimethylsilyl
tCA	<i>trans</i> -cinnamic acid
TMBD	<i>N,N,N',N'</i> -tetramethylbenzidine
TMS	trimethylsilyl
TRIR	time-resolved infrared
TRP	tryptophan
TRP-AuNP	tryptophan-conjugate functionalized gold nanoparticle
TRP-conj	tryptophan-conjugate
TPA	triphenylamine
ZnTPP	zinc tetraphenylporphyrin



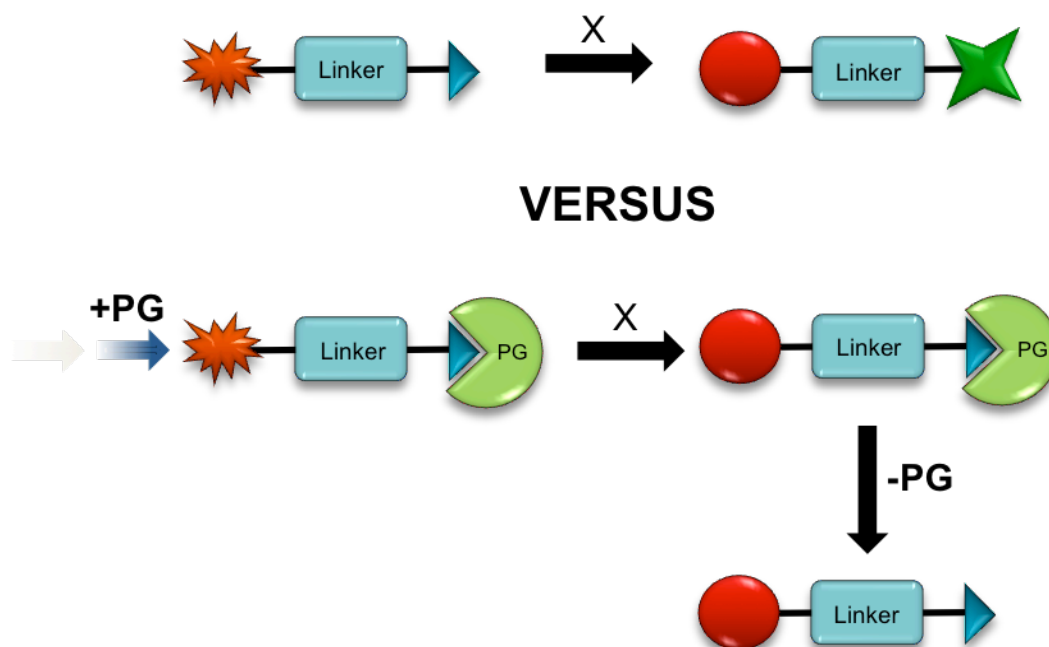
## **General Abstract**

The energy carried by visible light can be harnessed for many applications. In addition to using energy from the sun to provide power for electrical devices or to provide heat, visible light energy can be used to transform chemical compounds from one form to another. In a specific application, a compound can be introduced into an environment and remain benign towards everything in that environment until light is introduced. The light energy causes a chemical transformation that makes the compound capable of interacting with other components in its environment. In this way, interactions that the produced compound(s) have with other components can be studied in interesting systems such as biological tissues. This research has focused on the development of new systems that allow the use of visible light to quickly and efficiently produce final active compounds that are functional in biological or materials applications.

# 1 Photoremovable Protecting Groups

## 1.1 Introduction

The ability to selectively protect and restore the reactivity of functional groups has tremendous impact on the success of many fundamental research and applied pursuits. Chemists often must transform one particular functional group and still maintain close control over others. This can be challenging when one reagent reacts with multiple functional groups, sometimes in unpredictable ways. (Scheme 1-1) Additionally, many researchers require compounds to remain inactive until a certain time of their choosing. The study of biological processes, especially *in vivo* studies, often require strict temporal and spatial control over the adjustable variables to produce responses that can be studied.



**Scheme 1-1: Use of a protecting group to prevent transformation of a functional group**

A plethora of chemical protecting groups (PGs) have been designed to address some of these challenges by actively changing functional groups to be inert toward certain reaction conditions required for a particular synthetic transformation.<sup>1</sup> (Scheme 1-1) Subsequent exposure to a different set of conditions will remove the specific protecting group, restoring the original functional group. Alcohol protection with silyl derivatives, cleaved by acid workup serves as a commonplace example.

Despite the successful application of many chemical PGs, mostly for synthetic purposes, certain circumstances require greater control and milder conditions to effect deprotection. Most of the widely used PGs require acid, base, or other relatively harsh chemical conditions that can have adverse effects in sensitive environments encountered in biological systems. Additionally, the release of controlled amounts of these deprotection reagents is often difficult and typically cannot be directed only towards specific areas of a substrate.

Several of these disadvantages can be addressed by photoremovable protecting groups (PRPGs).<sup>2-4</sup> PRPGs can be removed by simple irradiation with light of the appropriate wavelength. In general, this allows for a milder and simpler means of deprotection as potentially harsh reagents are unnecessary. Additionally, since light can be directed to specific locations, a higher degree of spatial selectivity can be achieved. For example, protected substrates immobilized on a planar solid support can be addressed in particular regions with the use of lithographic masks or a sufficiently narrow irradiation source. (i.e. lasers) Several research efforts have focused on designing PRPGs that absorb at different wavelengths such that selective deprotection could be realized by simply changing irradiation wavelengths. Given these benefits, PRPGs are ideal for

biological applications.<sup>5,6</sup> Many biologically active compounds, such as ATP, neurotransmitters, and ions have been “caged” with PRPGs and photolysed to study certain physiological events with great precision.

A successful PRPG strategy requires the optimization of several important design criteria.<sup>2</sup> (1) The photoreaction should proceed efficiently with a high quantum yield for the release reaction ( $\Phi_{rel}$ , Eq 1-1). Other processes that compete with the bond scission

$$\Phi_{rel} = \text{molecules released/photons absorbed} \quad (1-1)$$

step should be sufficiently uncompetitive. (2) The chromophore should absorb light of sufficiently low energy (long wavelength) and the surrounding environment (biological or otherwise), substrate, and other compounds should not compete appreciably for absorption. (3) The products of deprotection should not compete with the chromophore for the irradiation light or interfere with further deprotection reactions. (4) The PRPG must be stable in the medium in which it is introduced and not decompose appreciably before photolysis. (5) Release of the protected compound should be sufficiently fast so to exceed the expected response that is monitored. Additional benefits include aqueous compatibility and a facile synthetic method to prepare protected compounds. While the ideal PRPG would embody all of these characteristics, each PRPG will invariably attain these goals to varying degrees.

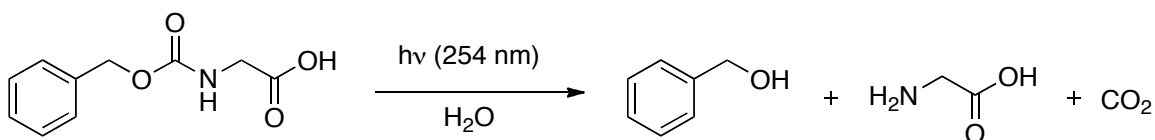
In quantifying the effectiveness of a PRPG, it is important to differentiate  $\Phi_{rel}$  from the photolytic efficacy ( $\Phi_{rel}\epsilon$ ).  $\Phi_{rel}\epsilon$  accounts for the molar absorptivity ( $\epsilon$ ) of a species at the irradiation wavelength and relates directly to the observed photorelease rate,  $k_{rel}$ .<sup>7,8</sup> While optimization of both  $\epsilon$  and  $\Phi_{rel}$  is important, a deficiency in one term can be overcome by the other. For example, a chromophore may have a low  $\Phi_{rel}$  but very

strong absorption in the wavelength range in which  $\Phi_{rel}$  was determined. The fact that excitation of a chromophore does not lead to a particular photochemical process frequently is less important simply because many excitations occur due to strong absorption. Photolysis times required for quantitative deprotection will be less than those for a species with a similar  $\Phi_{rel}$ , but lower  $\epsilon$ . Thus, for practical implementation of PRPGs,  $\Phi_{rel}\epsilon$  is a more meaningful metric for assessing the overall reaction rate and is a convenient means to compare different PRPGs.

Over the past several decades, two families of PRPGs have been the focus of attention. Protecting groups designed around a moiety that both absorbs light and fragments (Direct Deprotection PRPGs) comprise the majority of the literature and will be discussed presently. A second family relies on a photochemically-produced reactive ground state intermediate that subsequently releases the substrate in the return to a more stable ground state. Generating this intermediate can rely on photoinduced electron transfer (PET) to produce a reactive radical species. (PET-based PRPGs) This will be discussed at length in the following chapter.

## **1.2 Direct deprotection PRPGs**

By far, the most highly developed branch of PRPGs rely upon a rearrangement and/or radical mechanism that occurs within the chromophore after light absorption. Indeed, the first reported use of a PRPG was the direct photolytic release of glycine from *N*-benzyloxycarbamoyl glycine by Barltrop and Schofield.<sup>9</sup> (Scheme 1-2) The use of a single photochemical step for substrate release offers the potential to realize very high deprotection rates and efficiencies. However, this also presents a problem in the



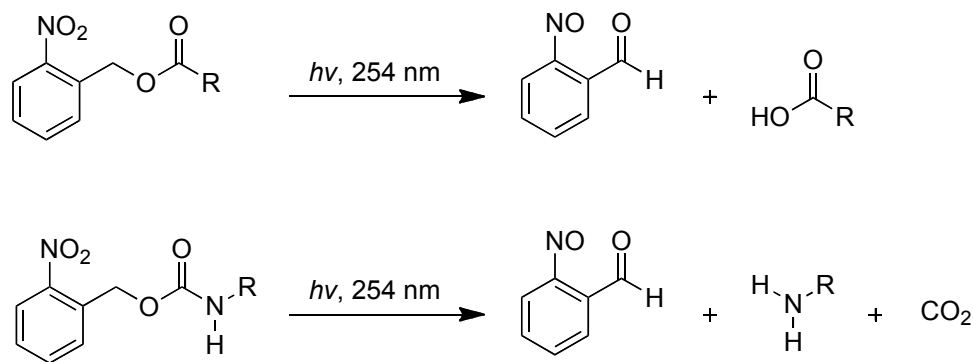
**Scheme 1-2: Photolytic release of glycine from *N*-benzyloxycarboamoyl glycine**

optimization of these systems, as structural modifications will invariably change rates, efficiencies, and photophysical properties. Many chromophores have been studied and developed as direct deprotection PRPGs including nitrobenzyl, benzoin, phenacyl, and coumarinyl derivatives. The development and application of these groups and the exploration of wavelength-orthogonal systems that attempt to combine several of these groups together in the same system will be discussed.

### 1.2.1 The *o*-nitrobenzyl group

Variants of the *ortho*-nitrobenzyl (ONB) moiety are the most heavily studied and broadly deployed PRPGs used for the release of alcohols, carboxylates, amines, and ketones. Studies have focused on elucidating the mechanism of photorelease and optimizing reaction efficiencies and absorption properties through substituent effects. Applications are quite diverse but have predominantly focused on the exploration of biological mechanisms and kinetics through the release of “caged” functional molecules such as ATP. Their use in the preparation of patterned substrates through lithographic masks illustrates applications in materials science.

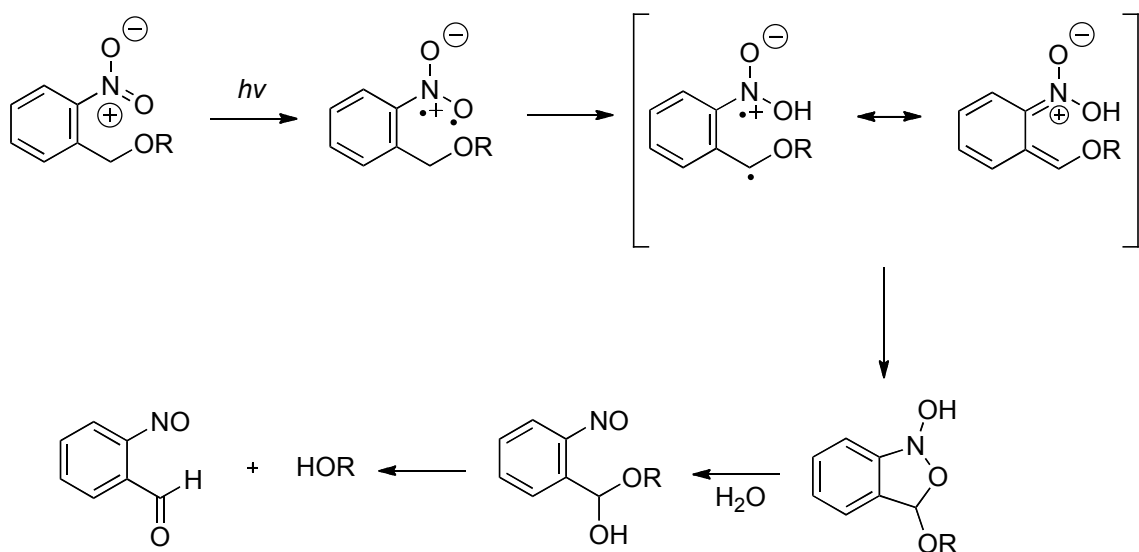
Originally introduced by Barltrop et al. for carboxylate and amine protection,<sup>10,11</sup> ONB and *o*-nitrobenzyloxycarbonyl (NBOC) groups (Scheme 1-3) have a strong UV absorption band centered around 275 nm ( $\epsilon_{275} = 5012 \text{ M}^{-1}\text{cm}^{-1}$ )<sup>4</sup> that, when excited, releases the protected substrate. Unfortunately, the original system requires short



**Scheme 1-3: Photolytic ONB carboxylate release and NBOC amine release**

irradiation wavelengths for prolonged photolysis periods. This limits the utility of unsubstituted ONB groups in sensitive biological systems as bio-active molecules inevitably will compete for absorption in this wavelength range. Additionally, photolysis generates a nitrosoaldehyde byproduct that is often reactive with other compounds in the system.

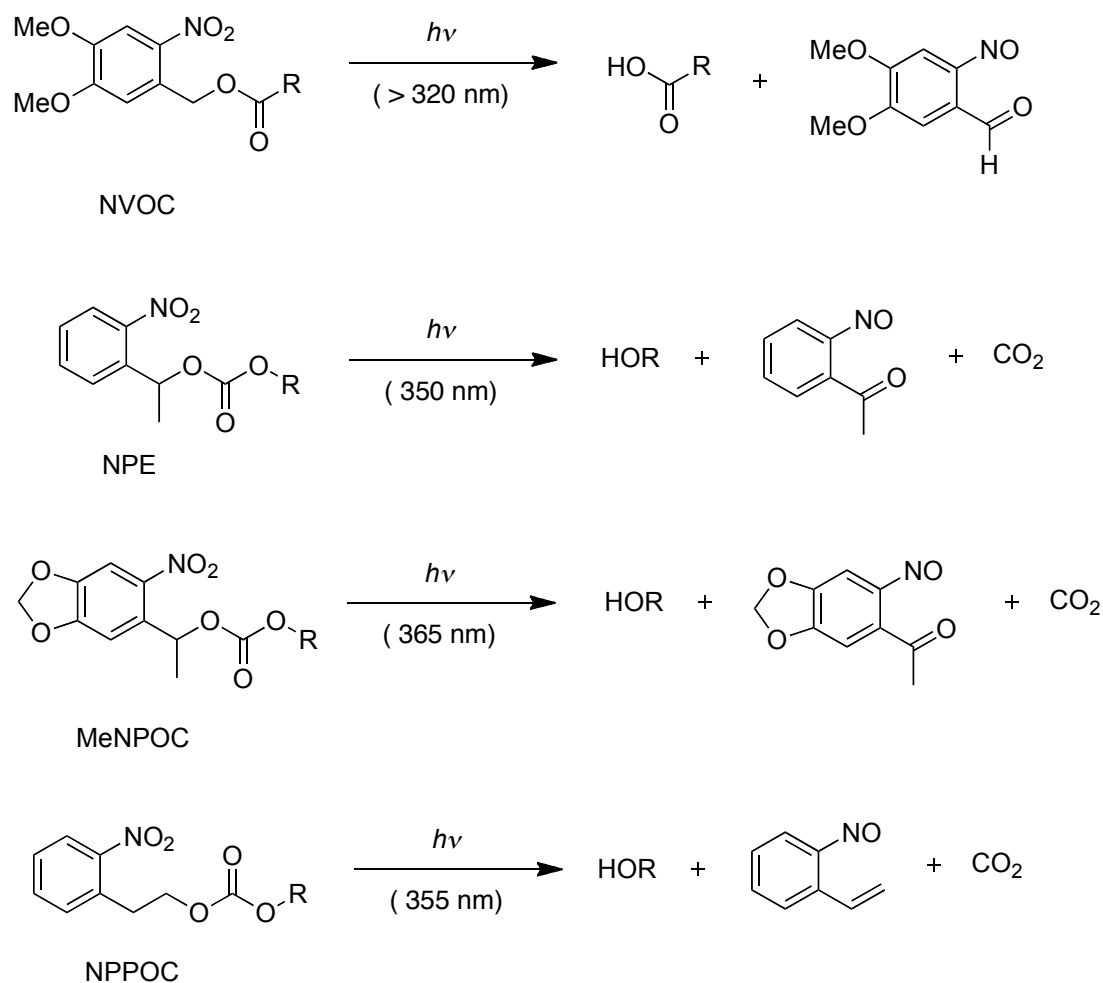
Extensive mechanistic studies have been undertaken on the ONB system by laser flash photolysis<sup>12,13</sup> and time-resolved infrared spectroscopy (TRIR).<sup>14,15</sup> Although details of the mechanism were initially difficult to correlate to observed data, Wirz et al. have proposed a mechanism that has largely remained consistent with the preponderance of spectroscopic data.<sup>16</sup> Deprotection in ONB systems begins with a Norrish II-type  $\gamma$ -hydrogen abstraction upon excitation with UV light to generate the *aci*-nitro intermediate.<sup>17</sup> (Scheme 1-4) Subsequent cyclization and general acid catalyzed ring-opening expels the protected compound. As the ring-opening step requires acid catalysis, the kinetics of the final release is solvent and pH dependent with faster release rates observed at pH < 7. Consequently, this poses a challenge for biochemical studies around physiological pH since reaction rates are minimized in that environment (pH 7.24).



**Scheme 1-4: ONB alcohol release**

Significant efforts have focused on shifting the ONB absorption band to longer wavelengths and improving substrate release efficiencies. The addition of substituents on the phenyl group and at the benzylic ( $\alpha$ ) position are the primary means by which several groups have attempted to produce these changes. Shortly after the development of the NBOC group, Patchornik et al. introduced the 6-nitroveratroyloxycarbonyl group (NVOC) containing two methoxy substituents (Scheme 1-5) that shifts light-absorption to longer wavelengths ( $> 320\text{nm}$ ).<sup>18</sup> Overlapping absorption by bio-active molecules in this range is minimal even in the presence of tryptophan, the most light sensitive amino acid. In the preliminary study, NVOC-protected amino acids and carboxylates were released in quantitative yield when in the presence of a carbonyl scavenger. Later, Ajayaghosh and Pillai suggested incorporating a methyl group at the benzylic position to form the less reactive nitroso ketone byproduct.<sup>19</sup> (NPE, Scheme 1-5) Additionally, this modification results in a more stable tertiary benzylic radical after hydrogen abstraction, however, the increased steric bulk combined with the statistically less-probable hydrogen abstraction





**Scheme 1-5: ONB derivatives as PRPGs**

does limit efficiencies. Cameron and Frechet reported  $\Phi_{rel} = 0.11$  for the methyl substituted system compared to  $\Phi_{rel} = 0.13$  for the parent ONB derivative.<sup>20</sup>

Alternatively, the combination of the  $\alpha$ -methyl with another *o*-nitro group results in the higher statistical probability of exciting a nitro group and subsequent  $\gamma$ -hydrogen abstraction leading to much higher quantum yields ( $\Phi_{rel} = 0.62$ ). A combination of the proposed beneficial qualities of the NVOC and NPE groups was realized to a certain degree in the introduction of the 5'-( $\alpha$ -methyl-2-nitropiperonyl)oxycarbonyl group by Fodor et al.<sup>21,22</sup> (MeNPOC, Scheme 1-5) This group allows the use of longer wavelength

irradiation due to the phenyl substituent and does not form the more reactive nitrosoaldehyde byproduct. A recently developed strategy extends the released compound from the *o*-nitrobenzyl unit by a methylene unit to generate [2-(2-nitrophenyl)propoxy]carbonyl protected compounds.<sup>23-25</sup> (NPPOC, Scheme 1-5)

Substituent effects on rates and efficiencies of release have been investigated by Pfleiderer et al.<sup>23,25</sup> The presence of a halogen at the 5-position of the phenyl group or elongation of the ONB- $\pi$  system with  $\pi$ -conjugated substituents enhanced release rates and efficiencies. The presence of an  $\alpha$ -methyl or second ONB group at the  $\alpha$ -position had the strongest rate and efficiency enhancements. Unfortunately, numerous studies<sup>24,26,27</sup> have also demonstrated that shifting the maximum wavelength absorption ( $\lambda_{max}$ ) of the ONB group to longer wavelengths has deleterious effects on the quantum efficiencies of release ( $\Phi_{rel}$ ). Aujard et al. observed a  $\Phi_{rel}$  decrease from 0.1 to 0.008 in changing from a *para*-chloro substituent to the NVOC system despite the significant bathochromic shift from 272 nm to 348 nm. Ultimately, rates and quantum yields of substrate release are determined by a complex combination of steric, electronic, and statistical factors.<sup>20</sup>

Many applications have utilized the ONB moiety for the investigation of biological systems. Many small bio-active compounds are even commercially available as the ONB-protected form. The “caging” and release of ATP (Figure 1-1) is one of the more heavily used applications of the ONB group, originally developed by Kaplan et al.<sup>28</sup> A number of groups have taken advantage of this design for study of ATP-activated intracellular processes.<sup>6</sup>

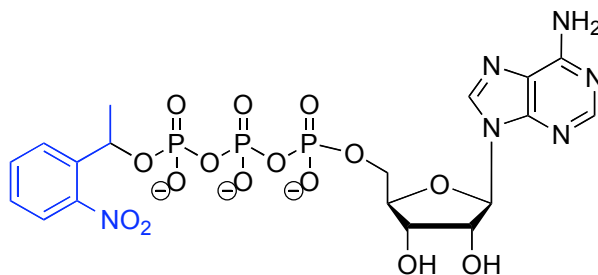
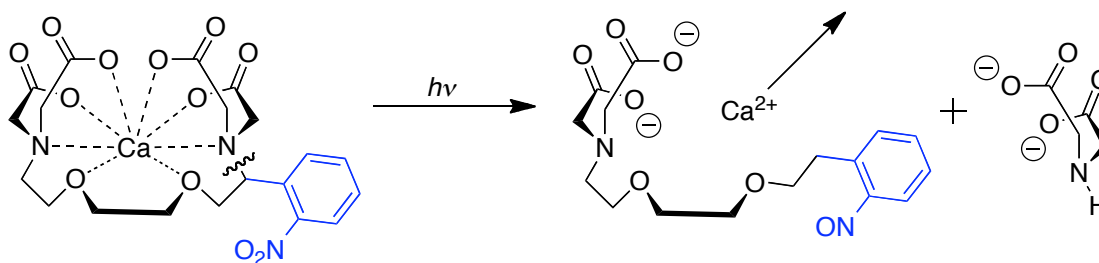


**Figure 1-1: ONB-Caged ATP**

Controlling ion concentrations in biological systems has also been a significant application. Ellis-Davies et al. have developed calcium cages based on ONB chemistry in which parts of the coordination complex fragment upon photolysis, thus releasing calcium into solution.<sup>29,30</sup> (Scheme 1-6) Adams et al. have also found a means to create controlled fast jumps<sup>31</sup> or drops<sup>32</sup> in calcium using ONB derivatives.

ONB PRPGs have also been applied to DNA (or oligonucleotide) synthesis and strand scission. ONB derivatives have been used for site-specific phototriggered bond cleavage of oligonucleotides or DNA strands.<sup>33,34</sup> Incorporation of an ONB derivative into a nucleoside before DNA synthesis allows scission of the formed DNA strand at that particular site upon photolysis. Fodor et al. have demonstrated a method for site-directed oligonucleotide synthesis using NVOC groups.<sup>35</sup> Since PRPGs can be addressed spatially by directing the irradiation beam or using a lithographic mask, specific areas of



**Scheme 1-6: Release of Ca<sup>2+</sup> from an ONB-based cage**

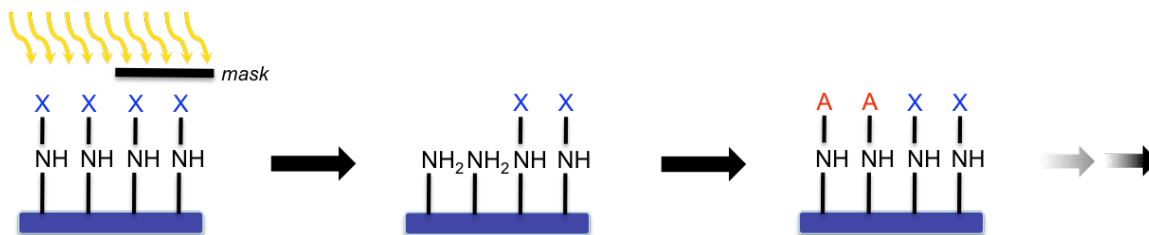


**Figure 1-2: Substrate patterning by deprotection through a lithographic mask**

a prepared substrate can be photolysed, thus “activating” that site by release of the PRPG. Subsequent reaction with a particular reagent allows for a specific surface pattern to be designed while other non-deprotected sites are left untouched. (Figure 1-2) In this manner, an NVOC-protected thymidine functionalized surface was irradiated through a checkerboard pattern mask to release free thymidine at only specific sites. The substrate was subsequently treated with a phosphoramidite-activated derivative of deoxycytidine, which would only react with the released thymidine. Attachment of a fluorescent probe to this moiety revealed the checkerboard pattern when visualized by fluorescence spectroscopy.

### 1.2.2 The benzoin (desyl) group

Benzoin or desyl groups (Figure 1-3) have become a popular method for photorelease of carboxylates,<sup>36</sup> amines,<sup>37</sup> alcohols,<sup>38,39</sup> and phosphates.<sup>40,41</sup> Benzoin derivatives absorb primarily 240-260 nm light and offer many advantages over their OBN counterparts, most notably, faster kinetic release, generally higher quantum yields of release, and relative inertness of byproducts formed. Unfortunately, benzoin-protected compounds typically have limited solubility in aqueous systems. The presence of the

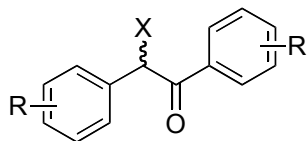
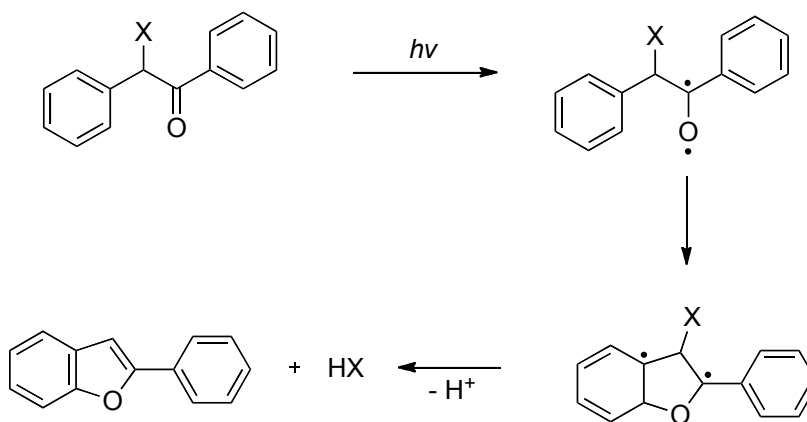


**Figure 1-3: Model benzoin derivative**

benzylic chiral center may also pose problems in systems requiring strict stereochemical control. A variety of substitution patterns have been explored to improve release efficiencies, absorption characteristics, and aqueous compatibility.<sup>42-44</sup> Benzoin release has been adapted for many biological studies in much the same way as OBN groups.

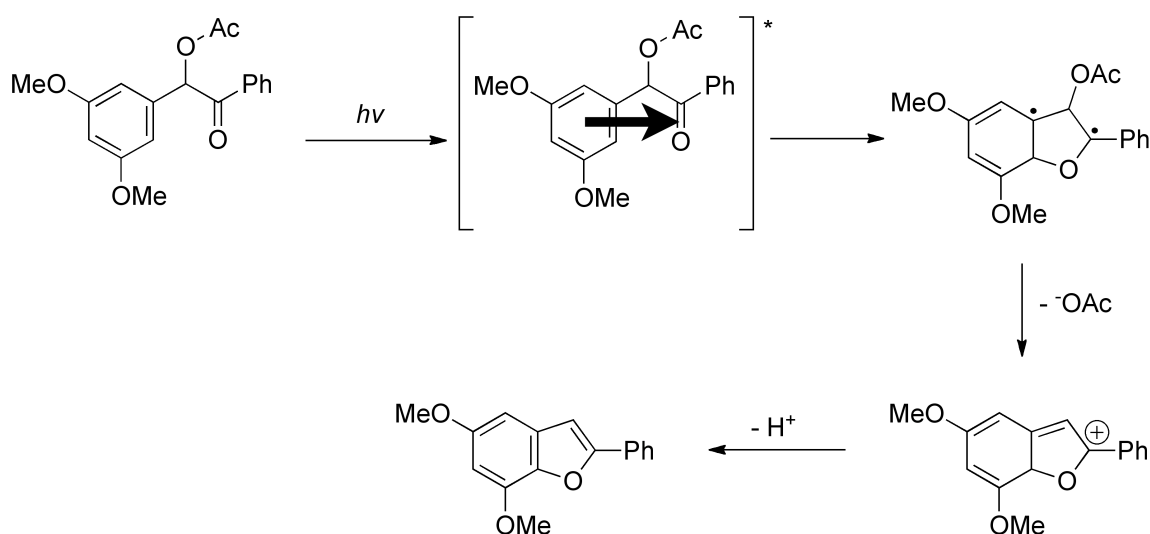
Upon photolysis with near-UV light, unsubstituted benzoin releases substrates attached  $\alpha$  to the carbonyl. The release of acetate from a benzoin derivative was first reported by Sheehan et al.<sup>45</sup> Excitation of the chromophore leads to homolysis of the carbonyl  $\pi$  bond. (Scheme 1-7) Subsequent cyclization results in expulsion of the leaving group and formation of a relatively stable benzofuran byproduct upon deprotonation. This byproduct absorbs strongly in the UV ( $\lambda_{\text{max}} \sim 300$  nm) thus allowing convenient monitoring of reaction progress. However, this also represents a drawback as the



**Scheme 1-7: Deprotection of unsubstituted benzoin PRPG**

benzofuran acts as an internal filter, competing with the protected benzoin for incident irradiation. Subsequent studies by Sheehan et al. explored the effects of substituents on either aromatic ring.<sup>42</sup> *m*-Methoxy substituents on the unconjugated phenyl group were found to greatly enhance deprotection yields while *p*-methoxy substituents decreased yields mildly. Methoxy substituents on the conjugated phenyl group generally decreased reaction effectiveness. The 3',5'-dimethoxybenzoin (DMB) derivative exhibited the most favorable results as high yields (> 99%) of photoproduct were obtained with high quantum efficiencies ( $\Phi_{rel} = 0.644$ ). Rates of photolytic release of acetate were on the order of  $10^{10} \text{ s}^{-1}$ . The DMB group has therefore been heavily studied and used in a variety of applications.

Mechanistic studies of the various substituted benzoin requires a departure from the classical unsubstituted benzoin mechanism.<sup>4</sup> Each substitution pattern seems to have subtle effects on determining the predominating mechanistic pathway. The exact mechanism for DMB derivatives is still under dispute, however, extensive studies by LPF have provided evidence for the intermediates in Scheme 1-8. Although Sheehan



**Scheme 1-8: 3',5'-dimethoxybenzoin (DMB) deprotection**

originally proposed the formation of a strained bicyclic oxetane intermediate as a result of a Paterno-Buchi reaction from the singlet excited state,<sup>42</sup> more recent work by Shi, Rock, and Wirz supports the formation of a biradical intermediate species. Shi et al. proposed a mechanism in which a charge transfer interaction occurs upon excitation between the electron rich DMB ring and the electron poor oxygen of the  $n,\pi^*$  singlet excited acetophenone, forming a singlet intramolecular exciplex.<sup>46</sup> Subsequently, heterolytic cleavage leads directly to a carbocation intermediate which they were able to observe by LFP. Rock et al. postulated the formation of a biradical before the formation of the carbocation in a similar 3',5'-bis(carboxymethoxy)benzoin with increased aqueous solubility<sup>44</sup> which was later confirmed by Boudebous et al. through femtosecond LFP.<sup>47</sup>

Benzoin derivatives have been studied for controlled photolytic release of a wide range of biologically significant compounds. Release of the phosphate group on caged cAMP occurs quantitatively and rapidly upon photolysis ( $10^8 \text{ s}^{-1}$ ), approximately 3-6 orders of magnitude faster than ONB analogues.<sup>48,49</sup> The amino acid neurotransmitters glutamate and  $\gamma$ -aminobutyric acid (GABA) have also been protected and released for mammalian brain receptor studies.<sup>50</sup>

In a continuation of previous work,<sup>35</sup> Pirrung et al. have extensively studied DMB carbonates as alcohol and phosphate protecting groups in the preparation of surface-bound arrays of oligonucleotides for solid-phase DNA synthesis.<sup>39,51</sup> 3'-DMB protected 3'-phosphotriesters were released to generate phosphodiester for coupling with free 5'-hydroxyl nucleotides.<sup>40</sup> If generated on a solid support, this offers an attractive option for generating "DNA chips" for detection of complementary sequences of unknown nucleic acids.

Finally, the benzoin moiety has been used to study protein folding directly by photolysis of an internal benzoin linker developed by Chan et al.<sup>36</sup> The *N* terminus of a protein is linked to an internal amino acid side chain using a benzoin group as the linker. This connection does not allow proper folding of the protein. Upon photolysis, the linear form of the protein is restored allowing the protein to fold into its lowest energy equilibrium state.

### 1.2.3 The phenacyl group

Phenacyl ester derivatives, particularly the *p*-hydroxyphenacyl (pHP) group<sup>52</sup> (Figure 1-4) have shown great promise as PRPGs and have been developed mostly for release of carboxylates<sup>53</sup> and phosphates.<sup>54</sup> In contrast to ONB derivatives, photoproducts are generally biologically harmless, release rates are fast, and most pHP derivatives are aqueous compatible. The primary pHP photoproduct has a blue-shifted absorption with respect to its precursor thus minimizing inner filter effects with the choice of appropriate irradiation wavelengths (generally >300 nm). The mechanism of photorelease has been extensively studied by a number of groups and the factors influencing the efficiencies are similar to those observed with other PRPG families. Their application in biological systems has been studied including the release of amino acids, neurotransmitters, and peptides.

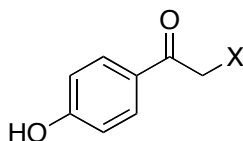
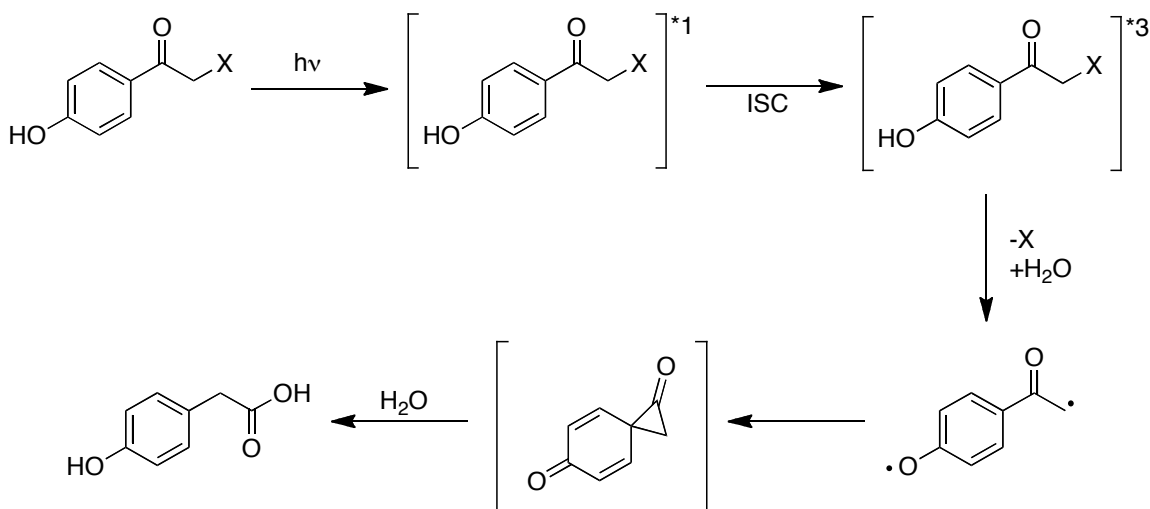


**Figure 1-4: Model *p*-hydroxyphenacyl protecting group**



The liberation of chloride from substituted phenacyl groups was first reported by Anderson and Reese.<sup>53</sup> Later, Sheehan et al. extended this system for the protection of carboxyl functionalities of several amino acids with *p*-methoxyphenacyl and  $\alpha$ -methylphenacyl groups.<sup>43</sup> These early studies demonstrated the significant effect that phenyl ring substituents have on release efficacy where *p*-methoxy and *p*-hydroxy substituents demonstrated the highest efficacy. Givens et al. later demonstrated the pHP group<sup>52,55</sup> for phosphate and carboxylate protection with high release rates, efficiencies, and improved aqueous solubility compared to previously used PRPGs. However, photorelease yields and efficiencies were found to be solvent dependent with carboxylate yields significantly enhanced in the presence of a hydrogen donor such as dioxane, ethanol, or water.

Although the pHP group is a relatively new PRPG compared to the ONB and benzoin derivatives, the mechanism of photorelease has been thoroughly studied. While the mechanism of release for unsubstituted phenacyl groups is believed to proceed through a hydrogen atom transfer to a ketyl radical followed by solvent-assisted release,<sup>56</sup> the mechanism for pHP release appears to follow a different pathway. Recent reports providing new data from ultrafast spectroscopy have helped elucidate some of the mechanistic details.<sup>57-60</sup> The generally accepted mechanism begins with excitation of the chromophore to an excited singlet state followed by efficient intersystem crossing.<sup>43</sup> (Scheme 1-9) Heterolytic release of the substrate proceeds with solvent assistance from at least two water molecules in aqueous solution to form a triplet biradical intermediate. Upon intersystem crossing, the singlet biradical then undergoes a Favorskii-type rearrangement to form a spirodione intermediate. Currently, there is no direct evidence



**Scheme 1-9: Release from pHP in aqueous solution**

for the spirodione intermediate, though its presence is expected due to the formation of phenylacetic acid derivatives as the final byproduct in high water concentrations.<sup>60</sup>

The absorption properties and quantum yields of these reactions are dependent on solvent pH and on the pKa of the phenolic proton. Givens et al. have illustrated the profound effect that the protonation state of the phenolic proton has on the quantum yields of release.<sup>60</sup> The conjugate base was found to be largely ineffective in releasing the protected substrate upon excitation, with  $\Phi_{rel} < 0.02$  in pH 9 solution compared to  $\Phi_{rel} \leq 0.2$  at pH 7. The absorption spectrum is also highly pH dependent as a bathochromic shift from 282 nm to 326 nm was observed between pH 7 and pH 9 solutions of pHP protected GABA. Photoinduced deprotonation was found to be an efficient “energy-wasting” pathway that competes with the Favorskii rearrangement from the triplet excited state. Thus, careful control over the protonation state of the phenolic proton must be maintained for optimal photorelease.

The addition of substituents on the phenacyl ring has been explored to shift the phenacyl absorption band and improve release efficiencies. Conrad et al. have introduced

the 3'-methoxy and 3',5'-dimethoxy pHP groups to red-shift the absorption range of the PRPG and avoid competitive absorption by aromatic amino acids and nucleotides.<sup>61</sup> The absorption maxima were shifted to 350 nm and 370 nm, respectively, tailing just below 400 nm. Unfortunately, quantum yields of release were significantly lower ( $\Phi_{rel}$  0.03-0.04) than their unsubstituted pHP counterparts. Other studies of substituent effects found that electron-donating substituents generally lower quantum efficiencies while electron-withdrawing substituents generally have the opposite effect. However, these changes also affect the pKa of the phenolic proton which may convolute the observation of these trends.<sup>4,60</sup>

pHP has been utilized for a number of biological applications including the caging and release of ATP,<sup>55,62</sup> GABA,<sup>52,60,63</sup> glutamate,<sup>52</sup> and the dipeptide Ala-Ala.<sup>52,64</sup> Compounds protected with the phenacyl moiety can also be released by reduction from an excited-state electron donor which will be discussed in the following chapter.

#### 1.2.4 The coumarinyl group

The use of coumarinyl derivatives as PRPGs<sup>65</sup> is fairly new (Figure 1-5), despite early reports of their photochemistry by Givens et al. while studying phosphate release from various PRPGs.<sup>41</sup> Coumarins are particularly attractive for PRPG use as the chromophore is highly stable under intense irradiation conditions, evidenced by their wide utility as laser dyes.<sup>4</sup> Also, absorption primarily falls in the near-UV and visible

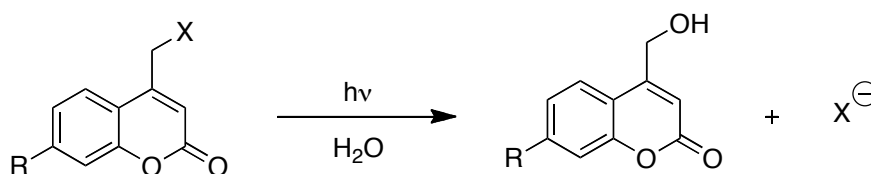
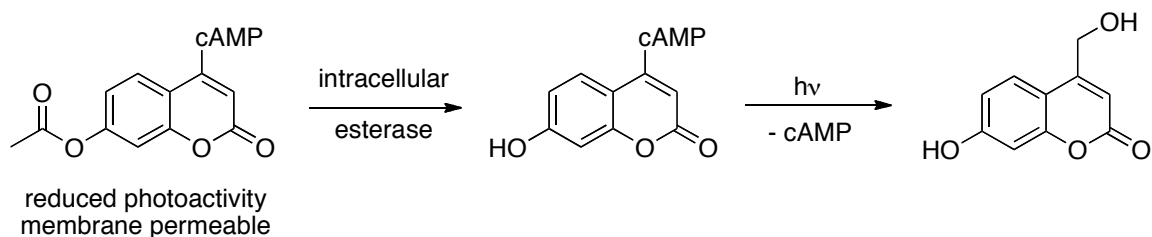


**Figure 1-5: 7-Substituted coumarin derivative as a PRPG**

regions, offering the ability to use low energy photolysis irradiation that will not be absorbed in biological systems. Through appropriate substitution, absorption can be tuned to even longer wavelengths in addition to altering fluorescence efficiencies. The highly fluorescent nature of the coumarin moiety also offers a convenient means to follow deprotection progress which is particularly attractive in biological applications. As such, coumarins have been used to protect carboxylates, phosphates, amines, aldehydes, ketones, alcohols, and an assortment of biologically significant molecules.<sup>65</sup> Quantum efficiencies of release are generally lower than other PRPGs however rates and yields of substrate release are still high.

The first significant application of the coumarin group as a PRPG was developed by Furuta et al. for the release of cAMP.<sup>66</sup> Although the quantum efficiencies of release from the 7-methoxycoumarinyl derivative were low ( $\Phi_{rel}$  0.07), molar absorptivity at the irradiation wavelength ( $\epsilon_{340nm}$ ) was 24 times larger than the NPE-protected analog. Thus the overall photoresponse, or photolytic efficacy ( $\Phi_{rel} \epsilon_{340nm}$ ), for the coumarin was about six times higher. Later, Furuta substituted an acyloxy group for the hydroxy group on a cAMP-protected derivative. This change limits PRPG release but increases biological membrane permeability.<sup>67</sup> Intracellular enzymes could subsequently hydrolyze the 7-acyloxy group to a 7-hydroxy group thus restoring the PRPG function. (Scheme 1-10)

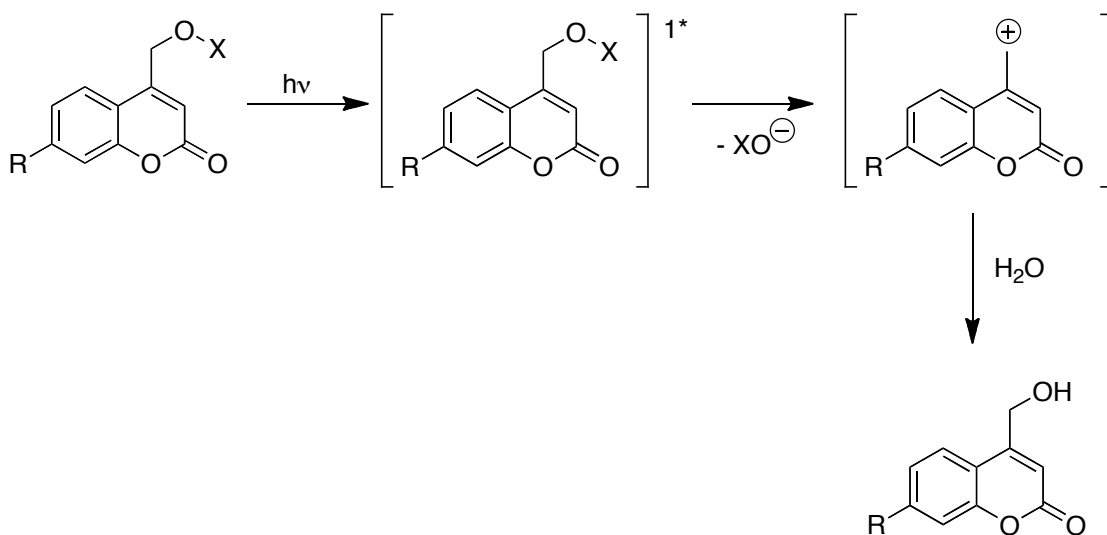


**Scheme 1-10: 7-acyloxycoumarins for improved membrane permeability**

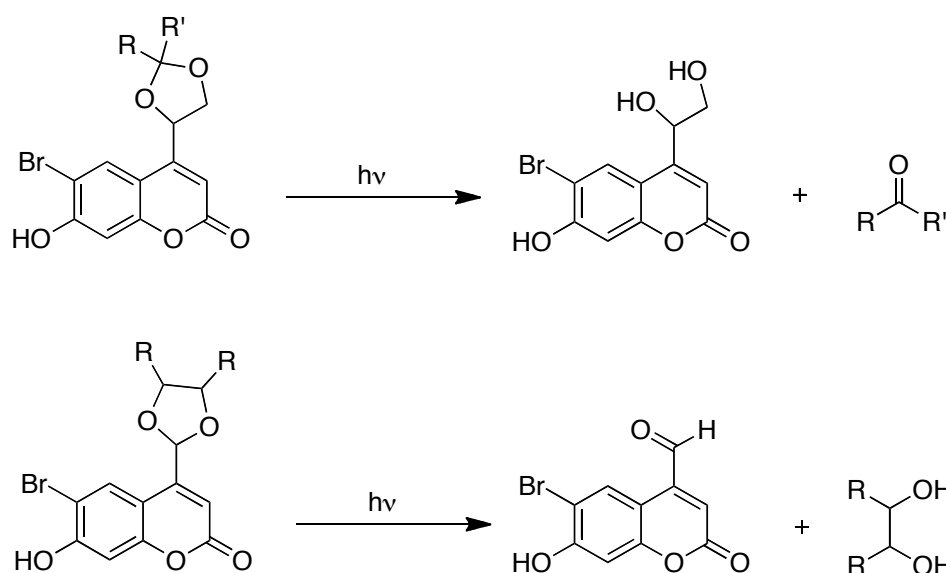
The exploration of several halogen-substituted 7-hydroxycoumarinyl derivatives for release of carboxylates and amines demonstrated their excellent two-photon absorption cross sections for improved spatially-addressable uncaging.<sup>68</sup>

The mechanism of photorelease from coumarin derivatives is generally agreed upon, though few studies have undertaken rigorous investigations. Schade et al. have proposed an excited-state S<sub>N</sub>1-type mechanism in which heterolysis occurs from the excited singlet state.<sup>69</sup> (Scheme 1-11) An ionic mechanism is supported by the increase in reaction efficiency with increasing amounts of polar protic solvent. <sup>18</sup>O-labeling experiments found incorporation into only the coumarin byproduct, therefore, cleavage of the C-O bond rather than the O-X bond predominates. The observation that increasing leaving group ability had a positive effect on  $\Phi_{rel}$  supports an S<sub>N</sub>1-type mechanism.

Coumarin groups have recently been adapted to protect diols,<sup>70</sup> aldehydes, ketones,<sup>71</sup> and alcohols.<sup>72</sup> Alcohols and phenols can be simply prepared as carbonate derivatives and release rates and efficiencies are comparable to carboxylate release.<sup>72</sup>



**Scheme 1-11: Release from Coumarin Derivatives**



**Scheme 1-12: Release of aldehydes/ketones and diols from coumarin derivatives**

Acetals or ketals prepared on the coumarin moiety generate the respective aldehydes and ketones along with the coumarin diol by-product. (Scheme 1-12) Alternatively, by substituting the coumarin at the carbon between the acetal/ketal oxygen atoms, the corresponding diol is released, generating the coumarin aldehyde by-product. Despite the poor leaving group ability of alcohols, the authors believe its release is assisted by the adjacent ether moiety of the acetal that subsequently stabilizes the carbocation. Quantum yields of release in both systems were generally low ( $\Phi_{rel} < 0.057$ ) although rates and yields of the release reaction were high. The coumarin group has also been explored for photoinduced pH changes.<sup>73</sup> Through the release of diethyl phosphates and sulfates, which have low pKa values, from (6,7-dimethoxycoumarin-4-yl)methyl and [7-(dimethylamino)coumarin-4-yl]methyl derivatives, controlled jumps in pH can be initiated with light in solutions of pH > 2. Surprisingly, these systems were characterized by high quantum yields of release ( $\Phi_{rel} \leq 0.79$ ) and may be useful in the exploration of proton-triggered biological processes.

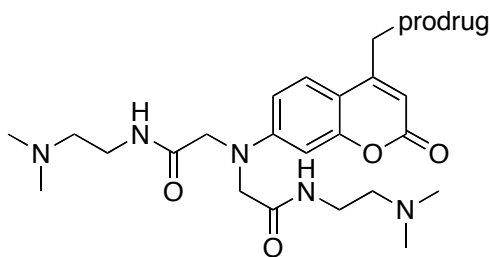
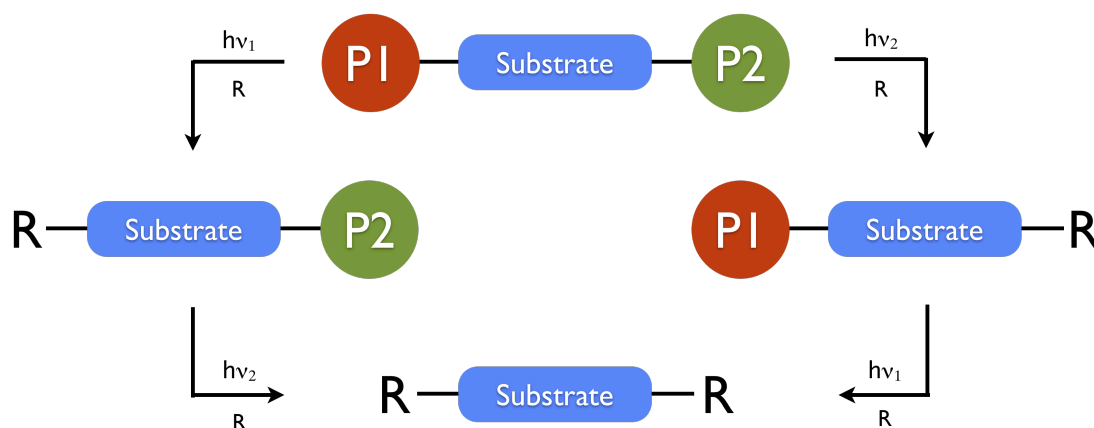


**Figure 1-6: Coumarin-based PRPG designed with improved aqueous compatibility for prodrug release**

Many applications have recently been developed around the release of bio-active molecules from coumarin moieties. The caging of important phosphates such as cAMP,<sup>66,67</sup> cGMP,<sup>74</sup> CDP,<sup>75</sup> and ATP<sup>76</sup> have all been reported. Hagen et al. reported the efficient release of cAMP and cGMP with 7-carboxy-substituted coumarins.<sup>77</sup> The substituent change significantly enhanced aqueous solubility without compromising reaction rates and efficiencies. Similarly, Noguchi et al. introduced a novel solubilizing substituent to the coumarin moiety as part of a tumor-targeting prodrug design.<sup>78</sup> (Figure 1-6) Water-solubility was found to increase considerably compared to the *N,N*-diethylamino-substituted system while high efficiencies and release yields were maintained. Combining the improved aqueous solubility of these new systems with the beneficial light absorption properties, ease of monitoring, and versatility of the coumarin moiety, this group will continue to be of great use as a PRPG in future applications.

### 1.2.5 Wavelength-orthogonal systems

Protecting group orthogonality refers to the ability to incorporate multiple protecting groups into the same system and selectively deprotect one group while the others remain intact, in any particular order. In practice, complete orthogonality is very difficult to achieve. Most protecting groups will have modulated lability<sup>79</sup> with respect to one another such that the order of deprotection will influence the final outcome. For instance, trimethylsilyl (TMS) ethers can be hydrolyzed in the presence of *tert*-butyldimethylsilyl (TBDMS) ethers, but introduction of TBDMS hydrolysis conditions in the presence of TMS ethers will deprotect both groups. Recently, efforts have been made, primarily by Bochet et al.,<sup>7</sup> to develop a wavelength-orthogonal system in which irradiation of different wavelengths is used to selectively release one PRPG over another.<sup>26</sup> (Scheme 1-13) Typically, two structurally different PRPGs with mismatched absorption profiles are utilized. However, since photolytic efficacy is proportional to the product of the molar absorptivity and quantum yield at the irradiation wavelength ( $\Phi_{rel}\epsilon$ ), manipulation of factors effecting quantum yields can also help selectivity. Modulated



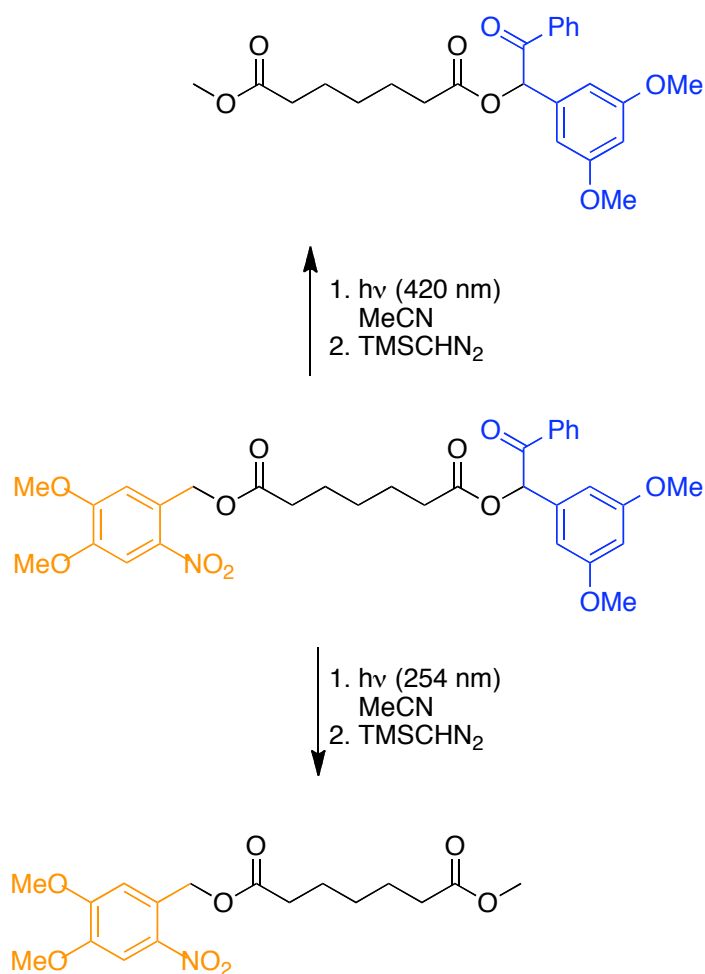
**Scheme 1-13: Wavelength-orthogonal deprotection of PRPGs**



lability has been demonstrated and the design of completely orthogonal systems has been described.

Preliminary attempts to design a wavelength-tunable system by Bochet et al. incorporated a nitroveratryl carbamate (NVOC) with a 3,5-dimethoxybenzyl alcohol derivative in the same solution.<sup>26</sup> The benzyl alcohol would be released with shorter wavelength (254 nm) light while the NVOC group would be released with longer wavelengths (350 nm). Unfortunately, wavelength selectivity was not realized as the higher-energy-absorbing benzyl alcohol seemed to act as a sensitizer for the NVOC-protected compound. Surprisingly, a degree of selectivity was observed when an NVOC-protected compound was combined with a different *o*-nitrobenzyl variant. Later, Bochet et al. were able to demonstrate partial orthogonality when incorporating an NVOC-derivative and a benzoin derivative separately in solution and in the linked system.<sup>80,81</sup> (Scheme 1-14) The NVOC group is addressed with 420 nm light and the benzoin derivative with 254 nm light. This design demonstrated much improved selectivity enabling them to isolate a 90:10 or 15:85 mixture of the released products when irradiated with 254 nm or 420 nm, respectively. In the linked system, 70% of the photoproduct was isolated from release of either PRPG. Energy transfer appears to be minimal in these systems.

Newer developments have utilized kinetic isotope effects (KIE) to increase orthogonality in concert with the wavelength absorption differences.<sup>82,83</sup> Since a rate-limiting step in the release of ONB-protected substrates is  $\gamma$ -hydrogen abstraction, substitution of this hydrogen with a deuterium atom should affect the rate and efficiency ( $\Phi_{rel}$ ) of this step and thus ONB-release. Thus, selectivity between the two PRPG release

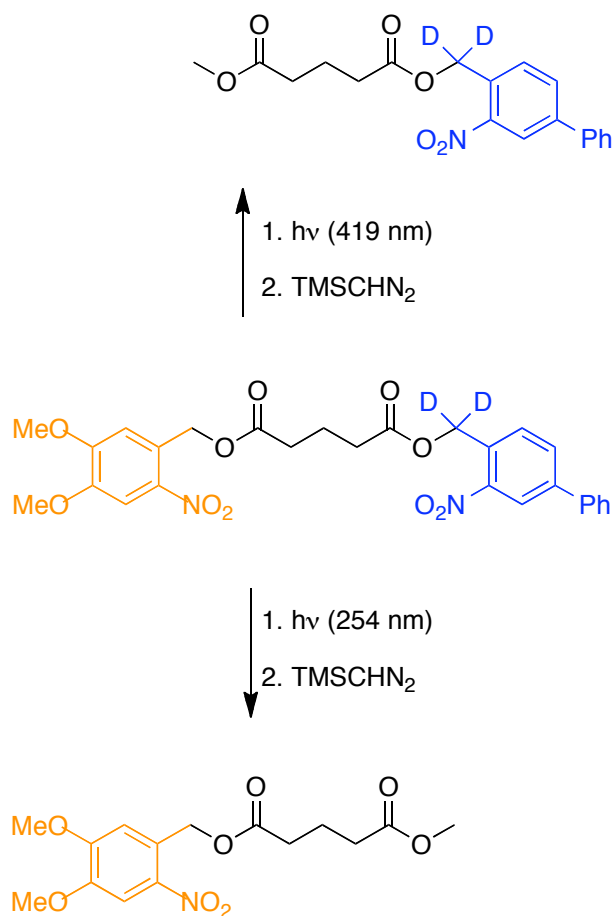


**Scheme 1-14: Wavelength-orthogonal photorelease utilizing ONB and benzoin PRPGs**

reactions should increase without significantly affecting the absorbance mismatch already in place. Bochet et al. incorporated this modification into a linked system that combines two different ONB moieties in an effort to modulate the ONB-release rate. (Scheme 1-15) The isotopically-substituted substrate demonstrated higher selectivity in the release reactions, 14:1 of the monoesters, compared to 2.4:1 with the undeuterated system when irradiated first with 420 nm light. Unfortunately, selectivity decreases when irradiated first with 254 nm light, thus the system is not formally orthogonal. However, optimization of spectroscopic parameters through modification of the ONB substituents

combined with the improved selectivity from the KIE lead to the development of a more chromatically orthogonal system.<sup>83</sup> By incorporating the 3,4-dimethoxy ONB derivative with the 3-phenyl ONB derivative, a 8.6:1 and 4.7:1 selectivity was achieved when starting from 420 nm or 254 nm irradiation, respectively.

While the potential applications for wavelength-orthogonal systems are numerous, there is much room for improvement. Some limited applications have been demonstrated by Bochet et al. in the use of the previously discussed system for solid-phase peptide synthesis.<sup>84</sup> Improved selectivity may be realized with the combination of



**Scheme 1-15: Improved wavelength-orthogonal photorelease by spectroscopic and kinetic parameter optimization**

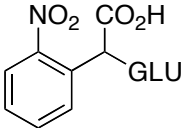
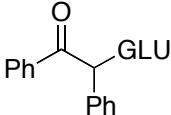
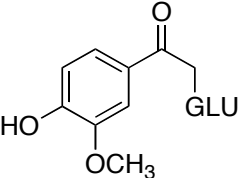
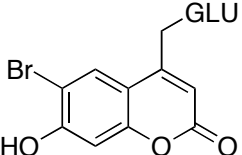
chromophores with significantly different absorption profiles, such as coumarins and ONB derivatives. Additionally, the use of two-photon absorption may improve selectivity by use of a chromophore with a high two-photon absorption cross-section. Photoinduced electron transfer based protecting groups may also provide opportunities for enhanced wavelength orthogonality.

### 1.3 Conclusions

Direct deprotection remains the most widely studied and heavily applied means of releasing compounds photolytically. Furthermore, the ONB and benzoin groups have been the centerpiece of several pioneering studies in biochemistry. Phenacyl groups continue to be applied and coumarinyl derivatives offer great promise due to their low energy absorption and high two-photon absorption cross sections. Innovative means to generate wavelength-orthogonal systems continue to be explored, but are still far from fulfilling their promise.

To facilitate comparison of the discussed PRPGs, photolytic efficacies for release of the  $\gamma$ -carboxylate-protected neurotransmitter glutamate from each of the discussed groups are collected in Table 1-1.<sup>8</sup> ONB and benzoin groups display large  $\Phi_{rel}$  values in comparison to the pHP and coumarin derivatives. However, the later groups compensate for this deficiency with high molar absorptivities. Thus, the ONB, pHP, and coumarin groups display comparable photolytic efficacies under the given irradiation conditions whereas the benzoin-protected glutamate is about an order of magnitude less effective.

**Table 1-1: Comparison of photolytic efficacy of various PRPGs for the release of glutamate (GLU) from  $\gamma$ -carboxylate-protected glutamic acid<sup>8</sup>**

Structure	PRPG Family	$\lambda$ (nm) <sup>a</sup>	$\epsilon_{\lambda}$ (M <sup>-1</sup> cm <sup>-1</sup> )	$\Phi_{\text{rel}}$	$\Phi_{\text{rel}}\epsilon_{\lambda}$
	<i>o</i> -nitrobenzyl	262	5100	0.14	714
	benzoin	347	170 <sup>b</sup>	0.14	24
	pHP	307	7930	0.035	278
	coumarin	369	19550	0.019	371

<sup>a</sup>Irradiation Wavelength

<sup>b</sup>Determined from a benzoin-protected phosphate group.<sup>85</sup>

Ultimately, exact photolytic efficacies of each PRPG will differ depending on substituent effects, solvent, as well as the identity of the protected substrate (among others), yet the data in Table 1-1 allow a convenient comparison of the discussed PRPGs.

Despite the successes of the aforementioned PRPGs, they all suffer from several drawbacks. Firstly, release of these groups is triggered by short wavelength irradiation that is less convenient to produce and potentially harmful to the surrounding environment in which they are placed. Attempts to shift absorption of these chromophores through structural modification generally leads to changes in efficiencies of release or changes in physical properties, such as solubility. Secondly, the chromophore used in each case is rendered ineffective towards inducing further deprotection reactions. This can be an inefficient use of resources as many synthetic steps are typically required to produce some of the more highly substituted PRPG chromophores. In response to these

challenges, several PRPGs have been designed around photoinduced electron transfer processes.

## **2 Photoinduced Electron Transfer (PET) Based PRPGs**

### ***2.1 Introduction***

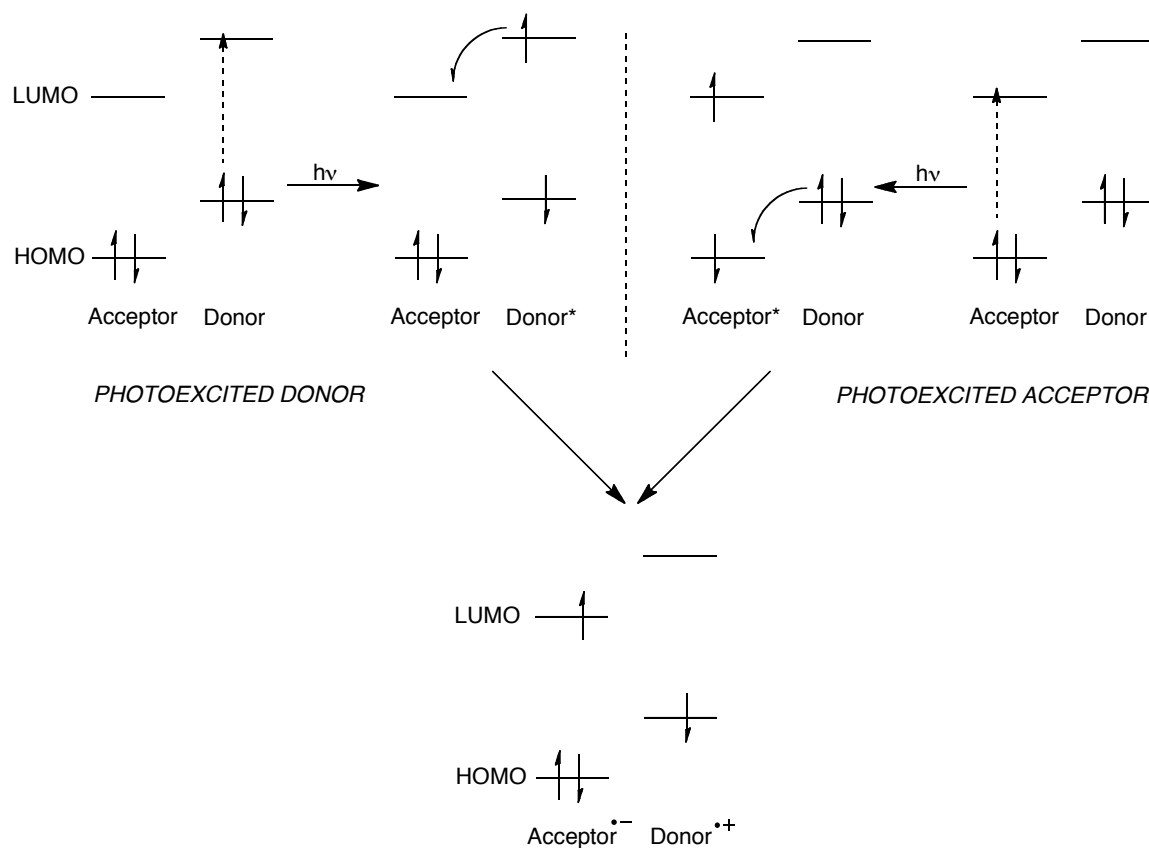
In contrast to direct photolysis PRPGs, photoinduced electron transfer-based PRPGs (PET-PRPGs) rely on the use of a sensitizer for substrate release. Sensitizers are designed to transfer electrons to or from the protecting group thereby initiating a cascade of events that eventually release the protected compound. Various PRPGs have been developed around this design utilizing the sensitizer as the electron source or sink (direct PET) or using the sensitizer to shuttle electrons between a donor or acceptor molecule and the PET-PRPG (mediated PET). In contrast to direct photolysis PRPGs, there is greater flexibility inherent in the design of PET-PRPGs, thereby facilitating optimization of light absorption characteristics and release efficiencies.

### ***2.2 Photoinduced electron transfer***

Photoinduced electron transfer (PET) is readily observed in a host of photochemical, biochemical, and biophysical interactions. Indeed, PET plays a profound role in sustaining life on earth as this process drives all biological photosynthetic apparatus. Although the effects of PET had been studied at least as early as the eighteenth century by Joseph Priestley, the direct observation and theoretical descriptions of PET were not possible until the later half of the twentieth century.<sup>86</sup> Since then, it has been extensively studied and exploited in a number of materials applications designed for solar energy conversion, photolithography, and molecular electronics.<sup>87,88</sup>

PET is an electron exchange interaction between a photoexcited moiety and a ground state species. Transfer occurs between an electron donor and an electron acceptor to generate the respective radical cation and radical anion pair (assuming both start with net zero charge). Photoexcitation can occur within either the donor or the acceptor moiety as the driving force and pathway for electron transfer are ultimately determined by the relative alignment of the ground state (HOMO) and excited state energy levels (LUMO) of the donor and acceptor. (Scheme 2-1)

The change in free energy for an electron transfer reaction ( $\Delta G_{ET}$ ) is the primary means to predict the success of an electron transfer reaction. As described by Weller et al.,  $\Delta G_{ET}$  can be approximated in terms of the ground state oxidation potential of the



**Scheme 2-1: Schematic representation of PET**





radiative ( $k_{nr}$ ) processes is generally competitive. In order for PET to occur, the donor and acceptor must diffuse into close proximity to one another, generating an encounter complex (EC). At this point, electron transfer ( $k_{ET}$ ) generates a contact ion pair (CIP) from which cage escape into solvent separated ions ( $k_{ss}$ ) competes with back electron transfer ( $k_{BET}$ ). The solvent-separated ground-state radical ions are typically sufficiently long-lived to potentially participate in additional reactions or to recombine to regenerate the original donor and acceptor molecules ( $k_{rec}$ ). Intersystem crossing to the triplet manifold ( $k_{ISC}$ ) may occur at any point between excitation and solvent separation of the ion pair depending on energy level alignment and the degree of spin-orbit coupling. Non-radiative decay ( $k_{nr}$ ) to the ground state is always a competitive process in each step of PET. The Weller equation (Eq 2-1) provides an approximation of the driving force ( $\Delta G_{ET}$ ) for the overall process from ground state donor and acceptor to solvent-separated ion pairs. To establish a relationship between  $\Delta G_{ET}$  and the rate of electron transfer ( $k_{ET}$ ), the theoretical work of Marcus must be considered.

Early theoretical studies by Marcus predicted a quadratic relationship between the free energy of electron transfer ( $\Delta G_{ET}$ ) and the rate of the electron transfer ( $k_{ET}$ ).<sup>90-93</sup> (Figure 2-1) Thus,  $k_{ET}$  is expected to increase with increasing exergonicity (the normal region). The reaction rate will eventually reach a maximum as the system is constrained to fewer optimal configurations for effective electron transfer. This is quantified as the reorganization energy ( $\lambda$ ) and accounts for solvent and vibrational changes. The maximum  $k_{ET}$  value on the Marcus curve is located where  $-\Delta G_{ET} = \lambda$ . Increasing

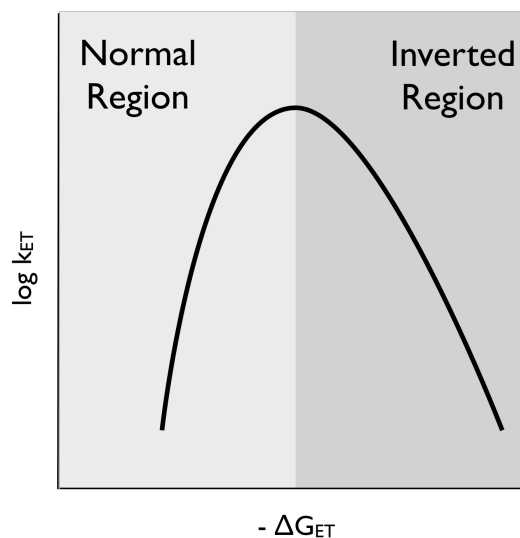


**Figure 2-1: Dependence of  $k_{ET}$  on  $\Delta G_{ET}$  as described by Marcus**

exergonicity beyond the maximum  $k_{ET}$  results in a decrease in  $k_{ET}$  due to the increasingly poor vibrational overlap between the product and reactant wavefunctions (the inverted region).

Preliminary experiments to explore Marcus' predictions confirmed the behavior expected for the normal region, but were unable to demonstrate the inverted region. Fluorescence quenching studies by Rehm and Weller showed a plateau at the molecular diffusion limit after a sharp rise with increasing exergonicity.<sup>94</sup> Since this work employed an intermolecular electron transfer reaction in solution, diffusion rates ultimately limited the observed rates at high exergonicity; donor and acceptor molecules were unable to diffuse into an encounter complex fast enough to observe the inverted region behavior. Subsequent studies by Miller et al. were able to provide clear evidence for the inverted region by measuring electron transfer rates in a rigid organic solid thus avoiding the diffusion-limiting problem.<sup>95</sup> Shortly thereafter, Miller and Closs were able to demonstrate the inverted region in solution by utilizing a linked donor-spacer-acceptor

system to again avoid the diffusion of donor and acceptor away from each other.<sup>96</sup>

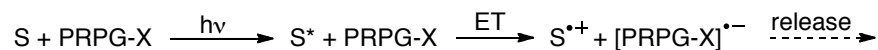
Several other groups have since confirmed these results in a number of different systems (including back electron transfer reactions in solution) utilizing modern spectroscopic techniques including laser flash photolysis and Electron Pair Resonance (EPR).<sup>87,97,98</sup>

### **2.3 Design of PET-based PRPGs**

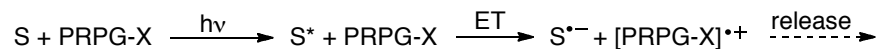
Release of caged substrates through PET requires that the protecting group be responsive towards oxidation or reduction. There are a number of modes in which this can take place. (Scheme 2-3) Direct electron transfer (DET) is the simplest process in which the PET-PRPG directly quenches the sensitizer excited state. Alternatively, electrons can be shuttled between the PET-PRPG and a good electron donor or acceptor through the sensitizer, now referred to as a mediator (mediated electron transfer, MET). (Scheme 2-3) For the desired electron transfer reactions to be realized, it is necessary to carefully consider the oxidation/reduction potentials of all compounds present in a given system.

## DIRECT ELECTRON TRANSFER (DET)

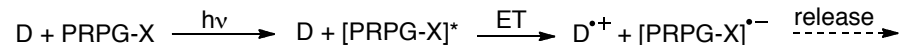
### *Sensitized Reduction*



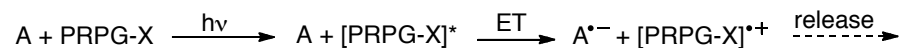
### *Sensitized Oxidation*



### *Direct Reduction*

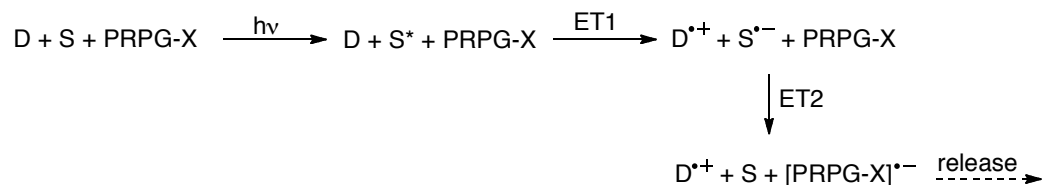


### *Direct Oxidation*

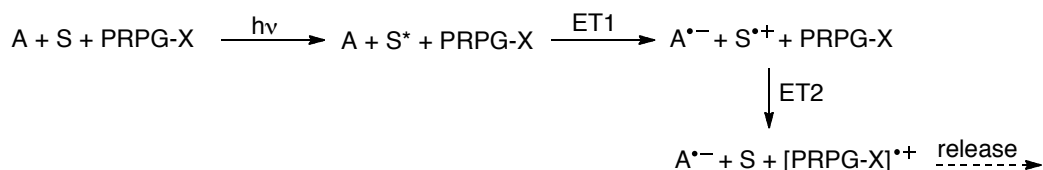


## MEDIATED ELECTRON TRANSFER (MET)

### *Reductive MET*



### *Oxidative MET*



**Scheme 2-3: Direct and mediated photoinduced electron transfer mechanisms**

### 2.3.1 Direct electron transfer

Direct electron transfer (DET) can occur by a reductive or oxidative mechanism, depending upon the fragmentation mechanism that releases the protected compound. (Scheme 2-3) As discussed in preceding sections, the success of a particular electron transfer pathway is predicted by calculating  $\Delta G_{ET}$  from the Weller equation. (Eq 2-1)

DET reactions can be further subdivided into sensitized and direct mechanisms. Direct mechanisms induce electron transfer by exciting a chromophore that is part of the PRPG. Abstraction or donation of an electron subsequently produces the radical anion or cation of the PRPG to begin the release reaction. Sensitized DET begins with excitation of a chromophore followed by inter- or intra-molecular quenching by the PRPG. This results in production of the geminate radical ion pair of the sensitizer/PRPG, which, upon cage escape, can proceed with the release reaction.

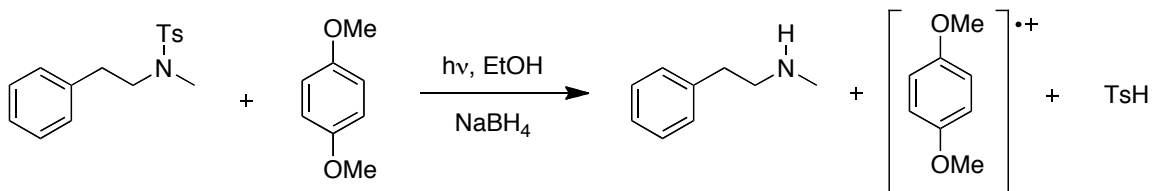
Thus, the primary difference between Sensitized and Direct DET mechanisms is the identity of the light-absorbing species. Direct DET offers the ability to use a wide variety of electron donors or acceptors as long as  $\Delta G_{ET}$  is still exergonic, however, the photophysics, and therefore the absorption profile, of the PRPG chromophore are fixed. As described in the preceding chapter, alteration of substituents to perturb the absorption profile of PRPGs often leads to changes in efficiencies and rates of release of the protected substrate. Frequently these changes are detrimental. Therefore, the main advantage of sensitized DET systems is the ability to choose sensitizers with a variety of absorption profiles so long as  $\Delta G_{ET}$  is still exergonic (i.e. the redox potentials of components in the system are now the primary design constraint). The bond fragmentation step should remain unaffected so long as electron transfer to the PET-PRPG is favorable. Therefore, custom-tailored chromophores can be chosen or synthesized to meet a particular irradiation wavelength range. This is particularly attractive for the design of PET-PRPGs to be used in biological systems, as chromophores absorbing longer wavelength visible and infrared irradiation could

potentially be used. Sensitized DET will be the main mode of DET discussed in this work, thus any further discussion of DET should be assumed to be sensitized DET.

The main disadvantage of DET strategies stems from the expectation that an oxidized or reduced sensitizer molecule is resistant towards further oxidation or reduction. Thus, at least a full equivalent of the sensitizer is required to quantitatively deprotect a particular system. This can represent a significant limitation as certain chromophores are only available in small quantities and at considerable cost. Nevertheless, direct PET is the simplest method for PET-based deprotection and several systems utilizing sensitized DET have been developed.

#### 2.3.1.1 Tosyl amide and esters

One of the seminal PRPGs developed for DET release is the tosyl amide group developed by Hamada et al. In the presence of a good electron donor and a coreductant, such as sodium borohydride, the *N*-tosylamine will afford the free amine upon photolysis in high yield.<sup>99</sup> (Scheme 2-4) The reaction was found to be promoted in polar, protic solvents and deactivated almost completely in nonpolar solvents. This observation was rationalized in terms of a sensitized reduction mechanism in which PET occurs from the electron rich donor to the tosyl amine acceptor. Hydrolysis then proceeds to release the amine and the reducing agent scavenges the sulfonyl radical or restores the donor



**Scheme 2-4: Photolytic tosyl amide deprotection**

compound. Hamada et al. extended their preliminary work by covalently tethering several aromatic donors to the tosyl group.<sup>100</sup> While several systems exhibited unsatisfactory yields and efficiencies, the 4-(4,8-dimethoxynaphthylmethyl) benzenesulfonyl group was able to release simple amines in high yields (77-90%) with quantum yields as high as 0.65.

Nishida et al. later extended the tosyl amide release reaction to tosyl ester photohydrolysis for alcohol release.<sup>101</sup> The use of (4,8-dimethoxynaphthyl)propionic acid or 1,5-dimethoxynaphthalene as an electron donors and sodium borohydride or hydrazine as coreductant released the respective tosylate-protected sugars and nucleosides in moderate to high yield (65-97%). Reaction rates were optimal in acetonitrile (versus aqueous ethanol). The best yields were observed with hydrazine acting as the coreductant.

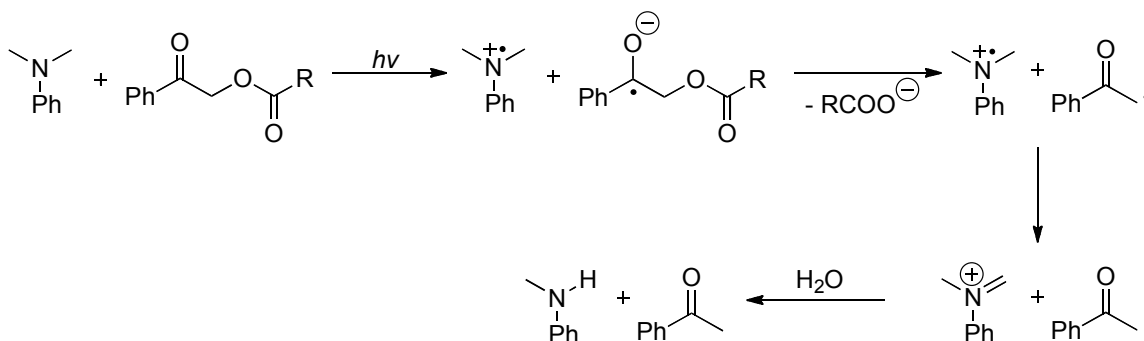
The tosyl amine/ester groups have been applied in a limited number of synthetic strategies and biochemical studies. Binkley et al. have used the tosylate group in conjunction with a benzyl and benzoyl group to protect hydroxyl groups on carbohydrates for  $\beta$ -disaccharides synthesis.<sup>102</sup> Regioselective deprotection of each group was demonstrated in good yield. Among other synthetic applications, Bruncko et al. have used a photocleavable tosyl group to protect the indole nitrogen of L-tryptophan in the synthesis of enantiomerically pure erythro- $\beta$ -alkylated derivatives<sup>103</sup> and Urjasz et al. have used the tosyl group to protect the amine function of thymidine derivatives in the synthesis of new 5' amino analogs of AZT (3'-azido-3'-deoxythymidine).<sup>104</sup> Attempts to release caged amino acids generally resulted in poor overall deprotection yields. Corrie



et al. have attempted to cage glycine but also observed only low yields.<sup>105</sup> Rapid decarboxylation of the amino acids is induced by electron transfer from radicals generated by earlier processes. Corrie found that substituting a carboxylate *ortho* to the sulfonamide diminishes the amino acid decarboxylation leading to an improved 30% yield. The additional substituent acts as a “sacrificial” carboxylate such that decarboxylation of the added carboxylate moiety is competitive with that of the amino group. Unfortunately, additional experiments showed that the effect is not additive, thus additional carboxylate substituents did not improve yields.

#### **2.3.1.2 Phenacyl ester derivatives**

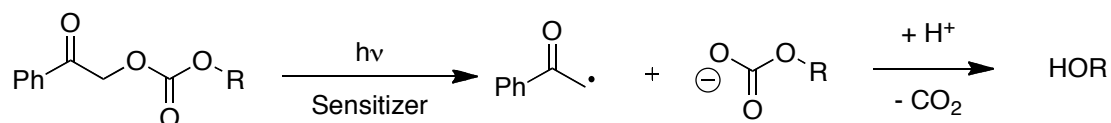
While the phenacyl ester group has been studied extensively as a direct photolysis PRPG (see Chapter 1) it also has been utilized in PET-based deprotection strategies. The majority of this work has been undertaken by Falvey et al. who initially reported deprotection of carboxylic acids from phenacyl ester cages in high yields by reductive sensitization from aromatic amines.<sup>106</sup> Excitation of the sensitizer, *N,N*-dimethylaniline (DMA), to its excited singlet state induces electron transfer to the phenacyl carbonyl, generating a radical ion pair. (Scheme 2-5) The protected carboxylate is subsequently released through heterolytic cleavage. H-atom transfer from the phenacyl radical to the amine donor radical cation results in the production of acetophenone and an iminium ion. Subsequent hydrolysis of the iminium results in *N*-methylaniline. The assigned mechanism is supported by fluorescence quenching studies and product analyses. In addition to simple carboxylic acids, the amino acids phenylalanine, glycine, and isoleucine were successfully released from phenacyl protection, demonstrating a marked advantage over the aforementioned tosyl amide systems.



**Scheme 2-5: Sensitized deprotection of phenacyl esters**

As discussed earlier, the sensitized phenacyl ester systems can take advantage of the modular design of the PET-PRPG systems by choosing a sensitizer that absorbs at higher irradiation wavelengths, provided that electron transfer to the phenacyl moiety is still favorable ( $-\Delta G_{ET}$ ). Falvey et al. explored this option by preparing an array of sensitizers with different absorption profiles and assessing their effectiveness in deprotection of the model compound phenacyl phenylacetate.<sup>56</sup> All of the sensitizers in these systems had  $E_{ox}$  values less negative than -2.0 V and  $\Delta G_{ET}$  values of at least -10 kcal/mol. Several of the compounds absorbed near the visible (387-407nm) and provided high yields of the free acid (70-90%). Two anionic sensitizers were also examined for incorporation into aqueous media, however a sacrificial reductant was needed in order to obtain good yields.

The phenacyl PET-PRPG strategy was also adapted for release of alcohols, phosphates, and diacids.<sup>107</sup> Modest  $\Phi_{rel}$  values observed for release of the free alcohol (a consequence of the poor leaving group ability of the alkoxide ion) resulted in the protection of the alcohols as carbamates. Upon photolysis, decarboxylation releases the free alcohol. (Scheme 2-6) In this manner, primary, secondary, and tertiary alcohols were released effectively from the phenacyl cage using 9,10-dimethylantracene, 9-



**Scheme 2-6: Photolytic release of alcohols from phenacyl carbonates**

methylcarbazole, and *N,N,N',N'*-tetramethylbenzidine as sensitizers. Successive deprotection of doubly-protected malonic acid was also investigated.<sup>107</sup> Sensitized photolysis showed production of the monophenacylmalonate in greater yields than malonic acid. However, since there is no discrimination between the two phenacyl protecting groups, the solution contained a statistical mixture of the mono-deprotected and fully deprotected malonic acid at any given point during photolysis.

In addition to intermolecular sensitization and deprotection, Falvey et al. studied linked donor-acceptor systems where intramolecular charge transfer results in the expulsion of the protected compound.<sup>108</sup> Protected acetic acid was linked to DMA or anthracene moieties (Figure 2-2). Laser flash photolysis (LFP) studies of the DMA-linked system revealed an intramolecular charge transfer state with a lifetime of 500 ns. This long-lived state partitions between bond scission and charge recombination pathways but, unfortunately, bond scission was generally slower than with the intermolecular analogues. While covalent linkage of the donors is expected to enhance forward electron transfer, back electron transfer is also enhanced in the process.

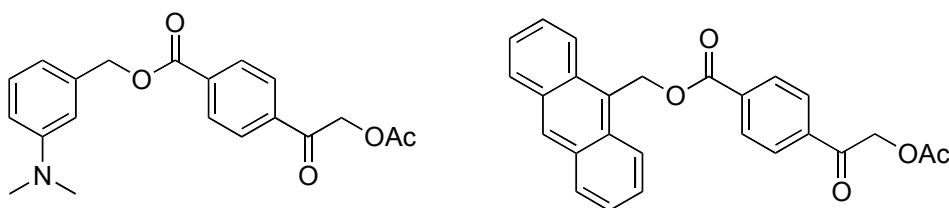


**Figure 2-2: DMA (left) & anthracene (right) linked donor-acceptor phenacyl release systems**

However, the DMA-based system still released acetic acid in high yields (70-85%). The anthracene-linked system released little or no acetic acid due to the rapid formation of a localized triplet state that is lower in energy than the charge transfer state. Thus, energy-wasting nonradiative relaxation from this state predominates instead of bond fragmentation.

### 2.3.2 Mediated electron transfer (MET)

The primary difference between MET and DET is the inclusion of a sacrificial electron donor or acceptor along with the PET-PRPG and the sensitizer. (Scheme 2-3) Since MET is a sensitized mechanism, sensitizers can be chosen with a variety of absorption characteristics as long as the electrochemical requirements are met. Using the Weller equation (Eq 2-1), the components are designed such that upon excitation, the sensitizer can donate or accept an electron from the sacrificial compound and then carry out the oxidation or reduction reaction with the PET-PRPG. Assuming a reductive mechanism, the first electron transfer reaction (ET1) can be described by equation 2-2, where  $E_{\text{red}}^M$  is the reduction potential of the mediator and  $E_{00}^M$  is the excited state energy of the mediator. The second electron transfer reaction (ET2) reduces the Weller equation to equation 2-3 since the reaction occurs in the ground state.

$$\Delta G_{ET1}(\text{kcal/mol}) = 23.06(E_{ox}^D - E_{red}^M - S) - E_{00}^M \quad (2-2)$$

$$\Delta G_{ET2}(\text{kcal/mol}) = 23.06(E_{ox}^D - E_{red}^A) \quad (2-3)$$

Thus, the sensitizer acts as a net electron shuttle or “mediator” between the sacrificial compound and the PET-PRPG.

The main advantage of this approach stems from the expectation that the sensitizer will be regenerated by the end of the electron cascade. Certain chromophores can represent a costly component of PET-PRPG strategies. In DET photolysis, the chromophore is oxidized or reduced by the end of a deprotection event and is thus resistant to further oxidation or reduction. This requires that at least a full equivalent of the sensitizer be included with a PET-PRPG in order for quantitative deprotection. Using a MET strategy, it should be possible to use a sub-stoichiometric amount of sensitizer provided that the sacrificial donor or acceptor is present in large enough concentrations. Thus, the sacrificial compound acts as an inexpensive electron source or sink for the mediator. The concentration of mediator is still important, however, as all electrons must pass through it to get to the PET-PRPG, thus an electron “bottleneck” would result if too little sensitizer were provided. The other added advantage in MET systems is that the second electron transfer reaction that initiates the bond fragmentation occurs in the ground state. Back electron transfer is thus significantly less competitive and the forward electron transfer reaction can be considered irreversible as long as  $\Delta G_{ET2} < 0$ . Higher bond scission efficiencies should thus be able to be realized. The main disadvantage of MET systems is the introduction of a third component into an already complex system. Two bimolecular processes must occur for successful deprotection and numerous energy and electron transfer processes compete with the desired productive pathway.

MET represents a subset of a larger array of electron transfer reactions. Indeed, successive electron cascade reactions to donors and acceptors pervade a variety of biological and materials processes from photosynthesis and solar energy conversion to organic electronic applications such as light-emitting diodes(LEDs). The use of MET for

photorelease of PET-PRPGs was explored using UV-absorbing mediators and has been improved upon as will be discussed later in this work. In both the preliminary studies and the projects to be detailed in upcoming chapters, the NAP group was utilized as the PET-PRPG since it offers several advantages over former PET-PRPG systems.

#### 2.4 The *N*-alkylpicolinium group as a PET-PRPG

The *N*-alkylpicolinium (NAP) group has been developed as a PET-PRPG to extend and improve upon previous PET deprotection strategies.<sup>109-112</sup> (Figure 2-3) The NAP group has demonstrated its utility as a carboxylate protecting group that releases the protected substrate by sensitized deprotection through DET and MET mechanisms using a variety of UV and visible light absorbing sensitizers.

A significant disadvantage of previously described phenacyl PET-based deprotection schemes is the need for a strongly reducing sensitizer to meet the low reduction potential of the phenacyl esters ( $< -2.2$  V). This severely limits the variety of sensitizers that can be used and constrains the absorption spectrum to mostly high energy UV light. Additionally, poor aqueous compatibility limits its application in biologically-related studies.

The NAP group evolved out of preliminary reports that utilized the 4-picolyl group as a conventional protecting group in peptide synthesis<sup>113,114</sup> and the caging of

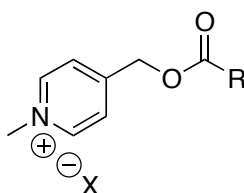
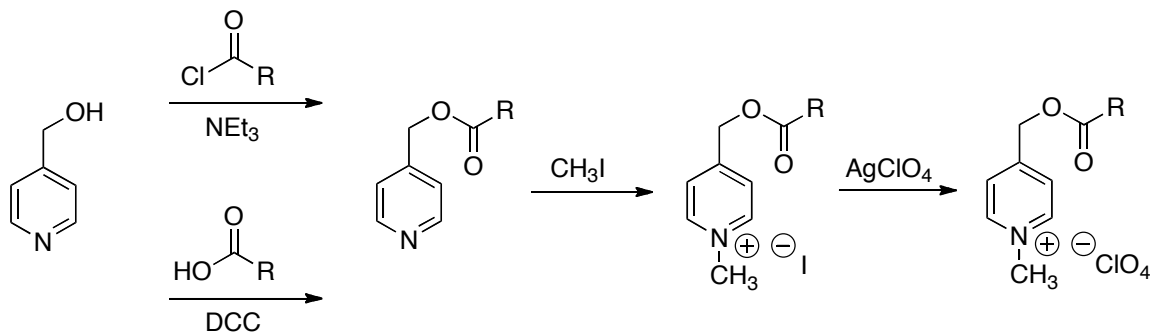


**Figure 2-3: Model NAP-protected carboxylate**

amino acids.<sup>115</sup> Deprotection could be initiated by catalytic hydrogenation, electrolytic reduction, and reducing metals, thereby making it a promising candidate for use with PET. Unfortunately, the 4-picolyl group is expected to have very negative reduction potentials, similar to those of pyridine around -2.6 V vs. SCE.<sup>116</sup> Preliminary experiments for sensitized release of several simple picolyl-protected carboxylates demonstrated little or no yield of free acid upon UV photolysis even with easily oxidized sensitizers such as *N,N,N',N'*-tetramethylbenzidine (TMBD,  $E_{ox} = 0.32$  V vs. SCE).<sup>88</sup> As expected, *N*-alkylation of the picolyl group elevates the reduction potentials to more positive values and yields of free acid increased considerably using TMBD as well as other more modestly reducing sensitizers such as triphenylamine. In fact, cyclic voltammetry of NAP-protected esters exhibited an irreversible reduction wave on average around -1.1 V vs. SCE demonstrating a substantial shift from the parent picolyl compounds.

An added advantage of NAP-protected carboxylates is their ease of preparation. (Scheme 2-7) Simple coupling of 4-pyridylcarbinol with the respective acid chloride analog of the carboxylate generally yields the ester in high yield. Coupling using the carboxylic acid with dicyclohexylcarbodiimide (DCC) also affords the ester in high yield.

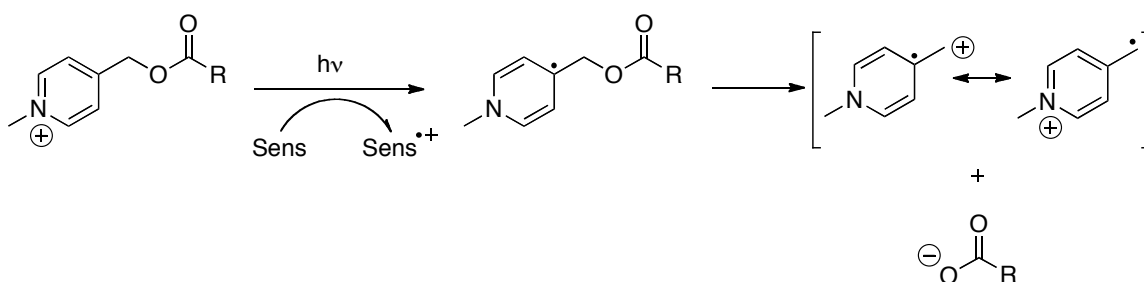


**Scheme 2-7: Synthesis of NAP-protected carboxylates**

Alkylation is carried out using an alkyl halide such as iodomethane. Due to the formation of a charge-transfer absorption shoulder in the near-UV, picolinium iodide esters were normally exchanged with a perchlorate counterion using silver perchlorate. This exchange eliminates the charge-transfer band such that the NAP-protected compounds do not absorb significantly above 290 nm. Using this method, several NAP-protected aromatic carboxylates were prepared in high overall yield.

Deprotection photolysis was initially carried out using UV absorbing sensitizers and typically required multiple hours for full consumption of the NAP-protected compound. Moderate to high yields (45-92%) were obtained after 3 h of irradiation, depending on the identity of the sensitizer. Direct irradiation of the charge-transfer band of the picolinium iodide salts also released the protected carboxylate in moderate yields. Quantum yields of release using 9-methylcarbazole (9-MC) as sensitizer were as high as 0.23 in methanol.

Fluorescence quenching and laser flash photolysis (LFP) studies helped to support the proposed photorelease mechanism. (Scheme 2-8) The excited-state sensitizer transfers an electron to the picolinium group generating the respective neutral radical. Subsequent heterolytic cleavage releases the carboxylate and picolinium radical. Quenching constants determined by fluorescence spectroscopy were diffusion limited for



**Scheme 2-8: Proposed release of carboxylate anions from NAP-esters**



each of the sensitizers used, indicating efficient electron transfer from the sensitizer to the NAP-ester. LFP data exhibited the expected radical cation signals for 9-MC in the presence of NAP-esters. Although a signal at 410 nm was observed for the picolyl radical, a signal for the picolinium radical following release was not observed. Preliminary photolysis experiments were unable to detect the byproduct either. In attempts to isolate this compound, 1,4-cyclohexadiene (CHD) was added to the photolysis mixture as a radical trap. The picolyl product was thus able to be identified and isolated in preparative photolysis experiments. Additionally, the presence of CHD in the photolysis mixture dramatically increased yields of the free acid as well as the quantum yields of release. For example, using 9-MC as a sensitizer, yields of phenylacetic acid increased from 37 % to 86 % over the same irradiation period (2 h) after addition of CHD. Quantum yields of release ( $\Phi_{rel}$ ) increased from 0.23 to 0.39. This increase in yield and efficiency was largely attributed to the trapping of the radical cation formed from the sensitizer thus suppressing back electron transfer as well as any unproductive radical side reactions.

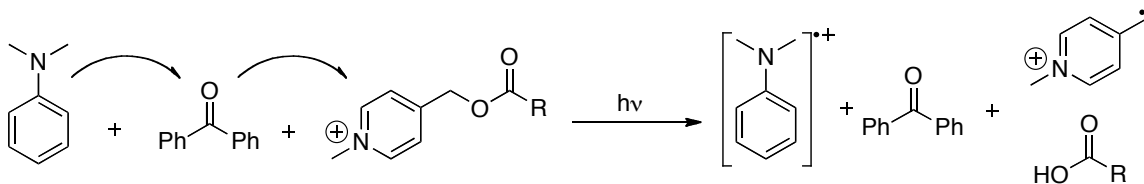
Later experiments utilized lower energy visible light absorbing sensitizers to initiate deprotection of NAP-protected carboxylates, amino acids, and phosphates.<sup>111</sup> The sensitizers absorbed 400-550 nm light and are derived from the pyrromethene and coumarin family of compounds, primarily developed for use in dye lasers. Protection of *N*-CBZ protected amino acids and phosphates with the NAP group was accomplished using picolyl chloride as the precursor. Deprotection photolysis using broad-band visible irradiation resulted in extremely fast release of the protected substrate in generally high yield. For example, in the presence of pyrromethene 546 and CHD, irradiation over 5

min released phenylacetic acid in 92% yield. Yields of the amino acids and phosphates were slightly lower and generally required longer irradiation periods for quantitative deprotection. Quantum yields of release were generally low ( $\Phi_{rel} < 0.05$ ), however, the photolytic efficacies ( $\Phi_{rel}\epsilon_{\lambda}$ ) were as high as 4460 using pyromethene 546 due to the large extinction coefficient of the dyes. Fluorescence quenching and LFP experiments supported the previously proposed mechanism for photorelease.

MET photorelease was preliminarily explored using NAP-esters in an effort to improve efficiencies of release through inhibition of the back electron transfer reaction by using triplet sensitizers.<sup>112</sup> These systems were designed to transfer electrons from a donor to the NAP-esters through the sensitizer (mediator), as previously described.

Benzophenone, a well studied triplet sensitizer, xanthone and diphenylanthracene were explored using *N,N*-dimethylaniline (DMA) as the electron donor. (Scheme 2-9)

Deprotection photolysis experiments resulted in high yields of the free carboxylate using benzophenone (78-100%) and diphenylanthracene (81-100%). For each sensitizer, LFP experiments clearly showed the generation of the anion radical of the sensitizer and the efficient quenching of that signal upon addition of ester. Quenching constants for the interception of the sensitizer radical ion by the ester were found to be near the diffusion limit for benzophenone and slightly lower for xanthone. The quantum yields of release were found to be markedly larger than DET systems, especially for benzophenone ( $\Phi_{rel}$



**Scheme 2-9: MET photolysis of DMA, benzophenone and a NAP-ester**

= 0.51) and xanthone ( $\Phi_{rel} = 0.39$ ). The impressive quantum yields obtained for the benzophenone system are attributed to the unity quantum yield for triplet formation after excitation thus making back electron transfer a spin forbidden process. While these systems offer promising results, they nevertheless require the use of UV-absorbing mediators.

Further attempts to improve the efficiency of release investigated covalently tethering the sensitizer directly to the NAP-ester.<sup>110</sup> This modification was expected to increase efficiencies due to the close proximity of the NAP group to the sensitizer. Unfortunately, the competing back electron transfer reaction is also enhanced. Linked NAP-esters that were designed to proceed through DET were prepared with 9-MC tethered to an *N*-alkyl chain. (Figure 2-4a) Despite observed quenching of the carbazole fluorescence, little to no yield of free acid was observed upon photolysis due to

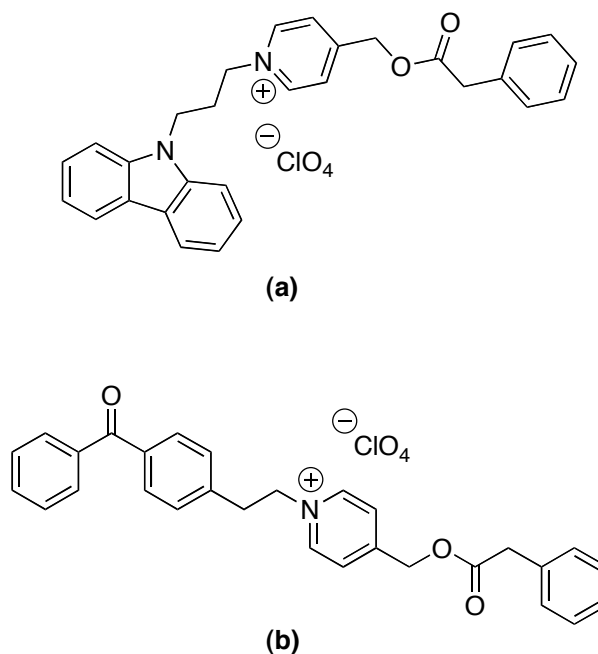


**Figure 2-4: (a) Carbazole-NAP linked system (b) benzophenone-NAP linked system**

rapid back electron transfer. MET release in the linked systems was explored by tethering the previously successful benzophenone mediator to NAP-esters. (Figure 2-4b) Photolysis of solutions containing DMA as the donor resulted in moderate to high yields of the free carboxylate within 2 h irradiation periods. Quantum yields of release were increased to 0.72 representing an improvement over the unlinked mediated system.

## 2.5 Conclusions

PET-PRPGs are an effective alternative to traditional direct photolysis PRPGs for release of functional molecules. Direct electron transfer (DET) from an excited-state sensitizer to tosyl, phenacyl, and *N*-alkylpicolinium (NAP) groups can release the respective substrates in high yields. PET-PRPGs allow the use of sensitizers that absorb lower energy visible light, offering a considerable advantage over the direct deprotection PRPGs, particularly for biological applications. Mediated electron transfer (MET) to NAP groups has improved upon the direct electron transfer pathway by increasing quantum yields of release considerably through the use of triplet mediators. Efficiencies and photolytic efficacies of several NAP-release systems are summarized in Table 2-1 for comparison.

**Table 2-1: Comparison of quantum yields of release ( $\Phi_{rel}$ ) and photolytic efficacies ( $\Phi_{rel}\epsilon_{\lambda}$ ) for NAP-release by DET and MET<sup>110,112,117</sup>**

DET/MET	Sensitizer	$\lambda_{ex}$ (nm)	$\Phi_{rel}$	$\epsilon_{\lambda}$	$\Phi_{rel}\epsilon_{\lambda}$
DET	9-MC	350 <sup>a</sup>	0.23 <sup>a</sup>	1300 <sup>b</sup>	299
DET	TMBD	345 <sup>a</sup>	0.05 <sup>a</sup>	4460 <sup>b</sup>	223
DET	Pyrromethene 546	493 <sup>c</sup>	0.06 <sup>c</sup>	81000 <sup>c</sup>	4500
DET	Pyrromethene 597	525 <sup>c</sup>	0.03 <sup>c</sup>	68000 <sup>c</sup>	1700
MET	Benzophenone	355 <sup>a</sup>	0.51 <sup>a</sup>	190 <sup>b</sup>	97
MET	Xanthone	355 <sup>a</sup>	0.39 <sup>a</sup>	1000 <sup>b</sup>	390

<sup>a</sup>In MeOH

<sup>b</sup>In EtOH

<sup>c</sup>In MeCN

<sup>d</sup>In H<sub>2</sub>O

<sup>e</sup>In MeCN/MeOH (1/1)

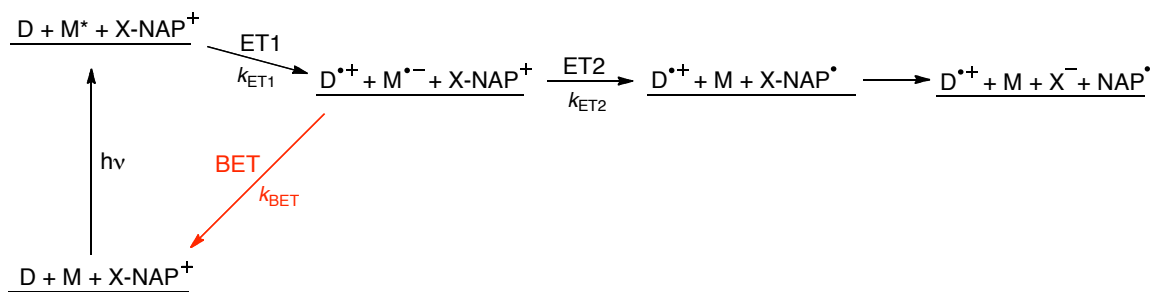
Much of the potential that MET can offer has not yet been realized. MET photorelease should be adaptable to visible light absorbing mediators that meet the required electrochemical characteristics. Furthermore, if mediators are indeed acting as net electron shuttles, it should be possible to use significantly sub-stoichiometric amounts in the presence of excess amounts of inexpensive electron donors to conserve the amount of costly sensitizer used. The development of robust, visible light absorbing MET systems that conserve sensitizer amounts will be the focus of the following work. Due to the demonstrated high yields and efficiencies of photorelease of the NAP system, new developments will build upon this successful platform. Subsequently, the utility of the produced systems will be demonstrated for application beyond chemical synthesis.

### 3 Ketocoumarin Dyes for Visible Light MET Photolysis

#### 3.1 Introduction

After preliminary studies demonstrated fast, efficient release of carboxylate anions from *N*-alkylpicolinium (NAP) esters via photoinduced DET and MET,<sup>109-112</sup> we chose to build upon this successful design. MET offers the possibility of very high quantum efficiencies, yet previous studies have utilized mediators that absorb primarily UV light.<sup>112</sup> MET also offers the possibility of using sub-stoichiometric amounts of sensitizer in the presence of excess electron donor. Therefore, the primary motivations of this work are to extend previously successful MET deprotection reactions to include visible light absorbing mediators and to demonstrate effective release using sub-stoichiometric amounts of those mediators. The use of visible light will allow for convenient photolysis and will allow the developed system to be applicable to sensitive environments, like biological systems. The use of sub-stoichiometric amounts of mediator will allow the use of very low amounts of potentially costly chromophores.

In addition to the aforementioned goals, we were interested in incorporating features to limit the competitiveness of back electron transfer (BET) reactions. BET is expected to limit the effectiveness of forward electron transfer processes. Previous experiments utilizing the mediator benzophenone displayed very high  $\Phi_{rel}$ , attributed to rapid intersystem crossing to the triplet state upon excitation.<sup>112</sup> Electron transfer from the donor to the mediator generates a triplet geminate radical pair from which forward electron transfer should be more competitive than the spin forbidden geminate recombination. (Scheme 3-1) Additional enhancement of the forward electron



**Scheme 3-1: Mediated electron transfer deprotection**

transfer process may be possible through careful consideration of the energetics and rates of the first electron transfer reaction (ET1) and corresponding back electron transfer reaction. Specifically, if the back electron transfer reaction can be designed to be significantly more exergonic than ET1, i.e.  $\Delta G_{BET} \ll \Delta G_{ET1}$ , then the rate of back electron transfer,  $k_{BET}$ , would be expected to be in the Marcus “inverted region” (Figure 2-1, Section 2.2) and thus lower relative to that of ET1 (i.e.  $k_{ET1} > k_{BET}$ ). With these objectives in mind, we established several criteria for choosing donors and mediators.

### 3.2 System design

Mediators were selected based upon the following design criteria: (1) significant light absorption above 400 nm, (2) high intersystem crossing quantum yield ( $\Phi_{ISC}$ ), (3)  $-\Delta G_{ET1}$  and  $-\Delta G_{ET2}$ , and (4)  $\Delta G_{BET} \ll \Delta G_{ET1}$ . Criteria (1) and (2) ensure visible light absorption and competitive formation of the mediator triplet excited state. These are intrinsic properties of the chromophore in question. Criterion (3) ensures the productive electron transfer reactions are exergonic and (4) targets the BET reaction for the Marcus inverted region. The successful realization of these criteria can be estimated using the modified versions of the Weller equation specific to MET deprotection. (Equations 2-2 and 2-3, Section 2.3.2)

With these criteria in mind, a survey of readily available or easily synthesized compounds was undertaken to find suitable mediators. Our investigation led to derivatives of the coumarin family of chromophores. Many coumarin dyes are well known for their highly fluorescent nature that, consequently, severely limits their intersystem crossing to the triplet manifold.<sup>118</sup> However, a class of coumarin dyes, termed “ketocoumarins,” were designed and prepared by Farid et al. specifically for use as triplet sensitizers and photoinitiators.<sup>119,120</sup> 3-Aroylcoumarins (Figure 3-1 (a)) can easily be prepared by condensation of salicylaldehyde derivatives with  $\beta$ -ketoesters whereas the carbonylbiscoumarins (Figure 3-1 (b)) are prepared from the ketodiester. Several derivatives of these compounds demonstrated strong absorption in the visible region of the spectrum in addition to high  $\Phi_{ISC}$ . We decided to explore two particular ketocoumarin chromophores, 7-diethylamino-3-thenoylcoumarin (DEATC) and 3,3'-carbonylbis(7-diethylaminocoumarin) (CBDAC), (Figure 3-2) since the reported values for  $\lambda_{max}$  and  $\Phi_{ISC}$  already met both conditions (1) and (2). (Table 3-1) DEATC was commercially available and CBDAC was prepared according to the aforementioned procedure.<sup>119</sup> After investigation of the redox properties of both ketocoumarins by cyclic voltammetry,  $\Delta G_{ET}$  calculations revealed that both would be sufficient to reduce NAP-esters and would be successful in MET deprotection reactions using *N,N*-

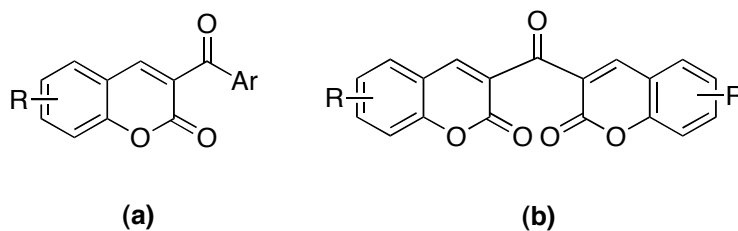


**Figure 3-1: Ketocoumarin dyes: (a) 3-aroylcoumarins (b) carbonylbiscoumarins**



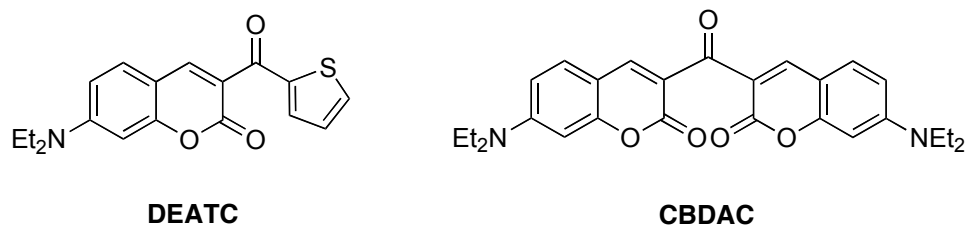


**Figure 3-2: Ketocoumarin dyes studied for triplet MET deprotection**

dimethylaniline (DMA) as the electron donor. Photophysical, electrochemical, and electron transfer calculations are presented in Table 3-1 for these two dyes. Both mediators meet criterion (3) by having exergonic forward electron transfer reactions and the BET reaction for both mediators is also considerably exergonic. Although a formal analysis to ascertain the position of the reaction on the Marcus curve was not performed, it is plausible to consider these reactions to be located in the Marcus inverted region based upon previous studies in which  $k_{ET}$  maximizes around -30 kcal/mol for similar multiple-ring systems in acetonitrile.<sup>87,98</sup> All desired criteria are thus met using either DEATC or CBDAC as mediators and DMA as the electron donor. Subsequently, deprotection photolysis experiments were undertaken to ascertain the effectiveness of the new mediators in photorelease reactions.

**Table 3-1: Photophysical and electrochemical data and electron transfer calculations for DEATC and CBDAC ketocoumarin dyes**

Compound	$E_{red}^a$ (V vs SCE)	$\lambda_{max}^a$ (nm)	$E_T^b$ (kcal/mol)	$\Phi_{ISC}^b$	$\Delta G_{ET1}^c$ (kcal/mol)	$\Delta G_{BET}^d$ (kcal/mol)	$\Delta G_{ET2}^d$ (kcal/mol)
DEATC	-1.32	422	52.00	0.83	-3.34	-50.04	-5.07
CBDAC	-1.21	457	50.80	0.92	-4.59	-47.60	-2.54

<sup>a</sup> In acetonitrile    <sup>b</sup> Reference <sup>119</sup>    <sup>c</sup> Calculated from Eq 2-2, Section 2.3.2

<sup>d</sup> Calculated from Eq 2-3, Section 2.3.2 using DMA as the electron donor

### 3.3 Deprotection photolysis

Several previously prepared NAP-esters were chosen for experimentation with the new mediators as representative examples to facilitate comparison with previous MET studies. (Figure 3-3) In addition to DMA, *N,N*-diethylaniline (DEA), and triphenylamine (TPA) were used as electron donors. DEA and TPA have oxidation potentials of 0.76 V and 0.98 V, respectively vs. SCE.<sup>88</sup> Samples were prepared by incorporating the mediator with a more than 100-fold excess of donor and a slightly less than 100-fold excess of NAP-ester in MeCN. 1,4-cyclohexadiene (CHD) was added in large excess as a radical trap and hydrogen-atom donor. Samples were degassed with N<sub>2</sub> and a dark control was maintained by removing an aliquot prior to photolysis and keeping it in the dark during the duration of the photolysis. Samples were photolysed for various periods of time by broad-band irradiation from the output of a 300 W tungsten-filament lamp. Photolysed and dark control samples were analyzed by <sup>1</sup>H NMR to determine free acid and starting material yields.

The use of DEATC demonstrated high yields of free acid over short irradiation periods. (Table 3-2) Quantitative yields of released product could be obtained over 10

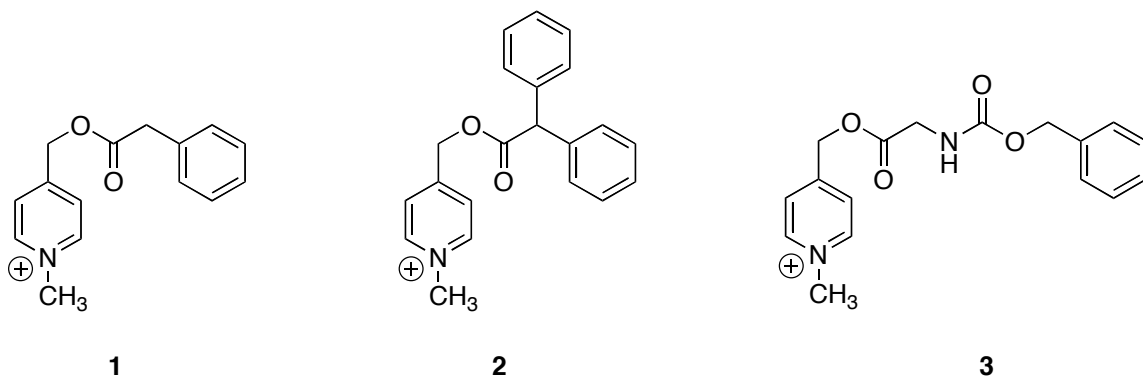


**Figure 3-3: NAP-esters used in deprotection photolysis experiments**

**Table 3-2: Deprotection photolysis data for release of carboxylates from NAP-esters with DEATC in MeCN**

Entry <sup>a</sup>	Donor	NAP-ester	Irradiation Time	% Yield <sup>b</sup>
1	DMA	<b>1</b>	30 min	99
2	DMA	<b>2</b>	40 min	81
3	TPA	<b>1</b>	10 min	100
4	TPA	<b>3</b>	60 min	100
5	DEA	<b>1</b>	30 min	100

<sup>a</sup>Each Sample: 3.33 mM NAP-ester, 0.057 mM DEATC, 9 mM Donor, excess CHD

<sup>b</sup>Yields determined by comparison of integration values in <sup>1</sup>H NMR of protons alpha to carbonyl in protected and released compounds in dark and irradiated samples, estimated error 5%

min of irradiation starting from NAP-ester **1** and TPA as the donor. Using DMA and DEA as donors exhibited similar results. There is, however, some variation in product yield based upon the structure of the NAP-ester. Release from NAP-ester **2** was generally lower than **1** or **3**. Although electron transfer occurs to the same picolinium moiety for each NAP-ester, there are clearly differences in release efficiencies. Despite the favorable yields and rates, there was noticeable photobleaching of the mediator over the course of the photolysis. A reduction and blue-shifting of the primary visible absorption band over time could be observed. While control photolysis solutions containing only DEATC showed a photobleaching effect with no shift in  $\lambda_{max}$ , solutions containing either DMA or NAP-ester in the presence of DEATC exhibited the photobleaching and  $\lambda_{max}$  shift. Thus, competing photoreactions are likely occurring and it is unclear what effect these side reactions have on eventual release from the NAP-esters.

Identical deprotection photolysis experiments were performed substituting CBDAC for DEATC. Moderate to good yields of the free acid were generally observed, although longer irradiation periods were usually necessary to achieve comparable yields to the DEATC system. (Table 3-3) Comparing each entry between Table 3-2 and Table 3-3 clearly demonstrates the higher overall deprotection rate of DEATC over CBDAC.

**Table 3-3: Deprotection photolysis data for release of carboxylates from NAP-esters with CBDAC in MeCN**

Entry <sup>a</sup>	Donor	NAP-ester	Irradiation Time	% Yield <sup>b</sup>
1	DMA	<b>1</b>	30 min	24
2	DMA	<b>2</b>	60 min	66
3	TPA	<b>1</b>	30 min	26
4	TPA	<b>3</b>	60 min	46
5	DEA	<b>1</b>	30 min	21

<sup>a</sup>Each Sample: 3.33 mM NAP-ester, 0.057 mM CBDAC, 9 mM Donor, excess CHD

<sup>b</sup>Yields determined by comparison of integration values in <sup>1</sup>H NMR of protons alpha to carbonyl in protected and released compounds in dark and irradiated samples, estimated error 5%

This is surprising given that CBDAC has a higher reported  $\Phi_{ISC}$  and better spectral overlap with the output of the irradiation source compared to DEATC. The photobleaching effect observed with DEATC was generally not seen with CBDAC. Extensive investigation into the processes competing with photorelease for both dyes was not within the scope of this work.

### 3.4 Mechanistic studies

Having demonstrated release of carboxylates from NAP-esters using DEATC and CBDAC by MET deprotection, we sought to confirm the mechanism of deprotection and determine efficiencies of photorelease. Laser flash photolysis (LFP) studies were pursued to confirm the formation and decay of the radical species expected in the MET mechanism. Solutions containing DEATC and DMA in MeCN were pulsed with 355 nm laser light and exhibited two signals at ca. 470 nm and ca. 510 nm. (Figure 3-4) The signal at ca. 470 nm is assigned to the previously characterized DMA radical cation.<sup>121</sup> The signal at ca. 510 nm is assigned to the radical anion of DEATC as it is produced concurrently with the DMA radical cation. Since O<sub>2</sub> is known to quench triplet states,

samples were purged with O<sub>2</sub> to assess whether the production of these signals occurs through a singlet or triplet state. Both signals were extinguished when samples were purged with O<sub>2</sub>, suggesting that electron transfer originates from the triplet

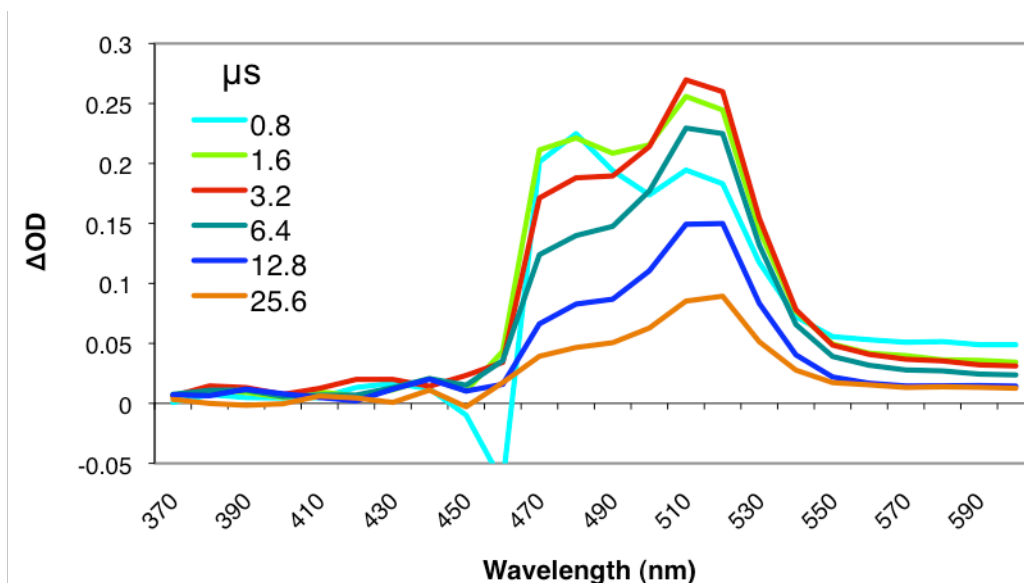


**Figure 3-4: 355 nm pulsed laser photolysis of DEATC and DMA (MeCN)**

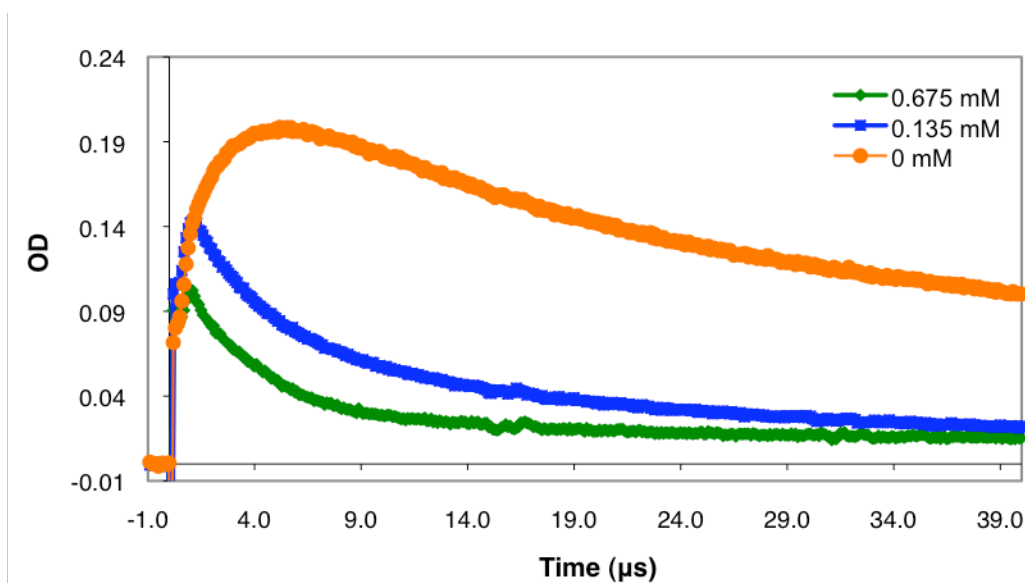


**Figure 3-5: Time-dependent traces after pulsed 355 nm laser excitation of DEATC + DMA + varying concentrations of NAP-ester 3, monitored at 510 nm**

manifold as expected. Upon addition of increasing amounts of the NAP-ester **3**, the signal at 510 nm is quenched significantly. (Figure 3-5) Thus, the expected electron transfer process from DMA through DEATC to NAP-ester **3** is supported. The radical anion of NAP-esters, normally observable at ca. 410 nm with this LFP setup,<sup>117</sup> cannot be detected due to significant absorption of the probe beam by the mediator in this region.

LFP studies were also performed with CBDAC as the mediator. Upon flash photolysis of CBDAC alone, a signal at ca. 510 nm was observed. This signal was assigned to the triplet state of the mediator as it was quenched by O<sub>2</sub>. Subsequent photolysis of CBDAC in the presence of DMA exhibited the CBDAC triplet at ca. 510 nm decaying concurrently with the growth of another signal at ca. 530 nm. (Figure 3-6) We assign this signal to the radical anion of CBDAC. The radical cation signal for DMA (ca. 470 nm) was not observable due to the significant absorption of the probe beam by the mediator in that region. Experiments to quench the CBDAC radical anion signal could not be performed as traces obtained at 530 nm exhibited considerably different

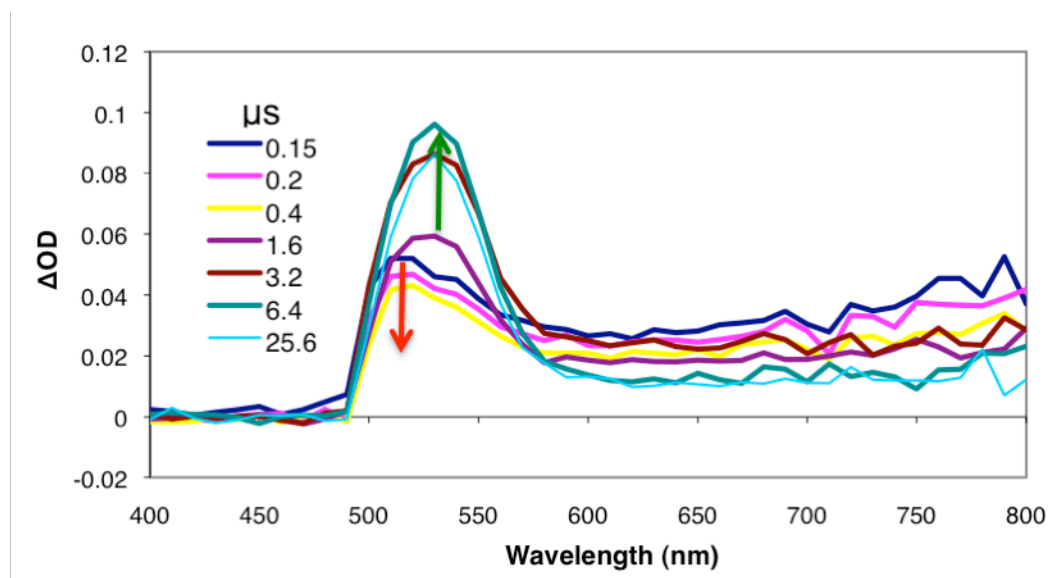


**Figure 3-6: 355 nm pulsed laser photolysis of CBDAC+DMA (MeCN)**

**Table 3-4: Quantum yields and photolytic efficacies determined for release of PAA from NAP-ester *1* with DEATC or CBDAC in MeCN**

Mediator	$\Phi_{rel}^a$	$\epsilon_{\lambda} (M^{-1}cm^{-1})^a$	$\Phi_{rel}\epsilon_{\lambda}$
DEATC	0.050	33500	1675
CBDAC	0.023	91739	2110

decay behavior.

In order to quantify the efficiency and efficacy of the overall release reaction, quantum yields of release ( $\Phi_{rel}$ ) and photolytic efficacies ( $\Phi_{rel}\epsilon_{\lambda}$ ) were determined for both DEATC and CBDAC. Solutions were irradiated with a 1000 W Xe lamp fitted with a monochromator tuned to the absorption maximum of each mediator ( $\pm 10$  nm). Since TPA provided the highest rates of release in the deprotection photolysis experiments, quantum yield determinations were performed using this donor with NAP-ester *1*. (Table 3-4) CBDAC release efficiency was about half that of DEATC which is consistent with the lower yields obtained for CBDAC in the deprotection photolysis experiments. Both of the determined efficiencies are considerably lower than those observed for previous mediated deprotection photolysis experiments. However, these quantum yields are comparable to those obtained for PRPGs in the coumarin family (see Chapter 1) The extremely high extinction coefficients of the mediators compensate for the low efficiencies to a certain degree resulting in high photolytic efficacies ( $\Phi_{rel}\epsilon_{\lambda}$ ). These values are higher than many previously determined for PET-PRPG release. (Table 2-1)

### 3.5 Conclusions

The use of visible light to induce mediated electron transfer deprotection of NAP-esters has been successfully demonstrated. The ketocoumarin dyes employed in this

study were used in sub-stoichiometric amounts yet observed release rates were generally fast, requiring short irradiation periods, and yields of the free carboxylate were generally high. The expected MET process has been supported by laser flash photolysis data for DEATC, but limited data is available for the CBDAC system and the mechanism could not be verified. Significant photobleaching of the DEATC dye over short time periods is a limitation that hinders application in situations requiring prolonged irradiation. Yet, DEATC consistently outperformed CBDAC in release rate and efficiency, despite the higher  $\Phi_{ISC}$  of CBDAC. Thus it is clear that although prevention of geminate recombination through the promotion of a triplet pathway should be advantageous, this is only one of many factors contributing to efficient deprotection. Exploration of the efficiencies of competing processes by fluorescence quenching, LPF, or trapping studies may help elucidate the source of release efficiency loss. Although both dyes exhibited low  $\Phi_{rel}$ , their photolytic efficacies are quite high due to their extremely high extinction coefficients.



## 4 Gold Nanoparticles as Aqueous Visible Light Mediators

### 4.1 Introduction

Visible light has been used to induce both DET and MET processes that result in release of NAP-protected substrates. However, photobleaching of the previously used ketocoumarin dye DEATC led us to consider more robust chromophores for improvement. We also wanted to adapt visible light MET to aqueous environments. Gold nanoparticles (AuNPs) or gold nanoclusters have recently attracted much attention as chromophores due to their unique optoelectronic properties that can vary greatly with changes in their preparation.<sup>122</sup> Additionally, they have proven to be robust under illumination and can be prepared in aqueous media in many cases. AuNPs with core diameters greater than 2 nm exhibit a characteristic broad visible absorption band, an effect of surface plasmon resonance (SPR) of conduction band electrons on the nanoparticle surface.<sup>122-124</sup> Recent electrochemical studies by Murray et al. have also suggested certain AuNP systems to have reduction potentials around -1.5 to -1.7 V that would be sufficient to reduce NAP-esters in a MET deprotection system.<sup>125</sup> AuNPs therefore seemed to be interesting mediator candidates for visible light MET photorelease experiments.

### 4.2 Preparation of gold nanoparticles

AuNPs can be prepared in a variety of sizes, from one to several hundred nanometers in diameter, and functionalized with stabilizing ligands that surround the bulk surface area.<sup>122</sup> The stabilizing ligand is a critical component and serves to segregate

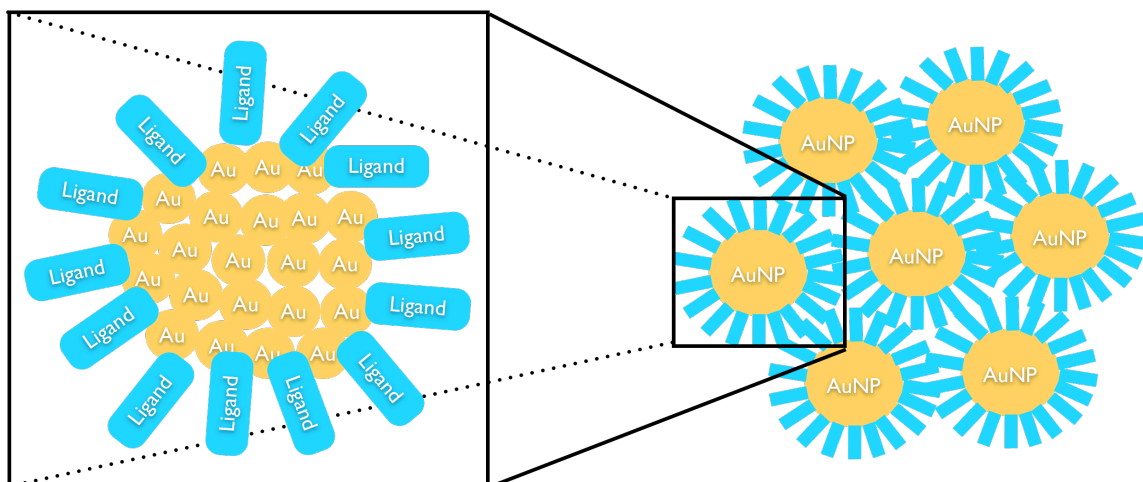


**Figure 4-1: Model representation of ligand-stabilized gold nanoparticles**

the nanoparticles from one another thereby avoiding rapid aggregation and precipitation. (Figure 4-1) The position of the absorption maximum ( $\lambda_{max}$ ) of the plasmon resonance band (PRB) is greatly influenced by size and shape of the nanoparticles as well as the nature of stabilizing ligands.<sup>126,127</sup> Our studies began with citrate-stabilized AuNPs (cit-AuNPs) due to their ease of preparation, narrow size distribution, and aqueous compatibility.

Synthesis of cit-AuNPs is easily accomplished using the citrate reduction method originally pioneered by Turkevich et al.<sup>128,129</sup> and later modified by Frens et al.<sup>130</sup> Sodium citrate is added to an aqueous solution of gold(III) chloride and refluxed for 20 minutes. By altering the concentration ratio of the two components, the average diameter of the approximately spherical AuNPs can be adjusted. cit-AuNPs of 16 nm average diameter were selected to be prepared for our experiments. For convenience of deprotection photolysis analysis, cit-AuNPs were prepared in D<sub>2</sub>O. After several minutes under reflux, the initial pale yellow solution changes to a deep red color, characteristic

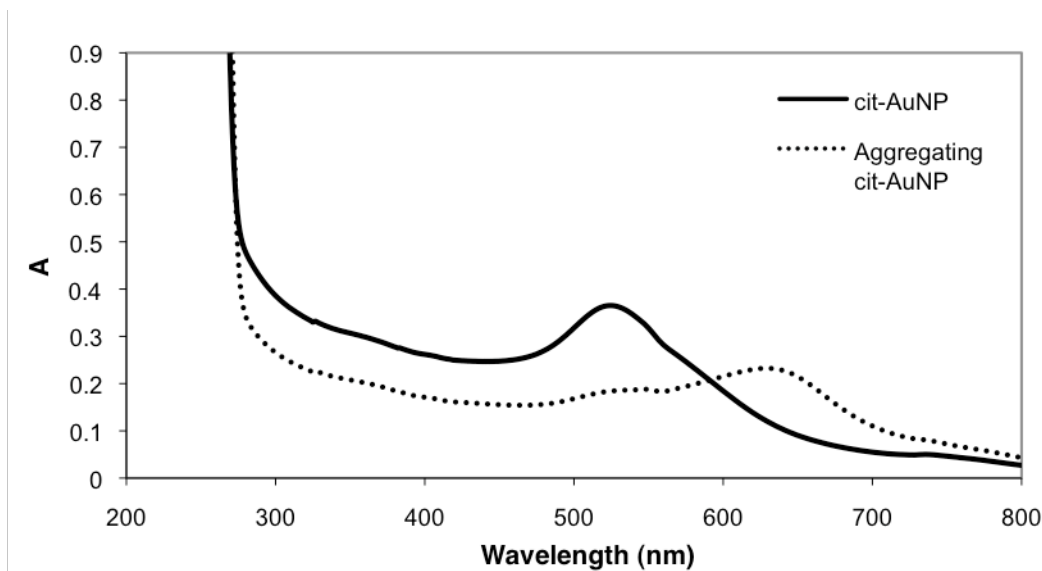


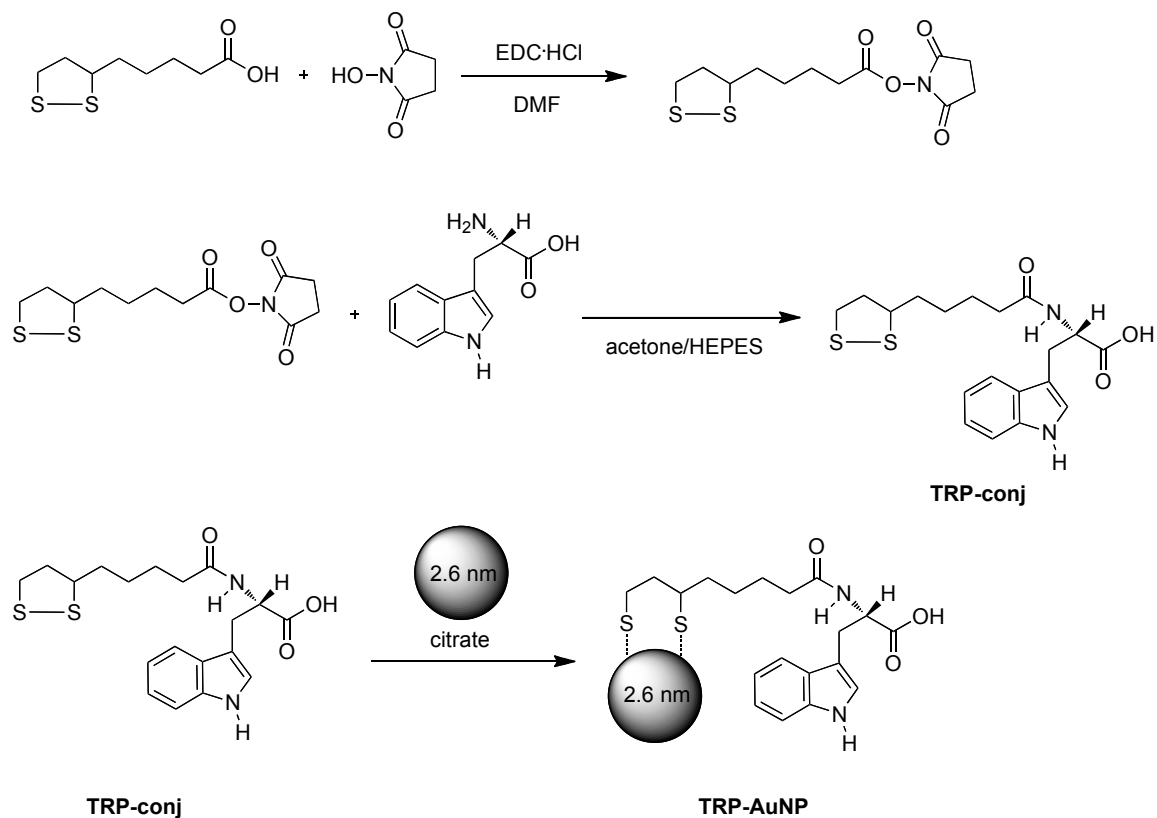
**Figure 4-2: Absorption spectrum of aqueous 16 nm cit-AuNPs and aggregating cit-AuNP**

of the PRB. Since the diameter of the AuNPs can be correlated with the position of the  $\lambda_{max}$ , comparison with literature values confirmed the formation of 16 nm cit-AuNPs. (Figure 4-2) Due to the weak interaction that citrate ligands have with gold surfaces, aggregation of the AuNPs can be triggered by a trace amount of many solution additives including acids, bases, and salts, among others. Aggregation results in a gradual reduction and blue-shifting of the PRB (Figure 4-2) and eventual precipitation of larger aggregates. This phenomenon severely limits any photochemical processes.

A separate AuNP system has been prepared by exchanging citrate ligands for a ligand that binds through sulfur coordination to the gold surface. An alternative method for preparing the starting cit-AuNPs reduces gold(III) chloride with sodium borohydride in the presence of sodium citrate.<sup>131</sup> This method allows AuNPs with smaller average diameters to be produced as the original citrate reduction method is generally limited to diameters larger than 10 nm. Preparation of AuNPs by the reduction of gold(III) chloride

using other reductants such as sodium ascorbate and white phosphorous has been reported.<sup>132</sup> A smaller distribution of AuNP sizes can generally be attained with this method. Thus, 2.6 nm cit-AuNPs were generated and subsequently combined with a tryptophan-dithiane conjugate (TRP-conj) as originally designed and synthesized by Park and DeShong to produce the tryptophan-functionalized AuNPs (TRP-AuNP).<sup>133</sup> (Scheme 4-1) Due to the relatively strong coordination of sulfur atoms to gold surfaces compared to the weak interaction from the citrate carboxylate groups, the ligand exchange reaction is very favorable and occurs rapidly. The incorporation of the TRP-conj onto the Au-NP surface is readily observable by the addition of the tryptophan shoulder at ca. 280 nm in the UV-VIS spectrum of the TRP-AuNP solution. (Figure 4-3) The weak emission from the tryptophan moiety at ca. 360 nm can also be detected by fluorescence spectroscopy.

The TRP-AuNPs offer several advantages over the cit-AuNPs. Most notably, TRP-AuNPs are generally more resilient against aggregation-inducing agents since the TRP-conj binds to the surface more strongly than citrate. Additionally, the acidic carboxylate proton enables a degree of control over aggregation behavior by adjustment of solution pH. Below pH 5, the TRP-AuNPs aggregate and precipitate out of solution, but pH values above 5 result in deprotonation of the carboxylic acid proton thus increasing the solubility and establishing an electrostatic repulsion between adjacent TRP-AuNPs. However, cycling of aggregation and solubility is not completely reversible and limited to <10 cycles in general.



**Scheme 4-1: Preparation of tryptophan-conjugate AuNPs (TRP-AuNP)**

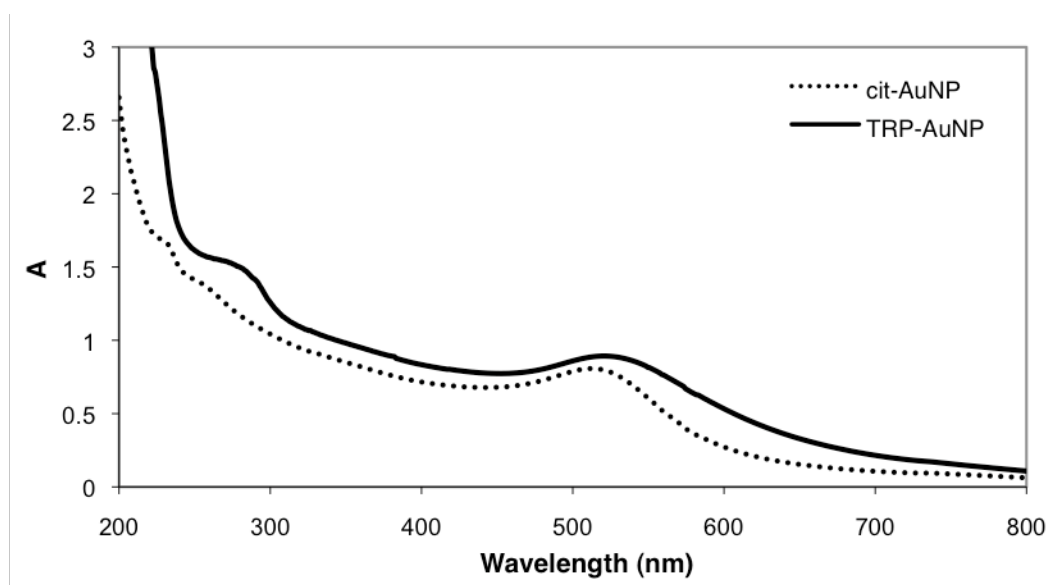


**Figure 4-3: UV-VIS spectra of cit-AuNP and TRP-AuNP**

Having successfully prepared two nanoparticle systems, deprotection photolysis experiments were subsequently explored to determine if MET release through the nanoparticles was possible.

### 4.3 Deprotection photolysis

#### 4.3.1 Citrate-stabilized gold nanoparticles

Deprotection photolysis experiments were initially performed using the prepared 16 nm cit-AuNPs as mediators. The NAP-ester *N*-methylpicolinium phenylacetate perchlorate (**1**) was chosen to be a model compound for these studies. As previously mentioned, cit-AuNPs are prone to irreversible aggregation due to the weak binding of the carboxylate moieties of the citrate ligands. Unfortunately, a correlation was established between the concentration of added NAP-ester **1** and the degree of cit-AuNP aggregation. (Figure 4-4) This was found to be a general observation as other NAP-esters and the model NAP group *N*-methylpicolinium perchlorate induced aggregation as

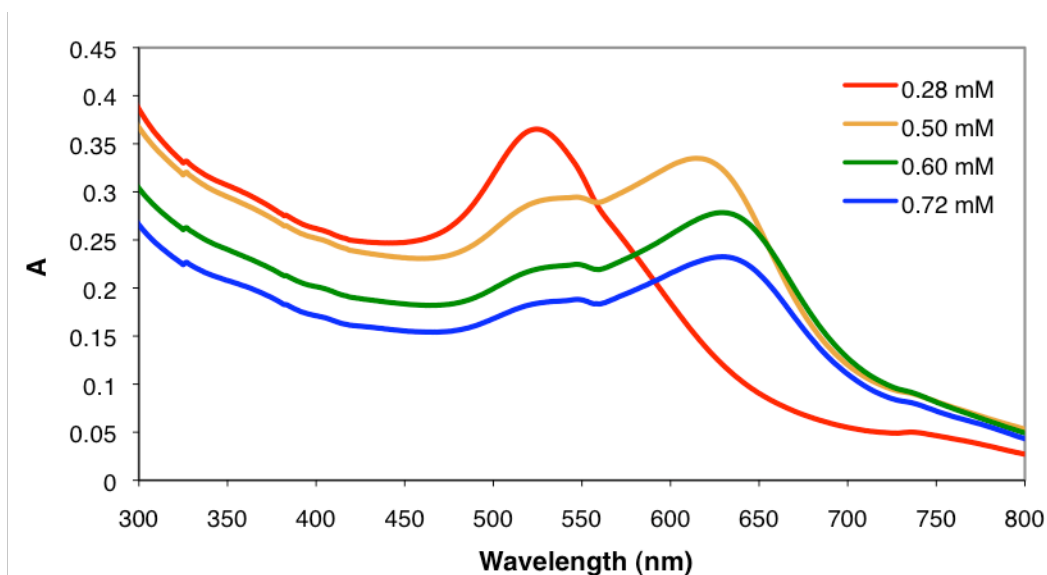


Figure 4-4: UV-VIS spectra of cit-AuNP with varying concentration of NAP-ester **1**

well. The reduction potentials of the nanoparticles could not be measured directly with our cyclic voltammetry system, therefore, electron donors for MET deprotection were chosen primarily on empirical observations. Several compounds considered for use as donors induced aggregation including ethylenediaminetetraacetic acid (EDTA) and ascorbic acid. The reductant DL-dithiothreitol (DTT) was an exception and cit-AuNP solutions remained stable in its presence. In fact, the addition of small concentrations of *1* to solutions of cit-AuNP and excess DTT (relative to *1*) were also stable for many hours. Thus, this system was explored further for deprotection photolysis experiments.

Solutions were prepared in D<sub>2</sub>O and an aliquot was set aside as a dark control. The samples were purged with N<sub>2</sub> for 10-15 min and irradiated with broad band visible light (400-800 nm) for predetermined periods of time. Free carboxylate yields were determined by analyzing samples directly by <sup>1</sup>H NMR. (Table 4-1) Yields were confirmed by HPLC of the final mixtures in several instances. Quantitative yield of free phenylacetic acid (PAA) is obtained after approximately 1 h of irradiation. Control photolysis experiments that lacked cit-AuNP, DTT, or both resulted in an insignificant yield of PAA (within experimental error). According to theoretical calculations of NP concentration (Table 4-1), significantly sub-stoichiometric amounts of sensitizer (cit-AuNPs) are being used in these experiments, far below levels previously used.

**Table 4-1: Deprotection photolysis data for release of PAA from NAP-ester *1* with cit-AuNP**

Entry	[NAP-ester <i>1</i> ] (mM)	[DTT] (mM)	[cit-AuNP] <sup>a</sup> (nM)	Irradiation Time (min)	% Yield of PAA <sup>b</sup>
1	1.24	12.5	1.9	60	64
2	1.24	62.2	0.95	60	80
3	1.24	62.2	1.9	60	95

<sup>a</sup>Theoretical concentrations assuming perfectly spherical 16 nm nanoparticles generated in 100% yield in the synthesis reaction <sup>b</sup> Determined by HPLC, relative to [*1*] in dark control, error ±10 %

In fact, concentrations reported in Table 4-1 are upper limits on the cit-AuNP amount in solution as the nitrogen purging step curiously resulted in partial nanoparticle aggregation. Absorbance at the PRB  $\lambda_{max}$  is reduced by an average of 29% after a 10 min nitrogen purge. Solutions containing only cit-AuNPs of identical concentration were unaffected by purging. The use of argon in place of nitrogen resulted in similar observations. The means by which nitrogen purging induces aggregation is unclear, but highlights again the difficulties of the cit-AuNP system.

The relative stability of the *I*/DTT/cit-AuNP system can be rationalized based on empirical and theoretical considerations. It is likely that the high concentration of DTT allows a certain percentage of DTT molecules to bind to the nanoparticle surface through reduction of the thiol groups, thus increasing the stability of the cit-AuNP towards aggregation. The remaining free DTT in solution can then act as a reductant to regenerate the cit-AuNPs upon electron transfer to *I* under irradiation. The challenges faced in using cit-AuNPs encouraged us to turn to the TRP-AuNPs for further deprotection studies.

#### **4.3.2 Tryptophan-stabilized gold nanoparticles**

The TRP-AuNPs are significantly more stable in a variety of different environments due to the strong binding affinity of the dithiolane linking moiety to gold. The ability to aggregate the TRP-AuNPs at low pH and restore their solubility at high pH highlights their relative robustness. TRP-AuNPs synthesized for deprotection photolysis experiments were prepared in pH 7.0 phosphate buffer. As opposed to the cit-AuNP system, the relative insensitivity to NAP-ester *I* and DTT concentration allowed a greater



**Table 4-2: Deprotection photolysis data for release of PAA from NAP-ester *1* with TRP-AuNP**

Entry	[ <i>1</i> ] (mM)	[DTT] (mM)	[TRP-AuNP] <sup>a</sup> (nM)	Irradiation Time (min)	% Yield of PAA
1	1.25	31.3	15	60	100
2	1.25	1.25	15	30	4
3	1.25	2.50	15	30	14
4	1.25	5.00	15	30	16
5	1.25	10.0	15	30	20
6	1.25	20.0	15	30	24
7	1.25	40.0	15	30	25
8	1.25	80.0	15	30	14
9	1.25	31.3	0.75	20	30
10	1.25	31.3	15	20	40
11	1.25	31.3	30	20	44
12	1.25	31.3	38	20	49
13	1.25	31.3	75	20	56

<sup>a</sup>Theoretical concentrations assuming perfectly spherical 2.6 nm nanoparticles generated in 100% yield in the synthesis reaction <sup>b</sup> Determined by HPLC, relative to [*1*] in dark control, error  $\pm 10$  %

exploration of the concentration parameter space for deprotection photolysis.

Additionally, nitrogen purging did not have a significant effect on aggregation behavior.

Samples were prepared in pH 7.0 phosphate buffer, purged with N<sub>2</sub> for 10-15 min and irradiated for prescribed periods of time. A small aliquot of the initially prepared solution was set aside as a dark control. Yields of PAA were determined by HPLC analysis of resulting dark and irradiated samples. (Table 4-2) Quantitative yield of PAA could be obtained after 1 h of irradiation. (Table 4-2, entry 1) Increasing concentrations of DTT (Table 4-2, entries 2-8) or TRP-AuNP (Table 4-2, entries 9-13) increased the deprotection yield of PAA for the same photolysis period. However, deprotection yield appears to maximize at ca. 1:25 1:DTT molar ratio for reasons that are unclear.

#### 4.4 Quantum yields

Quantum yields of release ( $\Phi_{rel}$ ) were determined for both the cit-AuNP and TRP-AuNP deprotection experiments. Samples were irradiated with 525 nm monochromatic light ( $\pm 10$  nm) from the output of a 1000 W Xe arc lamp and deprotection yields were measured by HPLC. For the cit-AuNP system,  $\Phi_{rel} = 0.4$  whereas for the TRP-AuNP system  $\Phi_{rel} = 1.4$ -4.5. In the case of the cit-AuNP system,  $\Phi_{rel}$  is comparable to previous MET systems using UV-absorbing mediators. Using TRP-AuNPs, the quantum yields are extremely high and may suggest the involvement of a radical chain mechanism. Since there are many components in the system that are potentially redox active, including the tryptophan moieties on the surface of the nanoparticles, the precise mechanism of this radical chain process is unclear. However, it is conceivable that the methylpicolinium radical generated in the deprotection event acts to catalyze some further radical reactions that eventually lead to additional deprotection reactions. Thus, the electron cascade established through the absorption of one photon may be able to effect release of several NAP-ester molecules, leading to higher than unity quantum yields. The photolytic efficacy ( $\Phi_{rel}\epsilon_{\lambda}$ ) of the nanoparticle-based systems could not be evaluated due to the inability to determine accurate molar absorptivities ( $\epsilon_{\lambda}$ ) of each system.

#### 4.5 Conclusions

Release of a NAP-protected carboxylate has been demonstrated using visible light absorbing gold nanoparticles and an included reductive additive. The initially conceived

system using cit-AuNPs proved unreliable and very sensitive to the donor and NAP-ester concentrations, yet full deprotection is possible within an hour of irradiation if the reaction is prepared within a narrow range of concentrations. The TRP-AuNP system performed exceptionally well and proved to be a robust system that is less sensitive to additive concentrations. Quantum efficiencies were high for both systems and above unity for the TRP-AuNP system. Although the exact mechanism of photorelease has not been pursued in either case, it is likely that there are contributions from multiple radical pathways that lead to deprotection. Studies by LFP to detect the formation of the expected radical intermediates may help to elucidate some of these mechanistic details. Considering further applicability, the cit-AuNP system would be very difficult to adapt to other systems that desire the use of different reductants and PET-PRPGs. Aggregation from many sources mandates the careful adjustment of a select few components that are compatible with the free cit-AuNPs. In contrast, the TRP-AuNP system should be adaptable to other NAP-esters and potentially other PET-PRPG and donor combinations.

## 5 Metal-Centered Complexes as Mediators for Visible Light MET Photorelease

### 5.1 Introduction

Previously used mediators for visible light MET deprotection reactions suffered from significant photobleaching (ketocoumarin dyes) or instability in a broad range of environments (citrate-stabilized gold nanoparticles). These effects contribute negatively to overall release efficiencies and limit the broader applicability of our MET deprotection design. Thus, we sought more robust visible light absorbing chromophores that could act as electron mediators and remain stable under our irradiation conditions.

Many metal-centered “inorganic” complexes (MCCs), such as metalloporphyrins, ruthenium(II) tris(bipyridyl), and chromium(II) tris(bipyridyl) derivatives are known to have strong visible absorption bands and function as electron donors or acceptors upon irradiation.<sup>88,134,135</sup> (Figure 5-1) In fact, MCCs can be found in a wide variety of naturally-occurring chromophores, most notably chlorophyll, functioning primarily as

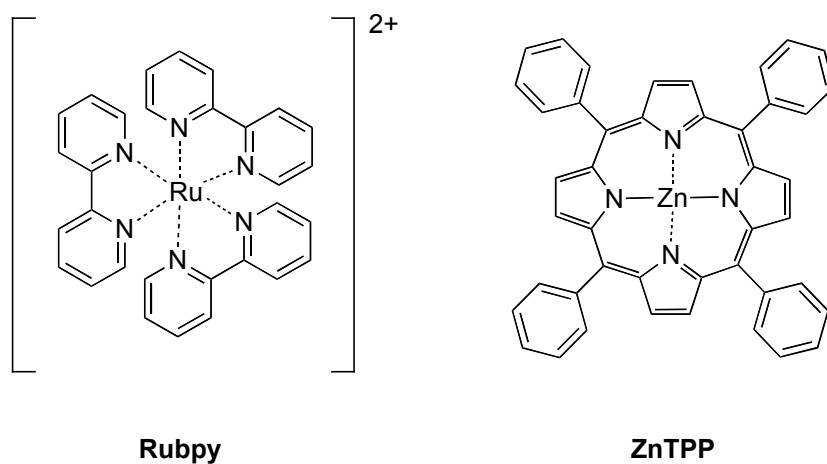
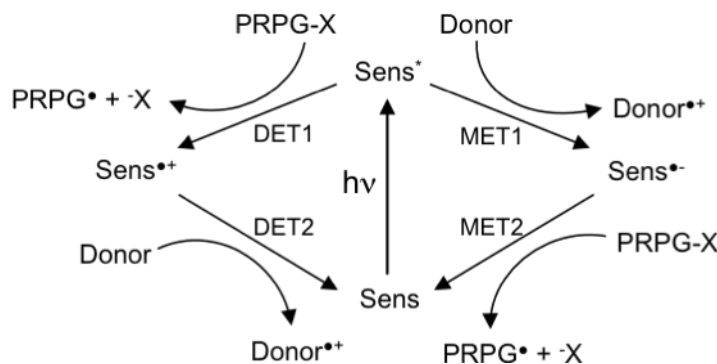


**Figure 5-1: Metal-centered complexes ruthenium(II) tris(bipyridyl) (Rubpy) and zinc(II) tetraphenylporphyrin (ZnTPP)**

photodriven redox mediators. Many MCCs have therefore been heavily investigated for inclusion in dye-sensitized and photoelectrochemical solar cells.<sup>136-140</sup> The lower energy visible absorption band in these complexes is primarily a result of a charge transfer interaction between the metal center and the surrounding ligands.<sup>141</sup> The lowest excited state generated by irradiation of this metal-to-ligand charge transfer (MLTC) band is typically very long lived due to strong spin-orbit coupling as a result of the presence of the (heavy) metal atom.<sup>134</sup> Thus, quenching of this excited state by an appropriate redox active species (such as NAP-esters or electron donors) should be a fairly competitive process. Many derivatives of MCCs are also aqueous compatible. For these reasons, MCCs seemed to make excellent candidates as sensitizers for deprotection reactions.

Despite the favorable attributes of MCCs, oxidation and reduction potentials and excited state energies of many of these compounds are comparatively modest. This can potentially pose a limitation when considering the two main mechanistic pathways through which MET can occur with these sensitizers. (Scheme 5-1) The primary mechanism discussed thus far occurs through reductive quenching of the sensitizer excited state and subsequent donation of an electron from the sensitizer radical anion to the NAP-ester. (Scheme 5-1, MET) However, since MCCs can typically access multiple reductive and oxidative states more easily than organic chromophores, oxidative quenching of the sensitizer excited state by the NAP-ester is another potential pathway to contribute to photorelease. (Scheme 5-1, DET) In this direct electron transfer (DET) mechanism, the oxidized sensitizer is subsequently reduced by the electron donor to regenerate the original electrochemical state of the sensitizer.



**Scheme 5-1: Mechanistic pathways for MET deprotection with MCCs**

Comparison of the electrochemical potentials of Rubpy and ZnTPP along with calculated  $\Delta G_{ET}$  values for the DET and MET photorelease processes using ascorbic acid as the sacrificial electron donor ( $E_{ox} = 0.29$  V vs. SCE) illustrates these considerations. (Table 5-1)  $\Delta G_{ET}$  values have been calculated using MET Eqs 2-2 and 2-3 in Section 2.3.2. The MET1 and MET2 processes using Rubpy are clearly exergonic whereas only MET2 is expected to be exergonic using ZnTPP. However, the DET pathway is endergonic for both sensitizers effectively eliminating that mechanistic pathway. For efficient use of these sensitizers, it would be desirable for all mechanistic pathways leading to deprotection to be accessible to avoid limiting release efficiencies. Options to rectify this situation include altering the sensitizer to make it a better electron donor or altering the NAP group to be a better electron acceptor. In an effort to make the NAP

**Table 5-1: Electrochemical data and electron transfer calculations for sensitizer/ascorbic acid/NAP-ester system**

Sensitizer	$E_{red}^a$	$E_{ox}^a$	$E_{oo}^b$	$\Delta G_{MET1}^b$	$\Delta G_{MET2}^b$	$\Delta G_{DET1}^b$	$\Delta G_{DET2}^b$
Rubpy	-1.35	1.29	48.9	-9.70	-5.77	7.60	-23.1
ZnTPP	-1.35	0.71	36.7	2.50	-5.77	6.42	-9.69

<sup>a</sup> in volts vs. SCE (MeCN) <sup>b</sup> in kcal/mol

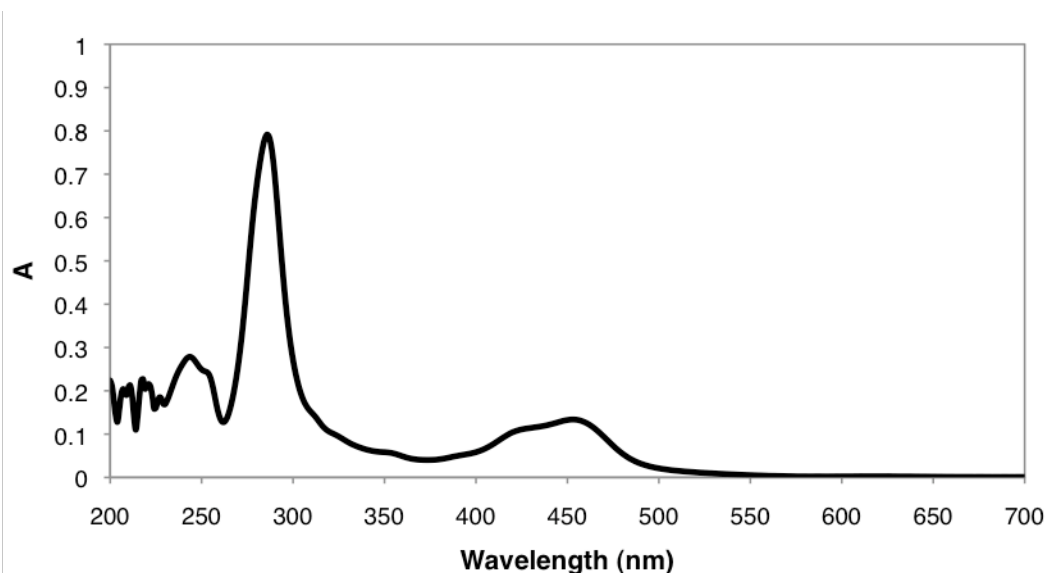


**Figure 5-2: UV-VIS spectrum of Rubpy in H<sub>2</sub>O**

group more broadly applicable to a variety of MCCs, we have chosen to alter the NAP group to make a better electron acceptor. We also chose to begin experimentation with ruthenium(II) tris(bipyridyl) (Rubpy) as the mediator due to its strong visible absorption band between 400-500 nm and because its redox and photochemical properties have already been extensively studied.<sup>142-144</sup> (Figure 5-2)

## **5.2 Modification of the NAP group**

It was expected that substitution of the existing NAP group with an electron-withdrawing substituent would raise the reduction potential to more positive values, thus generating a stronger electron acceptor. Although many such substituents could potentially be introduced, we began by considering a cyano substituent due to its strong electron-withdrawing ability. Additionally, conversion of a cyano substituent to the less

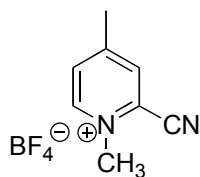


**Figure 5-3: Cyano-substituted NAP model compound**

electron-withdrawing amide derivative should be synthetically facile should we decide to consider experimentation with that substituent at a later time. To test the extent that a cyano-substituent would shift the NAP group reduction potential, the model compound *N*,4-dimethyl-2-pyridiniumcarbonitrile tetrafluoroborate (Figure 5-3) was prepared and analyzed by cyclic voltammetry. Compared to the original NAP-esters, the first reduction potential had shifted by ca. +0.5 V to -0.63 V (vs. SCE). This represents a substantial increase in the electron accepting ability of the NAP group. Factoring this shift into the electron transfer calculations performed previously for the MCC sensitizers shows that both the MET and DET pathways for Rubpy are now exergonic. (Table 5-2) The DET pathway for ZnTPP is also predicted to be exergonic, enabling the use of this mediator. Thus, several simple 2-cyano-NAP (mPCN) esters were prepared for further experimentation.

Synthesis of the mPCN-esters can be accomplished by modifying the 4-pyridylcarbinol precursor before the esterification step of the corresponding NAP-ester synthesis. Modification of a procedure reported by El Hadri and Leclerc generates the 4-

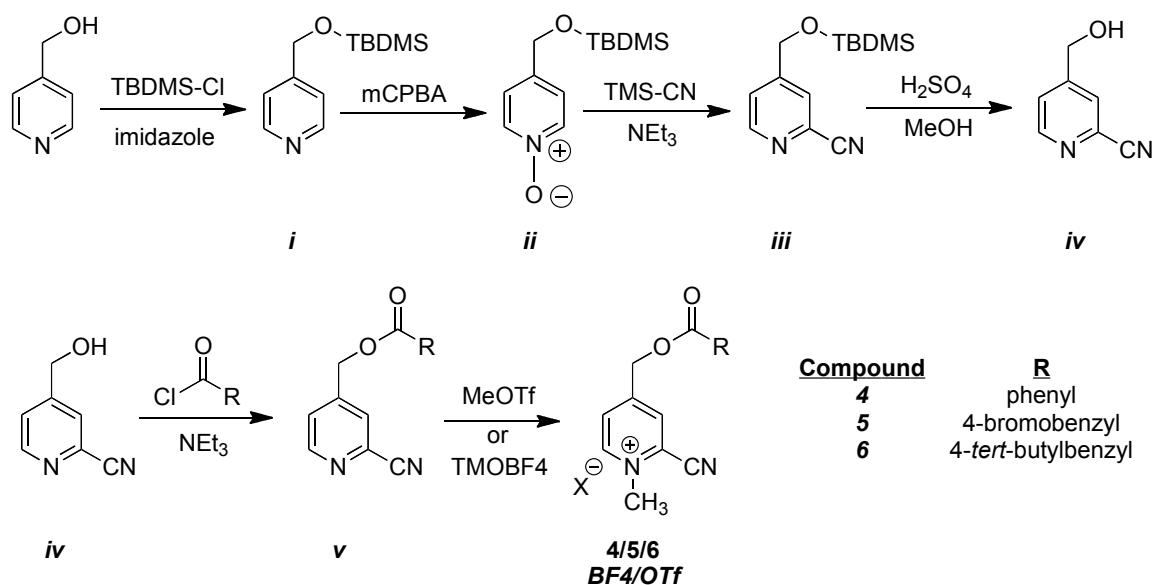
**Table 5-2: Electrochemical data and electron transfer calculations for sensitizer/ascorbic acid/cyano-substituted NAP system**

Sensitizer	$E_{\text{red}}^a$	$E_{\text{ox}}^a$	$E_{\text{oo}}^b$	$\Delta G_{\text{MET1}}^b$	$\Delta G_{\text{MET2}}^b$	$\Delta G_{\text{DET1}}^b$	$\Delta G_{\text{DET2}}^b$
Rubpy	-1.35	1.29	48.9	-9.70	-16.6	-3.24	-23.1
ZnTPP	-1.35	0.71	36.7	2.50	-16.6	-4.42	-9.69

<sup>a</sup> in volts vs. SCE (MeCN) <sup>b</sup> in kcal/mol



(hydroxymethyl)picolinonitrile precursor.<sup>145</sup> (Scheme 5-2) Protection of the 4-pyridylcarbinol hydroxyl group using *tert*-butyldimethylsilyl (TBDMS) chloride (**i**) is followed by oxidation with *meta*-chloroperoxybenzoic acid (mCPBA) to generate the *N*-oxide of the pyridyl group (**ii**). Installation of the cyano substituent (**iii**) is thereby accomplished by treatment of the *N*-oxide with trimethylsilylcyanide (TMS-CN) in triethylamine (NEt<sub>3</sub>). Subsequent deprotection of the TBDMS group with aqueous acid results in the cyano-substituted 4-pyridylcarbinol precursor (**iv**). Overall yields for this synthetic process were generally modest (42%). Esterification of **iv** is subsequently accomplished by acid chloride coupling. Yields of **v** were generally higher (> 90%) than the analogous NAP group esterification reactions (60-90%). It is likely that the decreased basicity of the pyridine nitrogen due to the cyano substituent reduces the competitiveness of processes that can occur at that position and thus potentially reduce yields of the ester.



**Scheme 5-2: Synthesis of cyano-substituted 4-pyridylcarbinol and mPCN-ester synthesis**

However, this effect is detrimental in the last step of the synthesis to produce the *N*-methyl salt. Attempts to methylate the esters, **ν**, with methyl iodide resulted in little or no yield of the methylated product. Stronger methylating reagents, such as trimethyloxonium tetrafluoroborate (TMOBF<sub>4</sub>) or methyl triflate (MeOTf), were required to generate the final mPCN-esters.

Analysis of the redox properties of the esters by cyclic voltammetry confirmed the results obtained for the mPCN model compound; the first reduction potential of the mPCN-esters was significantly shifted to more positive potentials compared to the original NAP-esters. (Table 5-3) Each ester exhibited an irreversible reduction wave at

**Table 5-3: First reduction potentials of prepared mPCN-esters**

mPCN-Ester	$E_{\text{red}} \text{ (V)}^a$
<b>4BF4</b>	-0.50
<b>5BF4</b>	-0.51
<b>6OTf</b>	-0.52

<sup>a</sup> Versus SCE, in MeCN, taken from the half-maximum current of an irreversible wave.

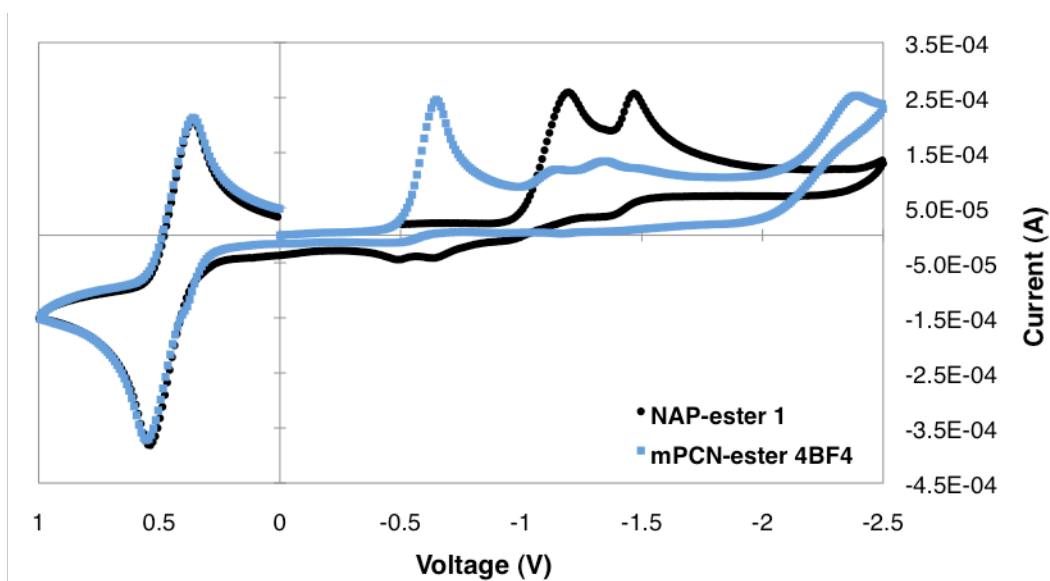
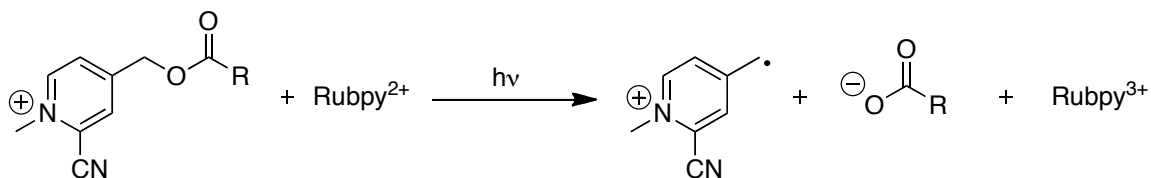


**Figure 5-4: Cyclic voltammograms of *1* and *4BF4*, referenced to ferrocene/ferrocenium couple in MeCN**

ca. -0.5 V (Figure 5-4). This value is approximately 100 mV more positive than the mPCN-ester model compound thus making the MET and DET electron transfer reactions more exergonic than calculated in Table 5-2. Having prepared the required esters, we turned to deprotection photolysis experiments to evaluate the MET photorelease reactions.

### 5.3 Deprotection photolysis

Preliminary deprotection photolysis experiments were directed at demonstrating photorelease using Rubpy as a sensitizer without any added electron donor (DET). (Scheme 5-3) According to the electron transfer calculations, deprotection through donation of an electron to the original NAP group from Rubpy is unfavorable. However, this deprotection reaction should now be accessible when using the mPCN-esters. Solutions were prepared in either MeCN/MeOH (1/1) or pH 4.0 acetate buffer and an aliquot was set aside in the dark as a control. The triflate mPCN-esters were generally more aqueous soluble than the tetrafluoroborate analogues, thus the triflate salts were used in all aqueous systems. Samples were purged with N<sub>2</sub> for 10 min and irradiated by a broad band tungsten filament source from which the output was passed through a 360 nm cutoff



**Scheme 5-3: Photolytic release of carboxylates from mPCN-esters by DET from Rubpy**

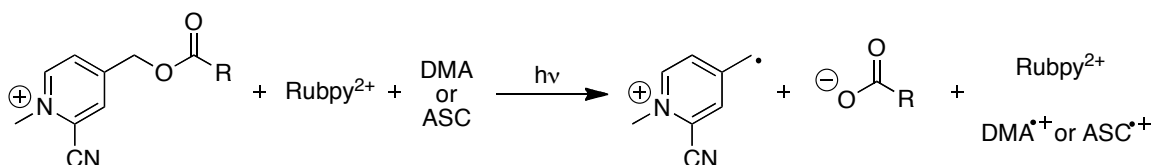
**Table 5-4: Deprotection photolysis data for release of carboxylates from mPCN-esters by DET from Rubpy**

Entry	Ester	[Ester] (mM)	[Rubpy] (mM)	Conditions	% Yield	% Conversion
1	<b>5BF4</b>	4.8	0.24	1 hr, MeCN/MeOH	10	22
2	<b>5BF4</b>	4.8	2.4	1 hr, MeCN/MeOH	24	29
3	<b>5BF4</b>	4.8	4.8	1 hr, MeCN/MeOH	15	14
4	<b>5OTf</b>	4.8	0.24	1 hr, acetate buffer	13	24
5	<b>5OTf</b>	4.8	2.4	1 hr, acetate buffer	16	21
6	<b>5OTf</b>	4.8	4.8	1 hr, acetate buffer	14	22
8	<b>5OTf</b>	0.6	0.3	30 min, acetate buffer	30	42

<sup>a</sup>Determined by HPLC, relative to [ester] in a dark control sample, corrected for any dark deprotection, estimated error <5%

filter and a Kopp 7093 IR light absorbing filter to ensure exclusively visible light irradiation entered the sample. According to the data (Table 5-4), DET is clearly a possible deprotection pathway in both aqueous and non-aqueous environments. Curiously, yields of the free acid seem to maximize at sub-stoichiometric concentrations of Rubpy. (Entries 2 and 5, Table 5-4) Control solutions lacking Rubpy or light resulted in a negligible yield of the free acid product (<5%). Solutions containing analogous NAP-protected esters resulted in insignificant yields after prolonged irradiation, confirming that the DET deprotection pathway is unfavorable for NAP-esters with Rubpy.

Having confirmed DET as a productive pathway for photorelease, a good electron donor was included in the system to add the MET deprotection pathway. (Scheme 5-4) Previous studies have reported the effective reductive quenching of Rubpy by DMA<sup>142,146</sup> with a quenching constant of ca.  $7 \times 10^7 \text{ M}^{-1}\text{s}^{-1}$ . Alternatively, 1,4-diazabicyclo[2.2.2]octane (DABCO) has a sufficiently low oxidation potential (0.57 V vs. SCE)<sup>147</sup> to quench Rubpy<sup>2+\*</sup> as well. For aqueous-based systems, ascorbic acid (ASC) is a well-known reductant and can effectively quench Rubpy.<sup>142</sup> We thus explored these donors for use in MET deprotection. Upon excitation, Rubpy<sup>2+</sup> is expected to



**Scheme 5-4: Photolytic release of carboxylates from mPCN-esters by MET from DMA or ASC through Rubpy**

abstract an electron from the donor, generating the Rubpy<sup>1+</sup> state. Subsequent reduction of the mPCN-esters by Rubpy<sup>1+</sup> should induce release of the free acid and regenerate Rubpy<sup>2+</sup>. Alternatively, oxidative quenching of Rubpy<sup>2+\*</sup> by the mPCN-esters, followed by regeneration of Rubpy<sup>2+</sup> by direct donation of an electron from the donor to Rubpy<sup>3+</sup> produces the same net effect. (Scheme 5-1)

Samples were prepared and photolysed in a similar fashion to the DET experiments utilizing an excess of the electron donor and sub-stoichiometric amounts of Rubpy. A large increase in the free acid yield is observed with the inclusion of the electron donor, compared to the DET experiments. (Table 5-5) For example, free acid yields were raised from 24% (Entry 2, Table 5-4) to 54% (Entry 2, Table 5-5) with the addition of DMA as the donor. Almost quantitative yields of the free acid are obtained

**Table 5-5: Deprotection photolysis data for release of carboxylates from mPCN-esters by MET from various donors through Rubpy**

Entry	Ester	Donor	[Ester] (mM)	[Ru(bpy)] (mM)	[Donor] (mM)	Conditions	% Yield <sup>a</sup>	% Conversion <sup>a</sup>
1	<b>5BF4</b>	DMA	4.8	2.4	9.6	1 hr, MeCN/MeOH	38	48
2	<b>5BF4</b>	DMA	4.8	2.4	24	1 hr, MeCN/MeOH	54	70
3	<b>5BF4</b>	DMA	4.8	2.4	24	3 hr, MeCN/MeOH	96	97
4	<b>5BF4</b>	DABCO	0.6	0.3	1.2	10 min, MeCN/MeOH	7	15
5	<b>5BF4</b>	DABCO	0.6	0.3	60	10 min, MeCN/MeOH	35	52
6	<b>5OTf</b>	ASC	0.6	0.3	3.0	10 min, acetate buffer	29	40
7	<b>5OTf</b>	ASC	0.6	0.3	6.0	10 min, acetate buffer	36	62
8	<b>5OTf</b>	ASC	0.6	0.3	60	10 min, acetate buffer	89	94

<sup>a</sup>Determined by HPLC, relative to [ester] in a dark control sample, corrected for any dark deprotection, estimated error <5%

after 3 h irradiation of this system. (Entry 3, Table 5-5) Substitution of DABCO as the electron donor generally resulted in higher yields of free acid for shorter irradiation periods. Unfortunately, a significant amount of deprotection occurs in the dark control sample for both the DABCO and DMA systems, generating yields of free acid as high as 50% in some cases. Furthermore, the dark free acid yield seems to be proportional to the concentration of donor. The dark electron transfer reaction between either donor and the mPCN-esters is predicted to be disfavored by ca. 30 kcal/mol. However, it is possible that base-catalyzed hydrolysis or methanolysis by the amine donors is a competitive side reaction under the experimental conditions.

Deprotection photolysis experiments for the aqueous system generally yielded more reproducible and stable results. Free acid yields are comparable to those obtainable in MeCN/MeOH using DMA or DABCO as donors. (Entries 6-8, Table 5-5) Rates of release are high, i.e. 89% yield of free acid is obtained after 10 min using 100 equivalents of ASC and 0.5 equivalents of Rubpy. (Entry 8, Table 5-5) Reduction of ASC concentration subsequently lowers the free acid yield for the same irradiation period. (Entries 6-7, Table 5-5) Dark control samples were significantly more stable in this system compared to using DMA or DABCO. Less than 3% deprotection occurs over 18 h and there is no apparent correlation between donor concentration and dark deprotection yield.

Unfortunately, a significant limitation exists in the current system. Solutions of the mPCN-esters in MeOH/MeCN or unbuffered aqueous solution develop a broad absorption band centered around 350 nm over time. Over prolonged periods of time, the band at 350 nm is reduced and a second band grows in at ca. 510 nm that remains

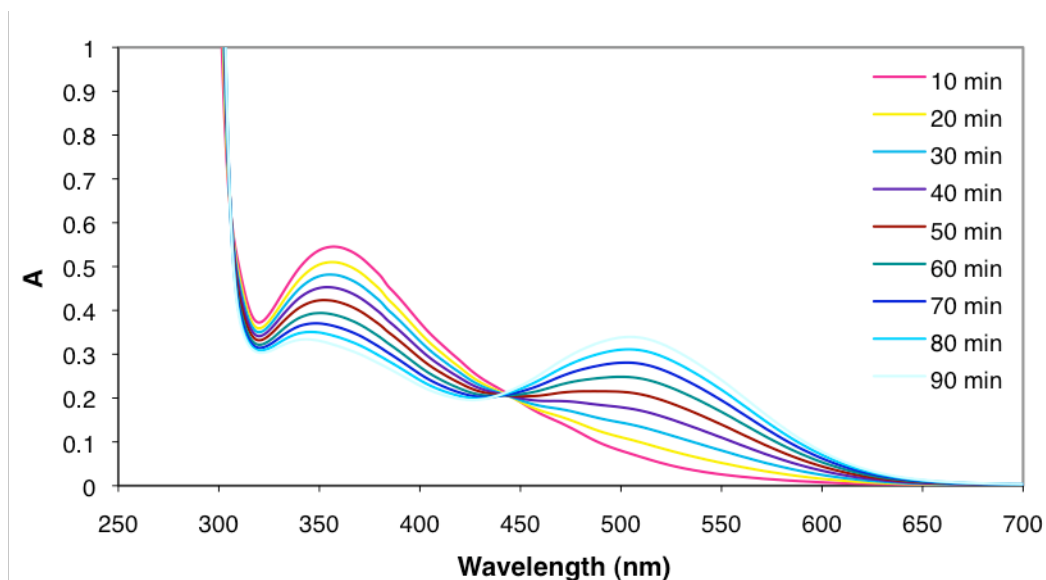


**Figure 5-5: UV-VIS spectrum of 5OTf in MeCN/MeOH over time**

persistent. (Figure 5-5) Curiously, there are no significant changes in the NMR spectrum over the course of these color changes and irradiation of this band does not result in any significant amount of deprotection products. As a result, this band competes with Rubpy for incident irradiation and is expected to lower deprotection rates and efficiencies.

While the exact identities of the species responsible for each absorption band have not been identified, the formation of the bands appears to be a consequence of deprotonation of a benzylic proton on the mPCN group. The increased electron-withdrawing power of the mPCN group decreases the pKa of the benzylic protons relative to the unsubstituted NAP group. This increased acidity has been confirmed by NMR studies of **5BF4** in CD<sub>3</sub>CN/D<sub>2</sub>O. Deuterium incorporation occurs at the benzylic position slowly over the course of 24 h and more rapidly in the presence of a catalytic amount of triethylamine. Studies of **5BF4** in MeCN/MeOH (1/1) with varying concentrations of triethylamine also support this suggestion, as all samples exhibited the 350 nm absorption band proportional to the concentration of base. After several minutes,

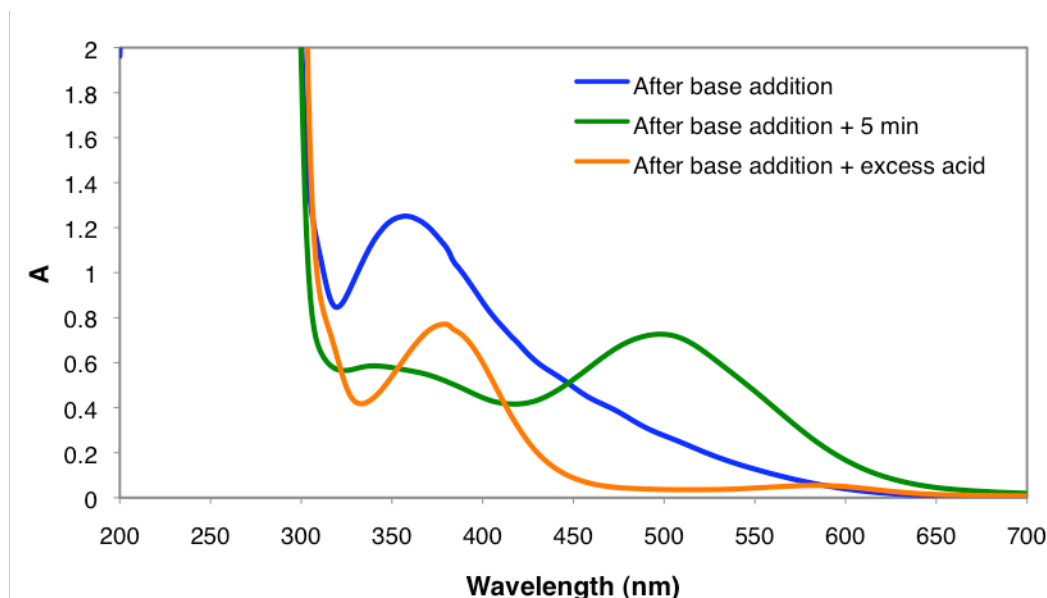
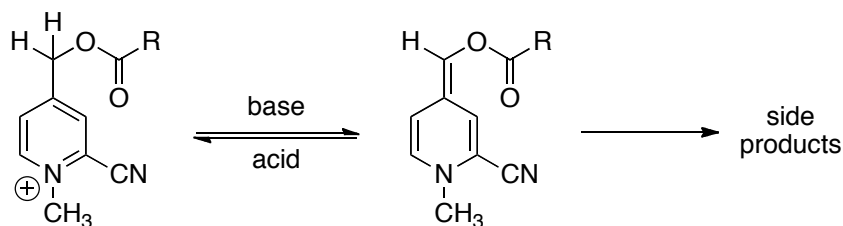


**Figure 5-6: UV-VIS spectrum of *5BF4* in MeCN/MeOH after addition of base ( $\text{NEt}_3$ ) and acid ( $\text{H}_2\text{SO}_4$ )**

the 350 nm band diminishes and the 510 nm band develops. Upon acidification with excess sulfuric acid, the 510 nm band diminishes and a band at ca. 380 nm persists.

(Figure 5-6) Samples of *5BF4* prepared in the presence of varying concentrations of sulfuric acid remained stable and colorless for several days. Therefore, it is evident that deprotonation of a benzylic proton contributes to the formation of the colored species. However, the behavior is more complex than a simple reversible acid/base reaction. It is likely that the deprotonated mPCN group participates in one or many slow, irreversible side reactions that result in the persistent 380 nm absorption. (Scheme 5-5) Fortunately, the preparation and photolysis of the mPCN-esters in acidic media, such as



**Scheme 5-5: Acid/base equilibrium and side reaction with mPCN-esters**



pH 4.0 acetate buffer used in the aqueous deprotection photolysis experiments, generally avoids the formation of the long wavelength bands. Nevertheless, the requirement for mildly acidic media is a notable limitation.

#### 5.4 Mechanistic studies

The proposed mechanistic pathways from which deprotection can occur were investigated by luminescence quenching and laser flash photolysis (LFP). Upon excitation, Rubpy<sup>2+</sup> forms a long-lived emissive MLTC triplet state (<sup>3\*</sup>MLTC) from which oxidative and reductive quenching can occur.<sup>142</sup> Luminescence quenching of the <sup>3\*</sup>MLTC by the donors and mPCN-esters was investigated to determine quenching constants ( $k_q$ ) of the electron transfer processes. Values for excited state lifetimes of <sup>3\*</sup>MLTC in MeCN ( $\tau_s$ = 850 ns)<sup>88</sup> and in aqueous solution ( $\tau_s$ = 620 ns)<sup>142</sup> have previously been reported. Confirming the deprotection photolysis results, **5BF4** and **5OTf** were

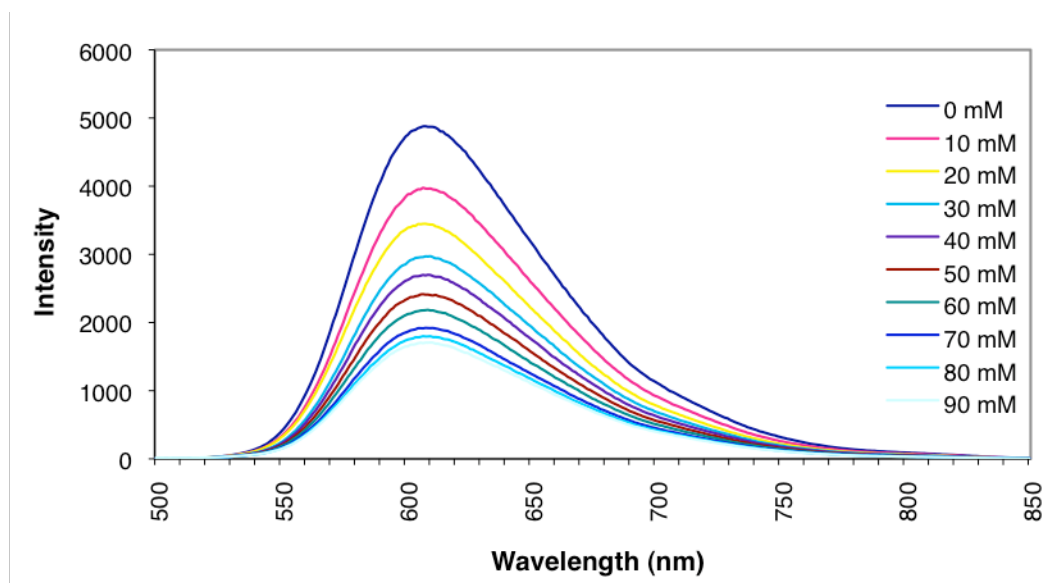
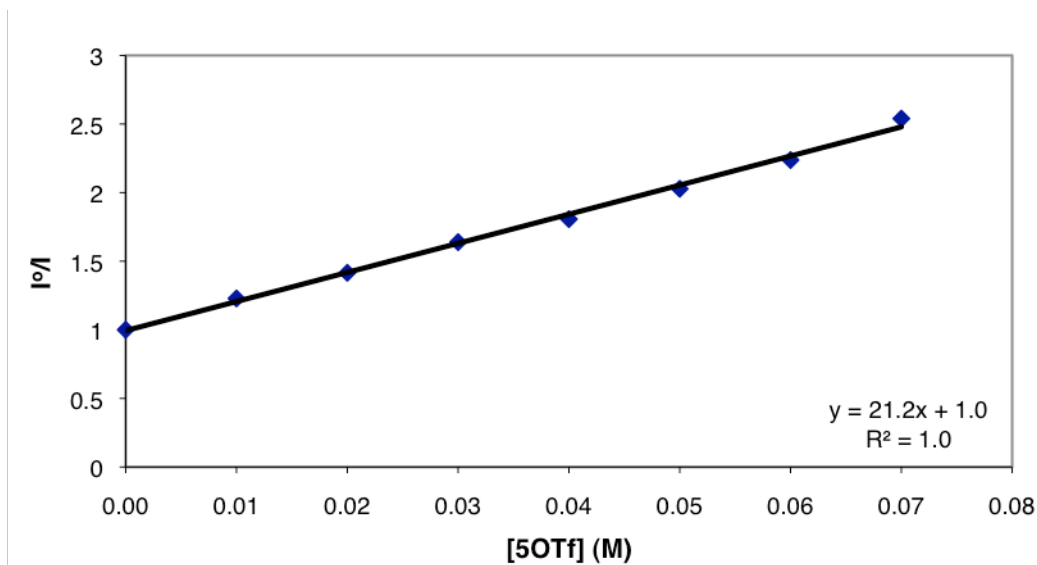


Figure 5-7: Luminescence quenching of Rubpy by **5OTf**



**Figure 5-8: Stern-Volmer analysis of Rubpy luminescence quenching by 5OTf**

effective quenchers of  $^3\text{MLTC}$  luminescence (Figure 5-7) and subsequent Stern-Volmer analysis (Figure 5-8) yielded  $k_q = 5.18 \times 10^8 \text{ M}^{-1}\text{s}^{-1}$  in MeCN/MeOH (1/1) and  $k_q = 3.42 \times 10^7 \text{ M}^{-1}\text{s}^{-1}$  in pH 4.0 acetate buffer. Similar quenching studies were performed on each of the donors and the determined  $k_q$  values are presented in Table 5-6. It is worth noting that the quenching processes occur at similar rates, including direct quenching of Rubpy  $^3\text{MLTC}$  by **5BF4**. Thus, oxidative and reductive quenching mechanisms appear competitive with one another. The predominating pathway will ultimately be determined by the relative concentrations of donor and mPCN-ester.

LFP experiments were performed to confirm and characterize the formation and

**Table 5-6: Observed quenching constants, quantum yields of photorelease, and photolytic efficacies for mPCN-ester release**

Ester	Donor	$k_q$ (MET1) ( $\text{M}^{-1}\text{s}^{-1}$ )	$k_{\text{obs}}$ (MET2) ( $\text{M}^{-1}\text{s}^{-1}$ )	$\Phi_{\text{rel}}$	$\Phi_{\text{rel}}\epsilon$
<b>5BF4</b>	DMA	$1.05 \times 10^8$	$3.17 \times 10^9$	0.02	260
<b>5BF4</b>	DABCO	$2.40 \times 10^6$	-	0.002	26
<b>5OTf</b>	ASC	$3.84 \times 10^7$	$1.77 \times 10^9$	0.01	130
<b>5BF4</b>	N/A	$5.18 \times 10^8$	N/A	0.001	13

quenching of intermediates of Rubpy formed in MET deprotection. Samples containing Rubpy and a large excess of any of the donors exhibited a broad signal in the transient spectra centered around 510 nm. This signal is assigned to Rubpy<sup>1+</sup> that has been previously characterized.<sup>142,148,149</sup> Addition of esters **5BF4** or **5OTf** results in a reduction in the signal intensity at 510 nm as well as an increase in the rate of decay. (Figure 5-9) Determination of quenching rate constants ( $k_{\text{obs}}$ ) for this process were accomplished by fitting the time-dependent decay curves to a second-order exponential decay function and plotting the extracted constants versus quencher concentration. (Figure 5-10) Rate constants for the MET2 process are near the diffusion limit for both the DMA and ASC systems. (Table 5-6) A rate constant could not be determined for the DABCO system due to interference from the previously discussed long wavelength absorption band forming during photolysis. The reduced mPCN group could not be directly observed by LFP experiments that utilized Rubpy. The expected signal (ca. 410 nm) is likely

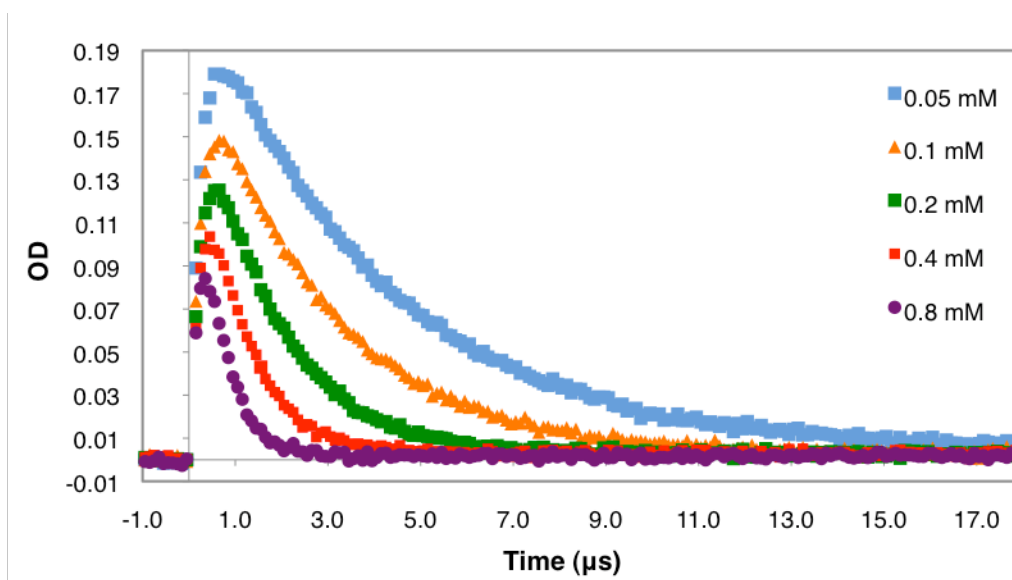


**Figure 5-9: Time-dependent absorption traces from 532 nm pulsed laser photolysis of Rubpy, ASC, and varying [5OTf], monitored at 510 nm**

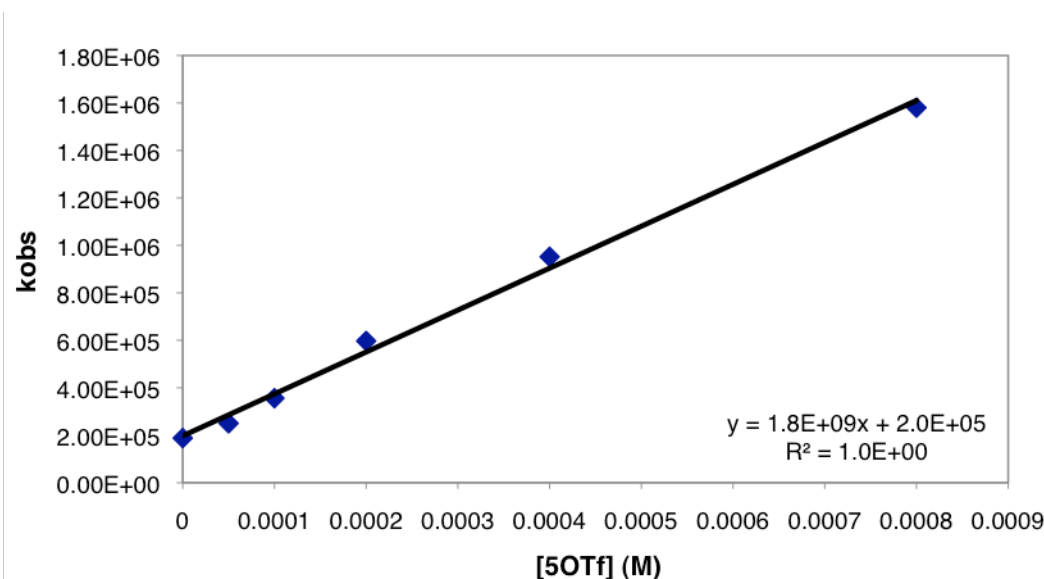


**Figure 5-10: Determination of  $k_{obs}$  for quenching of Rubpy<sup>1+</sup> by 5OTf**

bleached by the strong absorption of Rubpy in that region. However, a signal at 410 nm has been observed in LFP experiments using the UV-absorbing sensitizer 9-methylcarbazole with **5BF4**.

Efficiencies of the overall release reactions were assessed by determining quantum yields of release ( $\Phi_{rel}$ ). Using monochromatic irradiation at 450 nm ( $\pm 10$  nm),  $\Phi_{rel}$  was determined for each system and is presented in Table 5-6. These efficiencies are fairly low as it appears processes that do not lead to free acid release are fairly competitive. Substitution of the NAP group likely alters efficiencies of the release reaction which may contribute to the low  $\Phi_{rel}$ . However, photolytic efficacies ( $\Phi_{rel}\epsilon_{\lambda}$ ) of each system are comparable to those observed with traditional direct photolysis PRPGs. (Table 1-1)

## 5.5 Conclusions

A new adaptation of the NAP PET-PRPG has been created and has demonstrated effective release of carboxylate anions through visible light MET and DET. Compared to the original NAP group, the mPCN group allows a broader range of mediators to be used due to its more modest reduction potential. With the MCC dye Rubpy, the DET mechanistic pathway can be accessed in addition to the MET pathway, thus increasing the overall likelihood of deprotection upon photolysis. A higher degree of stability under irradiation was generally observed representing an advantage over the previously studied ketocoumarin and AuNP mediators. Additionally, this deprotection system is compatible with aqueous media using ascorbic acid as the donor in pH 4.0 acetate buffer. Laser flash photolysis and luminescence quenching experiments have confirmed and characterized the DET and MET mechanistic pathways and their kinetics. Moderately high photolytic efficacies have been obtained due to the high molar absorptivity of Rubpy compensating for low  $\Phi_{rel}$  values. The primary limitation of this system is the requirement for an acidic environment to prevent deprotonation at the mPCN benzylic site. This would significantly limit application in acid sensitive environments such as biological systems. In consideration of possible remedies for this issue, it is likely that substitution of the benzylic protons with alkyl groups would eliminate the problem. (see Appendix A)

## 6 A Quasi-Reversible Photorheological Fluid Based on Photorelease and Photoisomerization

### 6.1 Introduction

The NAP and mPCN groups have proven to be effective in releasing carboxylate anions in aqueous and non-aqueous environments using direct and mediated electron transfer induced by visible light. Aside from their potential synthetic utility, these deprotection schemes should be applicable to a number of situations where controlled release of carboxylate-containing compounds is desirable. Several PRPG systems have already been used to introduce the inactive protected version of a functional molecule into the system in which it would normally be utilized. (see Chapter 1) For example, ONB-caged ATP can be introduced with ATP-consuming enzymes and subsequently be photolyzed to restore functional ATP thereby initiating enzyme activity.<sup>28</sup> This type of application should be adaptable to the PET-PRPG systems developed in our lab. Thus, we surveyed a number of potential applications in which to utilize MET photorelease from the NAP or mPCN PET-PRPGs.

Recently, there has been much attention surrounding the development of fluids whose rheological properties (such as viscosity) can be modulated with external stimuli, such as electric or magnetic fields,<sup>150,151</sup> redox reactions,<sup>152</sup> and light.<sup>153-157</sup> These materials would be useful in improving vibrational damping systems, brakes, and microfluidic valves.<sup>150,151,158</sup> Advancements in microfluidic valve design would be particularly useful for “lab-on-a-chip” technologies.<sup>159-161</sup> The use of light as an actuator in chromophore-containing systems is particularly appealing as it allows temporal as well

as spatial control over the viscosity changes. For these systems to be successfully applied, reversibility of the different viscosity states is necessary. Currently, many of the systems that can achieve changes in viscosity are based upon surfactant solutions containing carboxylate-functionalized additives. We reasoned that it would be possible to protect these additives with the NAP group and thus modulate solution viscosity by photorelease.

Changes in solution viscosity are known to occur via formation, modification, or disruption of the molecular self-assembly of surfactant solutions. Self-assembly is a phenomenon observed with many amphiphiles, including many surfactants comprised of distinct hydrophilic and hydrophobic units. (Figure 6-1) Surfactants can spontaneously aggregate in solution as they seek to maximize attractive forces while minimizing repulsive forces between other surfactants and the bulk solution. These aggregates assemble thermodynamically in specific ways depending on the concentration of surfactant and the identity of the media in which they are placed. Thus, in aqueous solutions, hydrophobic units aggregate together while the polar hydrophilic groups aggregate and face outward toward the bulk solution. In nonpolar media, such as

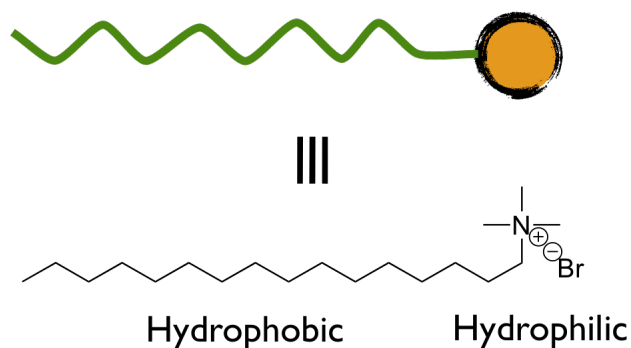


**Figure 6-1: Cetyltrimethylammonium bromide (CTAB) surfactant and surfactant model representation**

hexanes, the reverse is observed where hydrophilic units will segregate towards themselves placing the hydrophobic moieties in greater contact with the solvent.

Concentrations of surfactant above a threshold value, or the critical micelle concentration (CMC), tend to form supramolecular structures, termed micelles.<sup>162</sup> The overall structure of the micelles is governed by a number of factors, most importantly, the molecular structure of the hydrophilic and hydrophobic groups which determines how the surfactant molecules will pack together. While there is no definitive quantitative means of predicting supramolecular structure for any system, it is convenient to use the critical packing parameter (CPP) to approximate expected structures.<sup>162-165</sup> CPPs are calculated using Eq 6-1, where  $v$  is the volume of the hydrocarbon tail,  $a_0$  is the optimal headgroup area, and  $l_c$  is the maximum effective length of the hydrocarbon tail. Surfactants having an overall conical-type structure ( $\text{CPP} < 1/3$ ) will generally self-assemble into spherical-

$$\text{CPP} = v/a_0l_c \quad (6-1)$$

shaped micelles. (Figure 6-2, top; Figure 6-3) Surfactants with smaller effective headgroup areas tend to form truncated cones ( $\text{CPP } 1/3\text{-}1/2$ ) and cylindrical micelles. (Figure 6-2, bottom; Figure 6-3) Higher CPPs typically form flexible bilayers ( $\text{CPP} = 1/2\text{-}1$ ), planar bilayers ( $\text{CPP} \sim 1$ ) or inverted micelles ( $\text{CPP} > 1$ ).

While many supramolecular structures formed by surfactants in solution do not significantly alter physical properties (i.e. viscosity) of the bulk solution, cylindrical micelles can have a profound effect. These micelles can often elongate to great lengths and subsequently form tight interpenetrating networks that significantly constrict molecular movement or flow.<sup>163,166</sup> (Figure 6-3) This is manifested macroscopically



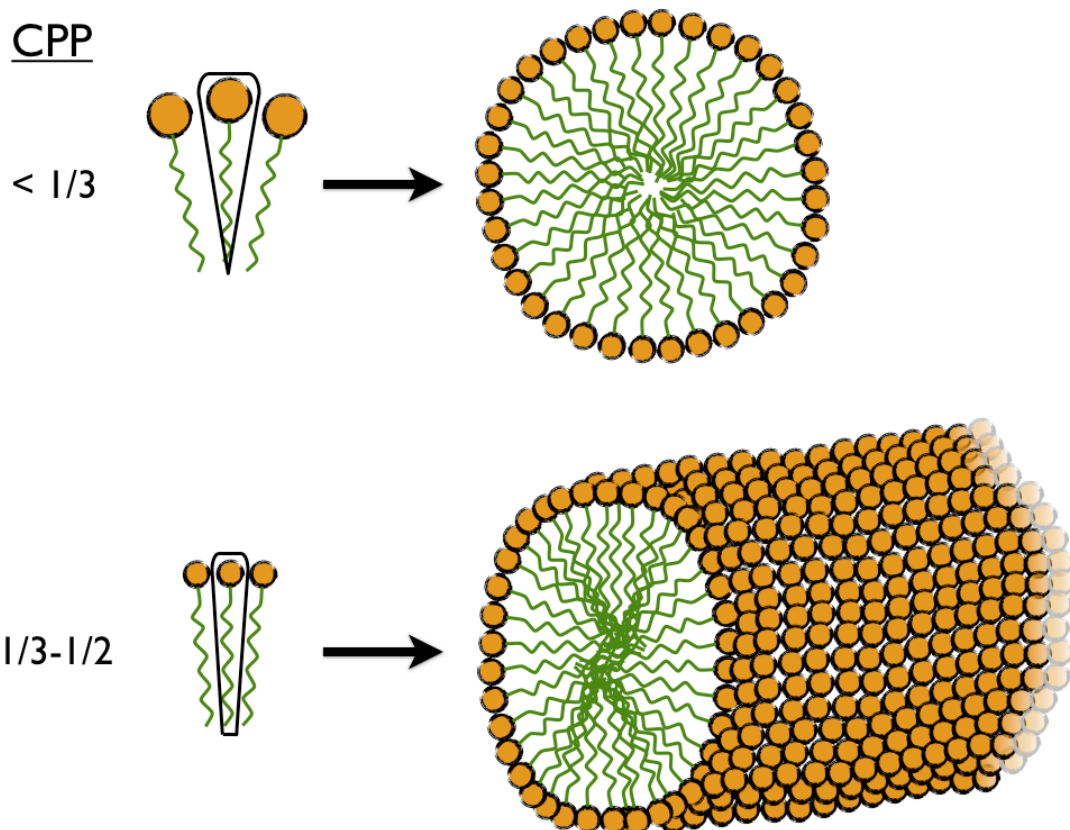


**Figure 6-2: Critical packing parameters and their relationship to expected packing of surfactant molecules and larger micelle structure**

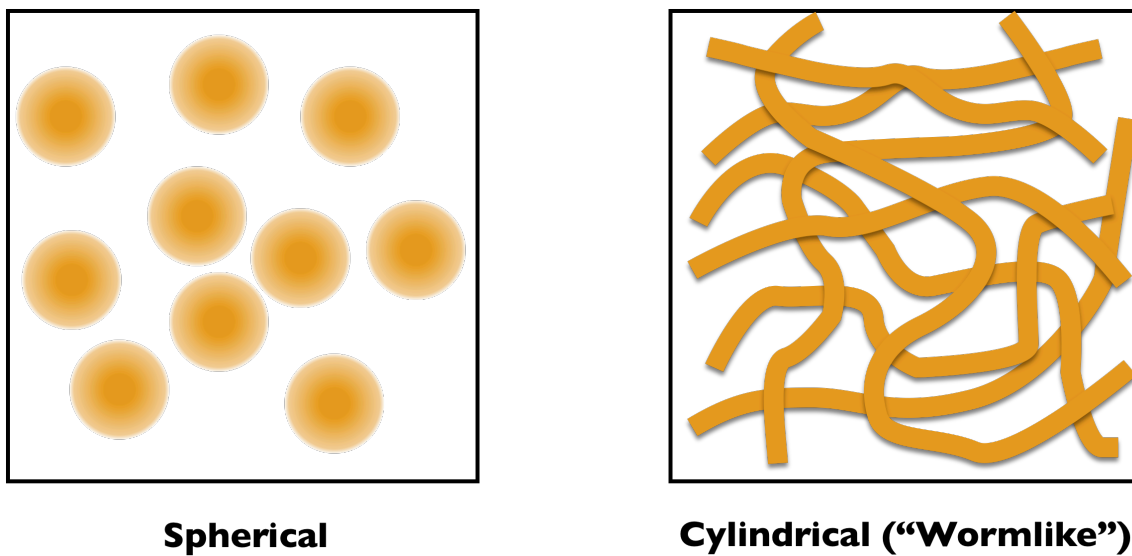


**Figure 6-3: Model representation of spherical (left) and cylindrical (right) micelle structures in solution**

as a highly viscous fluid or as a gel. Thus, slight changes in the surfactant structure and therefore its packing shape can have profound effects on the solution viscosity.

Furthermore, the effective packing shape of surfactant molecules can be adjusted by certain solution additives thereby inducing a change in overall viscosity. This phenomenon is central to the design of many tunable rheological systems.

Cetyltrimethylammonium bromide (CTAB) is an aqueous-soluble surfactant that is well-known to form micelles in solution.<sup>167</sup> Above its CMC, CTAB forms spherical micelles as its CPP is typically low. The large headgroup area and repulsive interactions between adjacent headgroups corresponds to a conical molecular geometry for each molecule ( $CPP < 1/3$ ). However, upon addition of simple salts, such as KBr, or organic salts, such as sodium salicylate (NaSal), the spherical micelles are transformed into long cylindrical “wormlike” micelles, thus greatly increasing solution viscosity.<sup>166,168-170</sup> This transition has been rationalized as a reduction of the effective positive headgroup charge (and therefore headgroup area) by the added salt anion. This reduces electrostatic repulsion between adjacent CTAB headgroups thereby allowing tighter packing in the headgroup region. Thus, the effective geometry of the CTAB molecules has changed to a truncated cone ( $CPP 1/3-1/2$ ) and wormlike micelles are the thermodynamically most stable form in which the system will self-assemble. This effect has been demonstrated in other systems including non-polar solvents.<sup>171,172</sup>

There are specific structural requirements of the organic additives that induce the formation of wormlike micelles in these surfactant solutions.<sup>168,170,173,174</sup> The presence of an aromatic hydrophobic unit coupled to hydrophilic units, such as hydroxyl or carboxylate groups, in specific geometric arrangements seems to encourage the transition.

It is believed that the aromatic unit buries within the hydrophobic pocket of the aggregated surfactant molecules while the hydrophilic moiety lines up with the complementary charge of the surfactant that is in contact with solution. Proper orientation of these groups is critical. For example, studies with CTAB and hydroxybenzoic acid have demonstrated that the acid becomes less effective in driving the transition as the hydrophilic hydroxy group is moved from the 3-position to the 4-position.<sup>168</sup> Changes in the substitution position of a methyl group in the same system did not have a similar effects since a methyl group would enhance hydrophobic permeability. Several examples of gelation-inducing additives are presented in Figure 6-4.

Since a number of these additives that induce gelation contain carboxylate moieties, we were interested in preparing a NAP-protected additive, such that deprotection would release the free additive. Thus, a solution containing the NAP-protected additive, a sensitizer, and CTAB would start at low viscosity and increase in viscosity upon irradiation due to release of the NAP group. Several systems that exhibit viscosity changes upon irradiation, called photorheological (PR) fluids, have already been described.<sup>153,175</sup> A chromophore is often incorporated directly into the surfactant

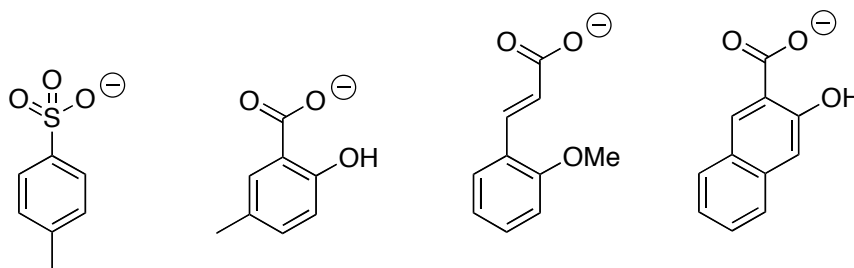


**Figure 6-4: Additives known to induce wormlike micelle formation in aqueous CTAB<sup>168,170</sup>**

molecule or into an additive present in the system. Since surfactant packing is very sensitive to slight changes in molecular structure, orientation, and electrostatics, photoisomerization or photorelease reactions can have profound effects on self-assembly. Chromophores such as stilbene<sup>157,176</sup> and azobenene<sup>155,156,177</sup> have been incorporated directly into surfactants to take advantage of photoisomerization reactions. The use of azobenzene moieties is particularly advantageous in the development of reversible PR systems due to the significant mismatch in absorption bands between the two isomers. Sakai et al. were able to observe a high degree of reversibility in their system that incorporates an azobenzene-containing surfactant into a CTAB/NaSal system.<sup>156</sup> (Figure 6-5) The use of photorelease to change solution viscosity has also been reported. A heavily studied system employs azosulfonates to change a hydrophilic site to a hydrophobic site upon photolysis.<sup>178-180</sup> A few studies have also used photodimerization reactions between anthracene or coumarin derivatives to radically change solution viscosity.<sup>154,181</sup>

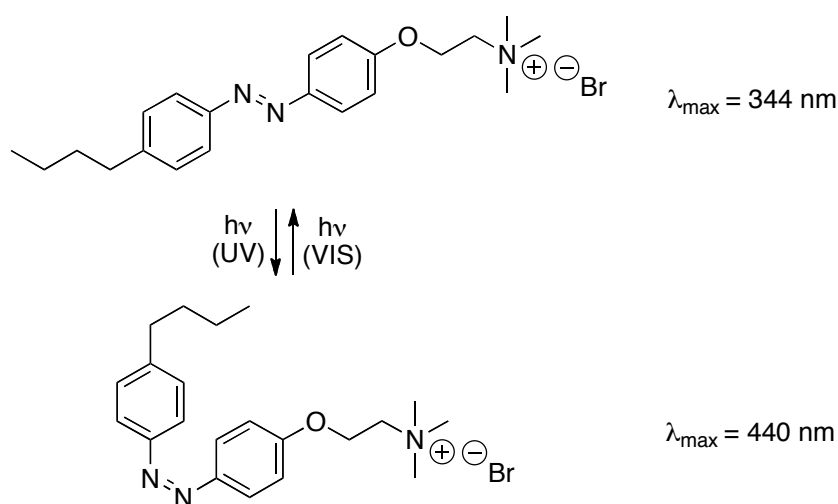
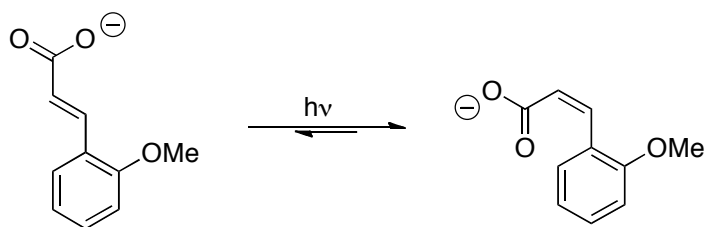


**Figure 6-5: Azobenzene surfactant derivative prepared by Sakai et al.**

Recently, Raghavan et al. have introduced PR fluids based on *ortho*-methoxycinnamic acid (OMCA) as an additive in surfactant solutions.<sup>182,183</sup> In the presence of CTAB, OMCA is effective in forming interpenetrating wormlike micelles that form a macroscopic viscoelastic fluid. UV photolysis of these solutions results in *cis-trans* isomerization of the  $\pi$  bond, greatly altering the geometric relationship of the hydrophobic and hydrophilic moieties. (Scheme 6-1) Thus, the uniformly arranged network of surfactant and OMCA molecules is disrupted, decreasing solution viscosity by approximately three orders of magnitude. In a complementary system, OMCA is combined with the zwitterionic surfactant erucyl dimethyl amidopropyl betaine (EDAB) to form spherical or short cylindrical micelles.<sup>183</sup> Upon photolysis, OMCA isomerizes and the solution viscosity increases. The OMCA anion has even been incorporated as the counterion for a cetyltrimethylammonium surfactant to achieve improved viscosity changes compared to the previously described systems.<sup>184</sup> While it is conceivable that the viscosity changes should be reversible in each system, this is difficult to achieve due to the similarities in absorption profiles between the two isomers. In fact, it is unlikely that all of one isomer could be converted to the other once a photostationary state is reached between the two.



**Scheme 6-1: Photoisomerization of *trans*-orthomethoxycinnamic acid (OMCA)**

The CTAB/OMCA system seemed particularly attractive for us as an application of the NAP group as it offers the potential to improve on previous systems by achieving a full viscosity change cycle (low to high to low). Protection of the carboxylate with the NAP group would allow the introduction of this compound to aqueous CTAB solutions without any change in solution viscosity. Photolysis of the NAP-protected additive would subsequently release the free acid, inducing wormlike micelle formation and increasing solution viscosity. Subsequently, photoisomerization of the OMCA additive would destabilize the cylindrical micelles and reduce solution viscosity. Thus, a quasi-photorheological system could be realized.

## 6.2 Photorheological fluid design

While OMCA was used in previous studies, we chose to use the parent *trans*-cinnamic acid (tCA) additive for NAP-protection as this compound displayed similar ability to induce the formation of gels in aqueous CTAB solutions. (Figure 6-6) We decided to use the NAP group over the mPCN group for protection of the tCA carboxylate due to the propensity for mPCN-esters to form a colored impurity in neutral

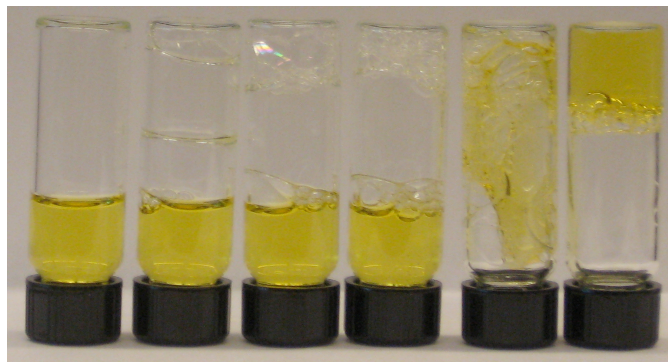


**Figure 6-6: 50 mM CTAB in H<sub>2</sub>O with varying concentrations of tCA, 0-50 mM tCA in 10 mM increments from left to right (Rubpy added for contrast)**

aqueous media which may compete for light absorption. (see Chapter 5) Additionally, gel stability in control solutions was reduced when prepared in the acidic buffer solution in which mPCN-esters are stable. Thus, the NAP-protected tCA (NAP-tCA) compound was initially prepared as the perchlorate salt as previously reported.<sup>109</sup> Unfortunately, upon addition to aqueous solutions of CTAB, NAP-tCA induced the precipitation of a white solid. Upon further investigation, it was determined that the perchlorate counterion included with NAP-tCA was likely the cause. Indeed, surfactant solutions and the formation of micelles are reportedly very sensitive to the presence of particular ions in solution.<sup>184</sup> A survey of inorganic salts added to a solution of CTAB revealed that bromide, chloride, and fluoride counterions did not cause precipitation. However, iodide, tetrafluoroborate, and perchlorate ions all generated the precipitate. Thus, we decided to synthesize the NAP group with a bromide counterion by addition of the ester precursor to bromomethane. Solutions prepared thereafter containing CTAB and NAP-tCA with a bromide counterion did not form a precipitate.

Since we desire the photoisomerization and photorelease reactions to be orthogonal to one another, the chosen sensitizer or mediator must absorb light in a different region from tCA. tCA absorbs primarily UV light (< 300 nm), therefore a visible light absorbing sensitizer would be convenient. Unfortunately, many of the visible light absorbing sensitizers that have previously been successful with the NAP group are not appreciably soluble in aqueous media. Rubpy would be a viable chromophore as it is aqueous soluble and its visible absorption band is isolated from the absorption of tCA. (Figure 6-7) DET deprotection is not a favorable pathway using the parent NAP protecting group. (see Chapter 5) However, MET deprotection using ascorbic acid

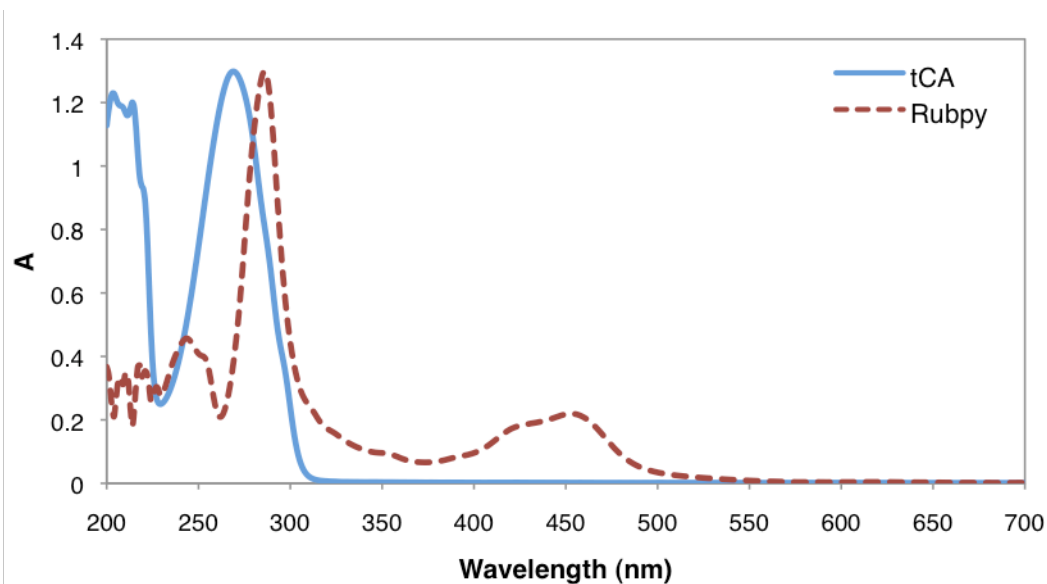


**Figure 6-7: Normalized UV-VIS spectra of tCA and Rubpy**

(ASC) as the electron donor could be utilized instead since this would be a favorable reaction according to electron transfer calculations. Therefore, we decided to explore this deprotection system for release of tCA.

Preliminary control experiments focused on verifying the formation of “stable” gels in the presence of the components required for deprotection. Solutions were prepared with 50 mM CTAB and 50 mM tCA. In general, equimolar amounts of CTAB and tCA form highly viscous gels that resist flow when inverted in sample vials. Gel stability was initially characterized qualitatively by observing the degree to which samples flowed when inverted. 50 mM CTAB and tCA was found to be a good compromise between compound solubility and stability of the gels. Stable gels formed in the presence of Rubpy even in relatively moderate concentrations (5 mM), however ASC seemed to have a destabilizing effect. While low concentrations of ASC (< 5 mM) results in stable gel formation, higher concentrations that would be required for quantitative deprotection ( $\geq$  50 mM) generally produce a viscoelastic fluid that will flow slowly when inverted. This



observation was extended to solutions containing Rubpy and ASC. CTAB also seems to impart improved solubility of these components together as tCA precipitates out of solution in the presence of ascorbic acid when control solutions lack CTAB.

Experiments to ascertain the influence of the picolinium deprotection byproduct on gel formation were unable to be performed as this compound was unavailable. Having explored some of the parameters of this system, we turned to photolysis experiments to evaluate any photoinduced changes in solution viscosity.

### **6.3 Photorelease and photoisomerization**

Initial control photolyses were performed in the absence of CTAB. Photolysis of aqueous solutions of equimolar Rubpy and NAP-tCA with broad band visible light (360 – 800 nm) resulted in 10 % consumption of NAP-tCA and a negligible amount of free tCA (as determined by HPLC). This result confirms expectations that the DET pathway is unfavorable, as determined from  $\Delta G_{ET}$  calculations. (Chapter 5) Subsequently, a solution was prepared with an excess amount of ASC, a sub-stoichiometric amount of Rubpy, and NAP-tCA for MET deprotection. Irradiation of this solution resulted in almost quantitative consumption of NAP-tCA while only a 28 % yield of free tCA was obtained. Control solutions of tCA irradiated with UV light for 2 h on a Xe arc lamp were cleanly converted to the *cis* isomer (as determined by HPLC) reaching a final *trans/cis* ratio of approximately 1/2. Solutions of NAP-tCA irradiated with UV light produced a mixture of products including the *cis* isomer of NAP-tCA and a negligible amount of free tCA. Despite the inexplicably low yield of tCA from visible photolysis, we decided to

determine if this released amount was sufficient to induce a viscosity change in the presence of CTAB.

Solutions were initially prepared with 50 mM CTAB and 50 mM NAP-tCA since equimolar amounts of surfactant and additive typically produced the highest viscosity gels in control experiments. A sub-stoichiometric amount of Rubpy (relative to NAP-tCA) was included and enough ASC was added to equal the NAP-tCA concentration. Photolysis of this solution resulted in approximately 24 % yield of free tCA despite 97 % consumption of NAP-tCA (Entry 1, Table 6-1), similar to the previous experiment without CTAB. Solution viscosity did not noticeably increase in this experiment. This is likely due to the high concentration of ASC, which was observed to hinder the formation of stable gels, as well as the low tCA/CTAB concentration ratio. (Entry 1, Table 6-2) Indeed, control experiments of only tCA and CTAB in this ratio were not appreciably viscous.

We reasoned that “pretreating” the solution with a small amount of tCA such that a smaller amount of ASC and released tCA is needed might lead to greater changes in viscosity. In fact, this strategy did lead to greater post-photolysis tCA concentrations and therefore higher viscosity after visible light irradiation. (Entries 2-5, Table 6-1) Although the change in tCA concentration was smaller than that observed for Entry 1, the ending  $[tCA]/[CTAB]$  was almost double. (Entries 2-5, Table 6-2) Solutions flowed very slowly when inverted in the cuvette. (Figure 6-8) After UV irradiation for two hours, concentrations of tCA decreased and *cis*-cinnamic acid concentrations increased. Solution viscosities decreased overall (Figure 6-8) presumably due to desorption of the

**Table 6-1: Deprotection photolysis and photoisomerization data for NAP-tCA/Rubpy/ASC PR fluid (all samples 50 mM CTAB, 30 mM ASC)**

Entry	[NAP-tCA] (mM) <sup>a</sup>	[tCA] (mM) <sup>a</sup>	[Rubpy] (mM)	Photolysis Conditions	VIS NAP-tCA Depletion <sup>a</sup> (%)	VIS [tCA] (mM) <sup>a</sup>	UV [tCA] (mM) <sup>a</sup>
1 <sup>b</sup>	51.3	-	5	3 h VIS, 2 h UV	97.0	12.1	4.3
2 <sup>c</sup>	30.7	14.2	5	2 h VIS, 2 h UV	96.7	22.0	7.9
3	31.7	14.0	2	2 h VIS, 2 h UV	97.3	18.8	5.7
4 <sup>d</sup>	29.0	19.5	2	1 h VIS, 2 h UV	94.9	28.6	9.7
5	29.5	18.6	2	10 min VIS	67.8	28.0	-

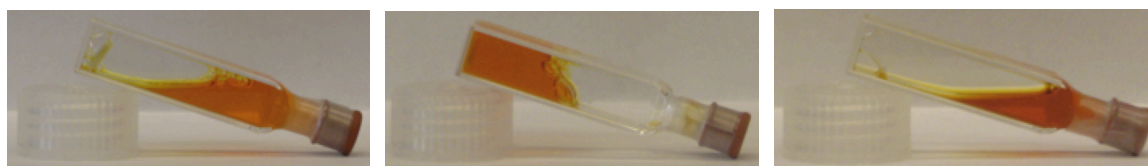
<sup>a</sup> Determined by HPLC, estimated error 5%

<sup>b</sup> Sample contains 50 mM ASC

<sup>c</sup> Average of 2 runs <sup>d</sup> Average of 4 runs

**Table 6-2: Concentration changes and ratios for NAP-tCA/Rubpy/ASC PR fluid photolysis (determined from values in Table 6-1)**

Entry	$\Delta$ [tCA] after VIS (mM)	VIS [tCA]/[CTAB]	$\Delta$ [tCA] after UV (mM)	UV [tCA]/[CTAB]
1	12.1	0.24	-7.8	0.09
2	7.8	0.44	-14.1	0.16
3	4.8	0.38	-13.1	0.11
4	9.1	0.57	-18.9	0.19
5	9.4	0.56	-	-



(a)

(b)

(c)

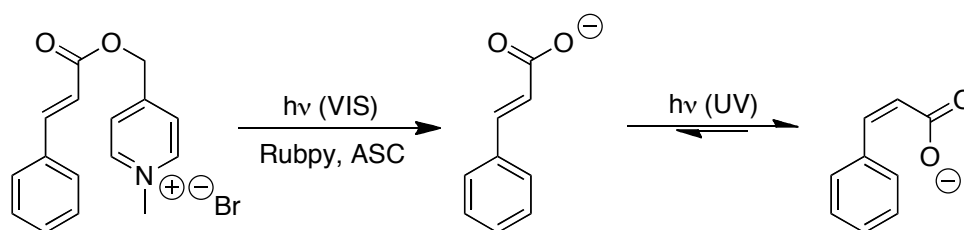


**Figure 6-8: Photoinduced viscosity changes; (a) starting solution, (b) after 1 h VIS irradiation, (c) after 2 h UV irradiation**

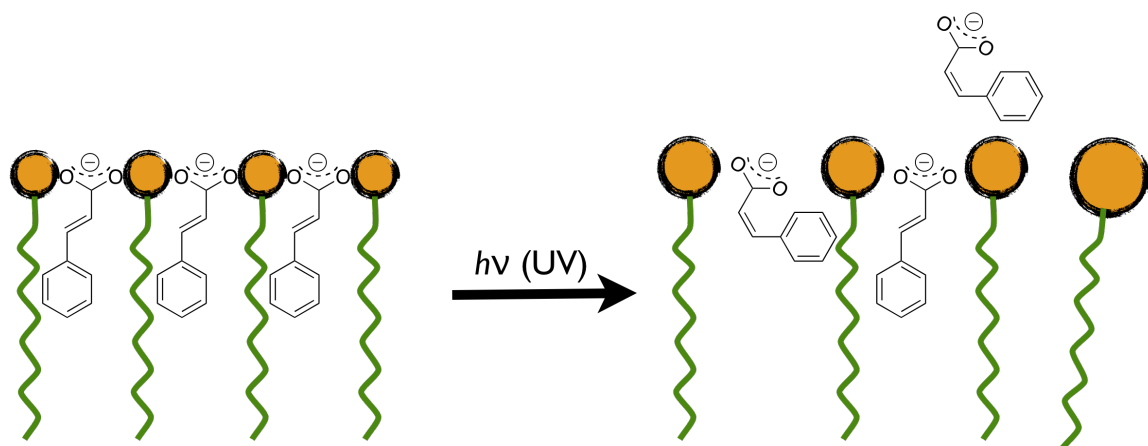


**Figure 6-9: Expected surfactant packing before and after conversion of tCA to the *cis* isomer**

cinnamic acid moieties from the area between the CTAB molecules thereby destabilizing the cylindrical micelle network. (Figure 6-9) Similar NAP-tCA consumption was observed when VIS photolysis periods were reduced to 1 h (Entry 4, Table 6-1), however, yields of free tCA were 30 % higher on average. As a result,  $[tCA]/[CTAB]$  after visible irradiation for these experiments was higher (Entry 4, Table 6-2) and viscosity changes appeared more pronounced. Interestingly, similar solutions irradiated with visible light for only 10 min exhibited similar levels of tCA concentration after photolysis (Entry 5, Table 6-1) and a similar  $[tCA]/[CTAB]$  value to 1 h irradiations despite the lower NAP-tCA consumption. (Entry 5, Table 6-2) These observations suggest that a competing photochemical process is depleting the amount of NAP-tCA or free tCA after release. Thus, longer visible irradiation periods result in less pronounced viscosity increases. Control experiments in which Rubpy was irradiated in the presence of NAP-tCA or tCA resulted in almost quantitative recovery of the starting materials. However, control experiments in which Rubpy, ASC, and tCA were photolysed in the presence of CTAB displayed a significant decrease in tCA concentration with photolysis

time. Thus, it is apparent that tCA from either “pretreatment” or released from NAP-tCA is participating in a competing photochemical reaction with Rubpy and ASC. The product of this reaction could not be detected by our HPLC setup. Studies to probe the mechanism of NAP-tCA photorelease and the side reaction will be described in a later section.

#### 6.4 Rheology

In an effort to quantify the viscosity changes observed in the photorelease and photoisomerization reactions, steady-shear rheological experiments were performed on solutions after each change. A solution prepared similar to Entry 4 in Table 6-1 and Table 6-2 was analyzed before any photolysis, after visible light photolysis, and after UV photolysis. (Figure 6-10) The starting solution behaves as a typical Newtonian fluid; viscosity does not change with increasing shear rate. After visible light photolysis,

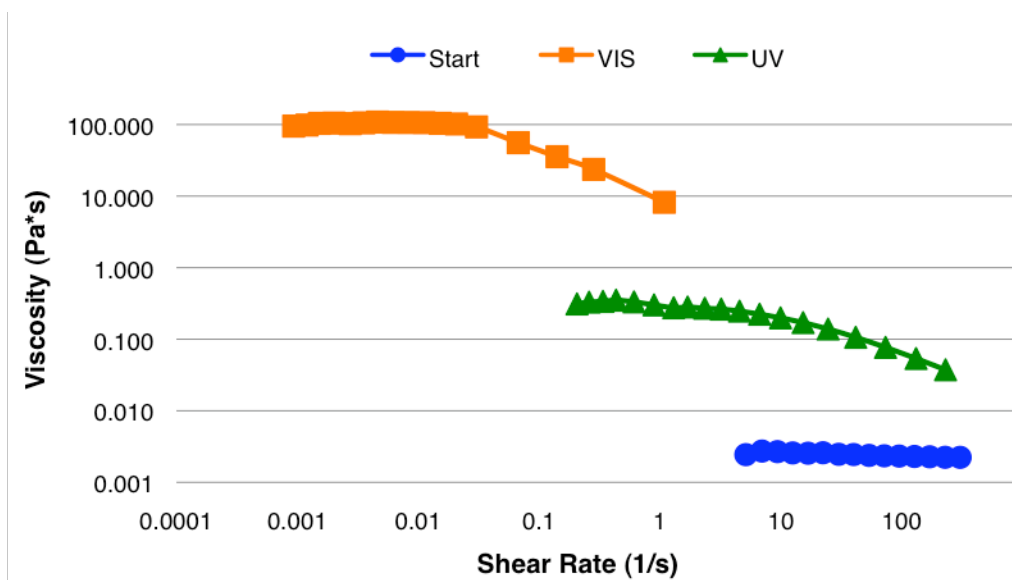


**Figure 6-10: Steady-shear rheology of a solution from Entry 4, Table 6-1**

solution viscosity at low shear rates increases by approximately five orders of magnitude. Additionally, this fluid exhibits shear-thinning behavior, indicated by the drop in viscosity at higher shear rates. This is an expected characteristic of viscoelastic fluids.<sup>182,183</sup> Subsequent UV photolysis of the viscoelastic fluid results in a decrease in solution viscosity by approximately two and a half orders of magnitude at low shear rates. This fluid still exhibits a degree of shear-thinning behavior and is noticeably more viscous than the starting solution. Nevertheless, this solution flows much more readily than the highly viscous solution after visible light irradiation. The observed increase and decrease in viscosity are comparable to changes observed in the two separate systems developed by Raghavan et al.<sup>182,183</sup>

The rheology experiments were repeated with the inclusion of an additional viscosity measurement after an aliquot was irradiated for 2 h with visible light. This additional time point was performed in an effort to correlate the observed drop in tCA yield over prolonged visible light irradiation to a drop in viscosity. As seen in Figure 6-11, solution viscosity increases by approximately four orders of magnitude at low shear rates between the starting solution and after 1 h visible light irradiation and subsequently drops after 2 h irradiation. Thus, over the course of the visible light irradiation period, solution viscosity most likely reaches a maximum coincident with the maximum in tCA concentration. After this maximum is reached, further photolysis results in a diminishment of the tCA concentration from the side reaction(s) thereby reducing solution viscosity.

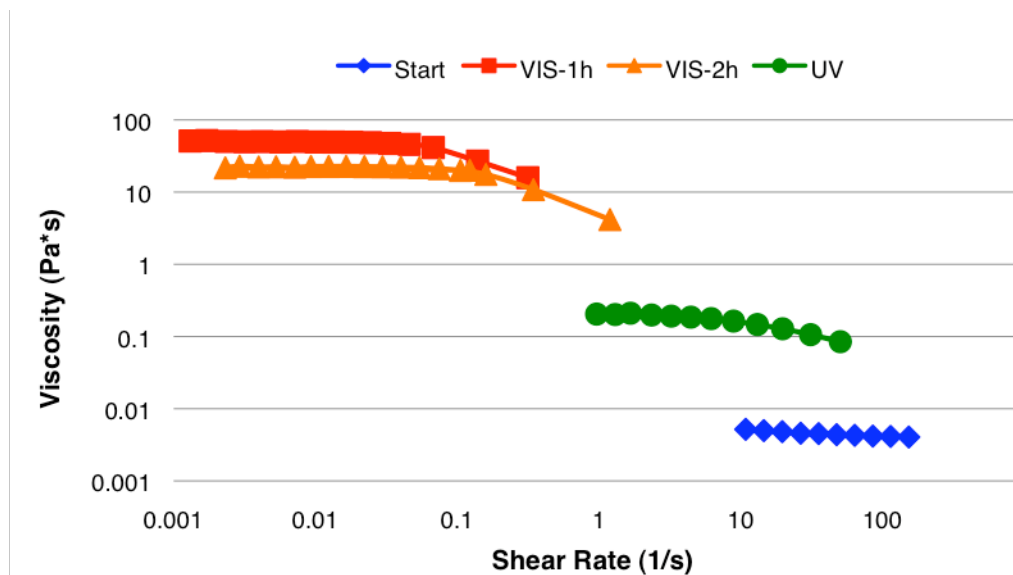


**Figure 6-11: Steady-shear rheology of a solution from Entry 4, Table 6-1 with additional VIS irradiation**

### 6.5 Mechanistic studies

Experiments to ascertain the success of the desired electron transfer reactions and gather information about the side reaction(s) were performed. Previous studies have shown the effective quenching of Rubpy<sup>2+\*</sup> by ASC to generate Rubpy<sup>1+</sup>. (see Chapter 5) Confirming deprotection photolysis experiments, Rubpy luminescence was not quenched with added tCA. Thus, since both the productive release of tCA from NAP-tCA and the side reaction with tCA appear to occur from Rubpy<sup>1+</sup>, we turned to laser flash photolysis quenching studies.

LFP solutions were prepared with a fixed amount of Rubpy and a large excess of ASC (steady-state) to ensure adequate production of Rubpy<sup>1+</sup>. Each solution contained

50 mM CTAB to ensure full solubility of ASC and tCA, however 10 % MeOH was added to inhibit the formation of micelles. Increasing amounts of Rubpy<sup>1+</sup> quencher (NAP-tCA or tCA) were added to these solutions and the growth and decay of Rubpy<sup>1+</sup> was monitored at 510 nm. Traces were fit to a model function containing exponential growth and decay terms with an added baseline correction term. (Eq 6-2)

$$O.D. = A + OD_0 \left( \frac{k_1}{k_2 - k_1} \right) (e^{-k_1 t} - e^{-k_2 t}) \quad (6-2)$$

Both tCA and NAP-tCA were observed to quench the signal from Rubpy<sup>1+</sup> (Figure 6-12), indicating that electron transfer from Rubpy<sup>1+</sup> to either compound is possible.

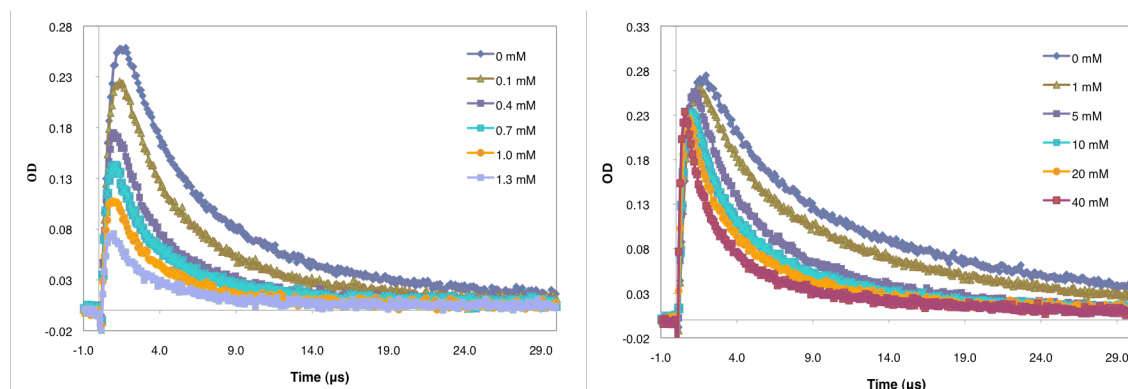


**Figure 6-12: Time-dependent absorption traces from 532 nm pulsed laser photolysis of Rubpy, ASC, and varying concentrations of (LEFT) NAP-tCA or (RIGHT) tCA, monitored at 510 nm**

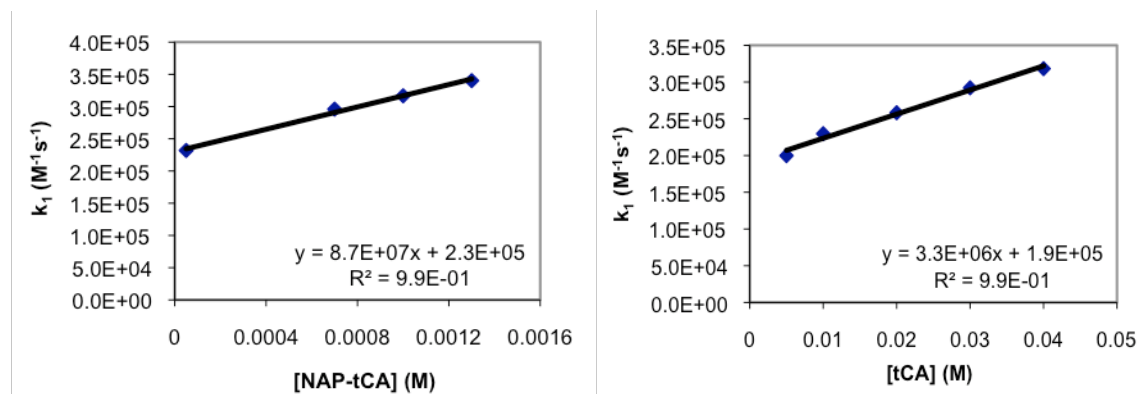


**Figure 6-13:  $k_1$  versus (LEFT) [NAP-tCA] or (RIGHT) [tCA] for LFP of Rubpy + ASC + quencher, monitored at 510 nm**



The decay rate constants ( $k_I$ ) for each of the curves were plotted versus quencher concentration to determine the quenching rate constant of each process. (Figure 6-13) The electron transfer process to NAP-tCA ( $k_I = 9 \times 10^7 \text{ M}^{-1}\text{s}^{-1}$ ) is apparently an order of magnitude greater than electron transfer to tCA ( $k_I = 3 \times 10^6 \text{ M}^{-1}\text{s}^{-1}$ ). Thus, electron transfer to NAP-tCA is the dominant process, however, an order of magnitude smaller difference in  $k_I$  for quenching of Rubpy<sup>1+</sup> by tCA indicates that this process is still fairly competitive when present in significant concentrations. It is likely that electron transfer to tCA is the dominant process leading to diminishment in tCA concentration during prolonged irradiation periods. However, the identities of the final products as a result of this process are unclear.

## 6.6 Conclusions

A quasi-reversible photorheological fluid has been created based on visible-light photorelease and UV light photoisomerization. A five order of magnitude increase in solution viscosity at low shear rates is obtainable after visible light irradiation and subsequent decrease by two and a half orders of magnitude is realized after UV irradiation. These changes are comparable to those observed in two separate systems created by Raghavan et al., yet they are presently combined into one system to achieve a full viscosity change cycle. The solution viscosity increase was confirmed to be directly related to the amount of tCA present. Unfortunately, the photochemical depletion of tCA induced by ASC and Rubpy is a competitive process, but high solution viscosities can still be realized with sufficiently short irradiation periods. Further improvements may

include the use of a gelation additive that is a poorer electron acceptor than tCA such that additive degradation can be avoided. Additional options for photorelease of gelation-inducing additives have been explored, including release from AuNP surfaces. (see Appendix B) While the current system is limited in that only one full viscosity cycle is possible, it nevertheless represents a convenient, orthogonal means of changing viscosity using two distinct irradiation wavelength ranges. From a broader perspective, the NAP group has been used for controlled photorelease of a functional molecule that participates in a larger chemical system, demonstrating its more general applicability.

## 7 Conclusions

Photoremovable protecting groups continue to offer a convenient means of releasing functional molecules for applications in chemical synthesis, biological studies, and materials science. Since potentially detrimental acidic or basic reagents are unnecessary, PRPGs offer a milder means of deprotecting certain functionalities. Additionally, the ability to direct light at specific locations offers spatial control over deprotection such that specific patterns may be obtained on reactive surfaces. Direct deprotection PRPGs have demonstrated their great utility but suffer from a number of undesirable qualities. Most of these groups absorb UV light and structural modifications to shift their absorption often have the unfortunate consequence of altering bond breaking efficiencies. Additionally, these groups have limited aqueous compatibility.

Photoinduced electron transfer based PRPGs (PET-PRPGs) offer several advantages over direct deprotection PRPGs as the light absorption and bond breaking processes are not electronically coupled. Thus, chromophores can be designed to absorb light at a variety of wavelengths so long as PET quenching of the PET-PRPG is still effective. This strategy has been successfully demonstrated with several PET-PRPGs, most notably the *N*-alkylpicolinium (NAP) group for protection of carboxylate anions. Release of the free substrate has been previously demonstrated using UV and VIS absorbing sensitizers. Additionally, mediated electron transfer (MET) was explored in which a good electron donor acts as a source of electrons for the sensitizer to shuttle to the NAP group. In these preliminary studies, MET demonstrated high quantum yields of release.

In an effort to build upon the success of the NAP MET deprotection strategy, we endeavored to meet several challenges to improve mediated photorelease:

- 1) Extend MET deprotection to visible light absorbing mediators
- 2) Improve photolytic efficacies ( $\Phi_{relE\lambda}$ )
- 3) Demonstrate that sub-stoichiometric amounts of mediator can initiate effective photorelease
- 4) Demonstrate MET release of NAP-protected substrates in aqueous media
- 5) Extend the applicability of the NAP group to a wide range of visible light absorbing sensitizers
- 6) Demonstrate the broader utility of the NAP group through the photorelease of a functional molecule into a larger chemical system

Each of these goals has been addressed in the work described in the preceding chapters. All of the sensitizers employed in this research have significant absorption in the visible and were successful, to varying degrees, in releasing protected substrates by a MET mechanism. Sub-stoichiometric amounts of sensitizer were used in each case. While the ketocoumarin dyes proved effective in photorelease of NAP-protected compounds in organic media, they suffered from significant degradation over prolonged irradiation. The extension of photorelease to aqueous systems was initially accomplished using visible light absorbing tryptophan-functionalized gold nanoparticles (TRP-AuNP) as mediators. This system demonstrated fast rates of release and very high quantum efficiencies using significantly sub-stoichiometric amounts of TRP-AuNP. The use of Rubpy as a mediator in conjunction with the modified NAP group offers several advantages over the aforementioned systems, namely, increased stability over long

irradiation periods and aqueous compatibility. Additionally, the modified NAP group should allow a broader range of mediators to be employed in these deprotection reactions, including many robust metal-centered complexes. Unfortunately, this system as currently designed must be kept in acidic media to ensure that undesirable byproducts are not formed. Finally, the NAP group has been successfully applied to generate a quasi-reversible photorheological fluid. Similar to applications employing other PRPGs, a higher order response (wormlike micelle formation) is inhibited while NAP-protection is maintained. Upon photorelease of the NAP group with visible light, a large increase in solution viscosity is observed when in the presence of CTAB. Thus, the expected system behavior is restored upon photorelease. Subsequent UV photolysis of the system reduces solution viscosity. This system also has been designed around MET and is aqueous compatible. Thus, all of the goals of this work have been met.

Comparison of the presently developed MET deprotection systems (Table 7-1) with previously designed “champion” MET and DET systems (Table 2-1) demonstrates the improvements developed. Irradiation wavelengths have been shifted substantially into the visible. Photolytic efficacies,  $\Phi_{rel}\epsilon_{\lambda}$ , are comparable to previous visible light DET systems, but substantially improved over previous MET systems. The lower  $\Phi_{rel}$  values obtained for the newer mediators are generally offset by the high molar extinction coefficients ( $\epsilon$ ) of the dyes. Additionally, the fact that sub-stoichiometric amounts of

**Table 7-1: Comparison of photolytic efficiencies and efficacies of studied MET PET-PRPG deprotection reactions**

Mediator	$\lambda_{ex}$ (nm)	$\Phi_{rel}$	$\epsilon_{\lambda}$	$\Phi_{rel}\epsilon_{\lambda}$
DEATC	420 <sup>a</sup>	0.050 <sup>a</sup>	33500 <sup>a</sup>	1675
CBDAC	460 <sup>a</sup>	0.023 <sup>a</sup>	91739 <sup>a</sup>	2110
TRP-AuNP	525 <sup>b</sup>	> 1 <sup>b</sup>	-	-
Rubpy	455 <sup>a</sup>	0.020 <sup>c</sup>	13000 <sup>a</sup>	260

<sup>a</sup>In MeCN

<sup>b</sup>In H<sub>2</sub>O

<sup>c</sup>In MeCN/MeOH (1/1)

mediator have been used in all cases and that gold nanoparticles and Rubpy have been incorporated into an aqueous compatible MET deprotection system represent significant advancements. The photolytic efficacies in Table 7-1 are also improved or comparable to those in Table 1-1 for the direct photolysis PRPGs. Excitation wavelengths used in the current systems are much longer than those required for the discussed direct photolysis PRPGs.

The use of low energy visible light to initiate PRPG deprotection in aqueous compatible systems will undoubtedly be useful in a number of applications. Furthermore, the use of sub-stoichiometric amounts of the sensitizer will facilitate conservation of potentially costly chromophores. With proper refinement and improvements in stability for some of the previously described systems, visible light MET photorelease should be adaptable to a number of important biological and materials science applications.

## 8 Experimental Section

### 8.1 General procedures

All  $^1\text{H}$  and  $^{13}\text{C}$  NMR were obtained on a Bruker 400 MHz spectrometer. Chemical shifts ( $\delta$ ) are referenced to TMS. Thin-layer chromatography (TLC) was performed on Merck silica-coated glass plates. Compounds were visualized under 254 nm UV irradiation or by treatment with  $\text{I}_2$ . All flash chromatography was carried out using Silicycle Silia-P Flash Silica Gel (60 Å pore diameter, 40-63  $\mu\text{m}$  particle size). UV-VIS spectra were obtained on a Perkin-Elmer Lambda 2S spectrophotometer. IR spectra were recorded on a Thermo Nicolet IR200 spectrometer. High pressure liquid chromatograph (HPLC) chromatograms were obtained on a dual Rainin HPXL pump system equipped with a  $\text{C}_{18}$  reversed-phase column and UV-VIS detector. Elution programs and solvent systems are described in the each respective section. Rheological studies were performed on a TA Instruments AR2000 stress controlled rheometer using a 20 mm couette geometry, maintained at 20° C by a Peltier-based temperature controller.

### 8.2 Cyclic voltammetry experiments

All electrochemical experiments were performed on a voltammetric analyzer with  $[\text{Bu}_4\text{N}][\text{PF}_6]$  as the supporting electrolyte. A carbon working electrode, a platinum auxiliary electrode, and an Ag/AgCl reference electrode were used to take measurements. The voltammograms were taken at a scan rate of 100 mV/s in dry acetonitrile after purging with nitrogen for 15 min. Measurements were taken in reference to the ferrocene/ferrocenium couple found at ca. 536 mV vs SCE.

### **8.3 Luminescence quenching**

Luminescence quenching experiments were performed using a luminescence spectrometer. Samples were prepared in a 1 cm quartz cuvette, sealed with a rubber septum, and purged with N<sub>2</sub> for 10 min. Samples containing Rubpy and DMA or DABCO were prepared in acetonitrile. Samples containing Rubpy and ASC or an mPCN-ester were prepared in 0.5 M acetate buffer (pH 4.0). Sensitizer concentrations were prepared such that the optical density of the sensitizer at the excitation wavelength was between 0.1 and 0.3. Quencher concentrations were prepared such that a linear relationship was obtained with respect to  $I^{\circ}/I$ .

### **8.4 Laser flash photolysis**

The prepared samples were placed in a 1 cm quartz cuvette and sealed with a rubber septum. Samples were stirred continuously during photolysis. Full transient spectra were obtained using a flow-cell setup to continuously refresh the photolysis solution over the course of the experiment. An Nd:YAG laser capable of 532, 355, and 266 nm pulses between 4-6 ns duration was used as the excitation source. A 350 W Xe arc lamp was used as the probe beam passed through a monochromator to a PMT detector. A 350 MHz digital oscilloscope was used to observe the traces which were subsequently recorded on a personal computer by a LabView data acquisition program. Growth and decay curves were fit to functions using the MathCAD software package.



#### **8.4.1 Ketocoumarin dyes**

Samples were prepared in anhydrous, distilled acetonitrile such that the optical density at the excitation wavelength, 355 nm, was 1-2. Samples were purged with N<sub>2</sub> for 10 min prior to photolysis.

#### **8.4.2 mPCN-esters**

Samples containing DMA or DABCO were prepared in anhydrous, distilled acetonitrile and those containing ASC were prepared in deionized water. Sufficient Rubpy was added such that the optical density at the excitation wavelength, 532 nm, was 0.1-0.5. Samples were purged with N<sub>2</sub> for 10 min prior to photolysis.

#### **8.4.3 Photorheological fluid**

Samples were prepared in deionized water containing 10% MeOH and sufficient Rubpy was added such that the optical density at the excitation wavelength, 532 nm, was 0.5-0.6.

### **8.5 Deprotection photolysis**

#### **8.5.1 Ketocoumarin dye photolysis**

*Materials.* 7-Diethylamino-3-thenoylcoumarin (DEATC), *N,N*-dimethylaniline (DMA), triphenylamine (TPA), 1,4-cyclohexadiene (CHD) were used as received from commercial sources. 3,3'-Carbonylbis(7-dithylaminocoumarin) (CBDAC) was prepared following previously reported procedures.<sup>119</sup>

*Methods.* A solution of 5-10 mg of the NAP-ester, an excess of the donor (at least 2 equivalents), and varying concentrations of the mediator was prepared in 5 mL acetonitrile and 1 mL of 1,4-cyclohexadiene was added. A 2 mL aliquot from this

solution was used as a dark control. Another 2 mL aliquot was transferred into a pyrex test-tube and purged with nitrogen for 15 min. The solution was irradiated by a 300 W tungsten-filament lamp with continuous stirring. The solvent in the photolyzed solution was evaporated and the residue redissolved in CD<sub>3</sub>CN with hexamethyldisiloxane or tetramethylsilane as the internal standard. Percent yields were determined by <sup>1</sup>H NMR integration of the resonance produced by the methylene protons α to the carbonyl, relative to the internal standard.

## 8.5.2 Gold nanoparticle photolysis

### 8.5.2.1 Citrate-stabilized AuNPs

*Materials.* *N*-Methylpicoliniumphenyl acetate (**1**) was synthesized as previously reported.<sup>109</sup> 16 nm citrate-stabilized gold nanoparticles were prepared as previously reported and confirmed by TEM and UV-VIS.<sup>130</sup> DL-Dithiothreitol was used as received from Acros.

*Methods.* Depending on final desired concentrations, **1** (3-10 mg) was dissolved in 50 μL MeCN and the solution was combined with dithiothreitol (0.07-0.08 g) dissolved in 0.95 mL D<sub>2</sub>O. Varying volumes of the starting material mixture and the nanoparticle solution were combined and diluted with D<sub>2</sub>O containing *tert*-butyl alcohol as an internal standard to a total volume of 0.8 mL. A duplicate mixture was created to use as a dark control. The solution was purged with nitrogen for 10 min and irradiated with a 300 W tungsten-filament lamp for a set amount of time. The mixture was then directly analyzed by <sup>1</sup>H NMR and deprotection yields were determined by integration of the aromatic protons of the released picolinium group relative to the internal standard. Yields were confirmed by HPLC analysis. Isocratic elution using a 3/1 phosphate buffer(50 mM, pH 4.0)/water

solvent mixture was sufficient to resolve the starting material and free acid peaks, monitored at 254 nm. Yields were calculated relative to the amount of unreacted *I* detected in the dark control samples.

#### **8.5.2.2 Tryptophan-functionalized gold nanoparticles (TRP-AuNP)**

*Materials.* TRP-AuNP were prepared as described in the Synthesis section.

*Methods.* *I* (3-10 mg) was dissolved in 50  $\mu$ L acetonitrile and the solution was combined with dithiothreitol (0.03-0.08 g) dissolved in 0.95 mL phosphate buffer (50 mM, pH 7.0). Varying volumes of the starting material mixture and the TRP-AuNP solution were combined and diluted with additional phosphate buffer to a total volume of 0.8 mL. A duplicate mixture was created to use as a dark control. The solution was purged with nitrogen for 10 min and irradiated with a 300 W tungsten-filament lamp for a set amount of time. Yields were determined by HPLC analysis. Isocratic elution using a 3/1 phosphate buffer(50 mM, pH 4.0)/water solvent mixture was sufficient to resolve the starting material and free acid peaks, monitored at 254 nm. Yields were calculated relative to the amount of unreacted *I* detected in the dark control samples.

#### **8.5.3 mPCN photolysis**

*Materials.* mPCN-esters were prepared as described in the Synthesis section. Tris(2,2'-bipyridyl)ruthenium(II) chloride hexahydrate (Rubpy) was used as received from Strem Chemicals. Ascorbic acid, *N,N*-dimethylaniline (DMA), and 1,4-diazabicyclo[2.2.2]octane (DABCO) were used as received from commercial sources.

*Methods.* A solution containing 0.6 – 4.8 mM mPCN-ester and 0.024 – 4.8 mM Rubpy was prepared in 5 mL MeOH/MeCN (1/1) when using the tetrafluoroborate salts and in 5 mL 0.5 M acetate buffer at pH 4.0 when using the triflate salts. In mediated photolysis experiments, a sufficient amount of donor was added to these solutions to produce the required concentrations. An aliquot of the solution was set aside as a dark control and a 2 mL aliquot was put in a thermostated water-jacketed test tube that was sealed with a rubber septum and purged with N<sub>2</sub> for 10 min. The solution was irradiated for various periods of time with continuous stirring and maintained at 20° C (+/- 1°). The irradiation source consists of a 300 W tungsten/halogen lamp the output of which is passed through a 330 nm cutoff filter and a Kopp 7093 IR-absorbing filter to ensure visible-light irradiation only. Dark control and irradiated sample mixtures were analyzed by HPLC. Gradient elution using an acetonitrile/acetate buffer (100 mM, pH 4.0) mixture that adjusts from 25% MeCN to 70 % MeCN over 20 min at a flow rate of 0.5 mL/min was sufficient to resolve the starting material and free acid peaks, monitored at 254 nm. Yields of free acid in the irradiated samples were calculated relative to the amount of unreacted ester plus any amount of free acid detected in the dark control sample.

## **8.6 Photorheological fluid photolysis**

*Materials.* NAP-tCA was prepared as described in the Synthesis section. Tris(2,2'-bipyridyl)ruthenium(II) chloride hexahydrate (Rubpy) was used as received from Strem Chemicals. Ascorbic acid (ASC), cetyltrimethylammonium bromide (CTAB), *trans*-cinnamic acid (tCA) were used as received from commercial sources.

*Methods.* Photolysis solutions were prepared containing 50 mM CTAB, 0-20 mM tCA, 30-50 mM ASC, and 2-5 mM Rubpy in deionized water. tCA was prepared in these solutions through dilution of a stock solution of equimolar tCA and sodium hydroxide in deionized water. 500  $\mu$ L of the photolysis stock was set aside in the dark as a control. The remaining amount was added to a 1 cm quartz cuvette fitted with a rubber septum. The solution was irradiated for prescribed periods of time with constant stirring by a 300 W tungsten/halogen lamp the output of which is passed through a 360 nm cutoff filter and a Kopp 7093 IR-absorbing filter to ensure visible-light irradiation only. UV photolysis of solutions was performed with constant stirring using the unfiltered output of a 350 W Xe arc lamp. Aliquots of the dark control, visible irradiated, and UV irradiated samples were removed at the appropriate time for HPLC analysis. Prior to injection, samples were diluted with MeOH/MeCN (1/1) to disrupt any self-assembly in the solutions. Gradient elution using an acetonitrile/acetate buffer (100 mM, pH 4.0) mixture that adjusts from 25% acetonitrile to 70 % acetonitrile over 20 min at a flow rate of 0.5 mL/min was sufficient to resolve the starting material and *cis* and *trans* isomers of the free acid, monitored at 254 nm.

#### **8.7 Quantum yield determination**

Solutions were irradiated with the light output from a 1000 W Hg-Xe lamp passed through a spectral energy monochromator with a 10 nm bandpass, set at the  $\lambda_{max}$  of the sensitizer. Solutions were prepared as optically thick samples (optical density greater than 3) using a substoichiometric amount of sensitizer and a large excess of donor, where applicable. Samples were placed in a 1 cm quartz cuvette and purged with nitrogen for

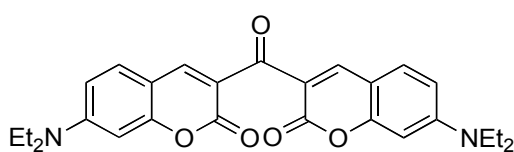
10 min. A variety of irradiation periods were selected such that deprotection yields fell below 30%. Deprotection yields were determined by  $^1\text{H}$  NMR or HPLC analysis as described for the deprotection photolysis experiments. Light intensities were measured by a radiometer calibrated by ferrioxalate actinometry.

## 8.8 Synthesis

### 8.8.1 NAP-Esters

NAP-esters **1**, **2**, and **3** were used as previously prepared or synthesized based on reported procedures.<sup>109</sup>

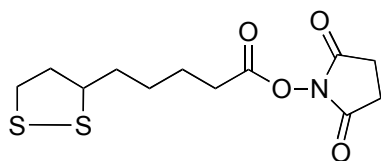
### 8.8.2 CBDAC



**3,3'-carbonylbis(7-diethylaminocoumarin)**  
**(CBDAC)**

CBDAC was prepared according to published procedures.<sup>119</sup> **Mp** 114-115 °C;  $^1\text{H}$  NMR ( $\text{CDCl}_3$ )  $\delta$  1.23 (t,  $J = 7.1$  Hz, 12H), 3.44 (q,  $J = 7.1$  Hz, 8H), 6.49 (s, 2H), 6.60 (dd,  $J = 8.9$  Hz,  $J = 2.4$  Hz, 2H), 7.38 (d,  $J = 8.9$  Hz, 2H), 8.16 (s, 2H);  $^{13}\text{C}$  NMR ( $\text{CDCl}_3$ )  $\delta$  12.5, 45.1, 97.2, 108.4, 109.4, 120.3, 131.1, 145.8, 152.3, 158.2, 160.4, 188.6 **UV-VIS** (benzene)  $\lambda_{\text{max}} = 450$  nm.  $^1\text{H}$  NMR, melting point, and UV-VIS data match published values.

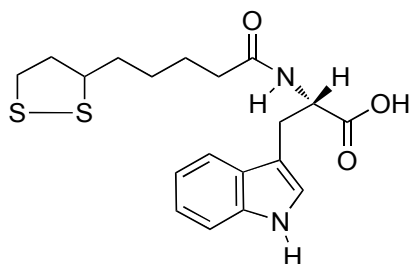
### 8.8.3 TRP-AuNP



**Thioctic ester**

A solution of thioctic acid (2.62 mmol, 0.540 g), *N*-

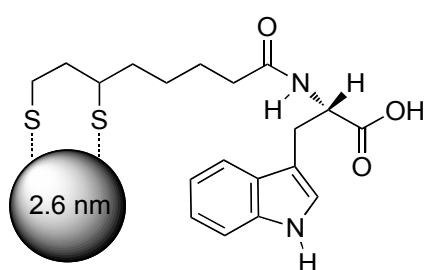
hydroxy succinimide (2.88 mmol, 0.330 g), 1-ethyl-3-(3-dimethylaminopropyl)-carbodiimide hydrochloride (2.88 mmol, 0.550 g) in anhydrous DMF (10 mL) was stirred at room temperature for 4 h under nitrogen atmosphere. The solution was diluted with EtOAc (50 mL) and washed with H<sub>2</sub>O (50 mL), sat. aq. NaHCO<sub>3</sub> (50 mL), and H<sub>2</sub>O (50 mL x 2). The organic layer was dried over MgSO<sub>4</sub>, filtered off, and concentrated in vacuo. Purification by recrystallization (EtOAc/hexane) afforded 0.768 g (97%) of the thioctic ester as light yellow crystals. **TLC** *R*<sub>f</sub>=0.46 (EtOAc/hexane, 1/1); **Mp** 93-94 °C; **<sup>1</sup>H NMR** (CDCl<sub>3</sub>) δ 1.52-1.62 (m, 3H), 1.69-1.83 (m, 3H), 1.93 (m, *J* = 6.8 Hz, 1H), 2.48 (m, *J* = 6.5 Hz, 1H), 2.63 (m, *J* = 7.4 Hz, 2H), 2.84 (s, 4H), 3.09-3.22 (m, 2H), 3.58 (q, *J* = 6.5 Hz, 1H); **<sup>13</sup>C NMR** (CDCl<sub>3</sub>) δ 24.4, 25.6, 28.3, 30.8, 34.4, 38.5, 40.2, 56.1, 168.4, 169.1



#### **Tryptophan conjugate (TRP-conj)**

To a solution of L-tryptophan (0.25 mmol, 0.052 g) in HEPES buffer (20 mM, pH = 7.4, 15 mL) was added a solution of the thioctic ester (0.33 mmol, 0.10 g) in acetone (15 mL) which was stirred at room temperature for 1 d (adjusted pH to around 7 with 0.2 M aq. NaOH after 4 h). The pH of the solution was adjusted to around 9 with 0.2 M aq. NaOH and washed with EtOAc (2x30 mL). The aqueous layer was acidified to around pH 3 with 0.2 M aq. HCl and extracted with EtOAc (2x30 mL). The organic layers were combined and washed with H<sub>2</sub>O (1x30 mL), brine (1x30 mL), and dried over MgSO<sub>4</sub>, filtered off, and concentrated in vacuo. Purification by column chromatography (CH<sub>2</sub>Cl<sub>2</sub>/MeOH, 10/1) afforded 0.064 mg (64%) of tryptophan conjugate (TRP-conj) as a

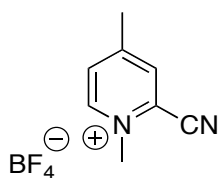
light yellow solid:  $R_f=0.23$  (MeOH/CH<sub>2</sub>Cl<sub>2</sub>, 1/10); <sup>1</sup>H NMR (CDCl<sub>3</sub>)  $\delta$  1.20-1.30 (m, 3H), 1.44-1.53 (m, 3H), 1.75-1.81 (m, 1H), 2.06 (t,  $J = 7.2$  Hz, 2H), 2.27-2.38 (m, 1H), 3.00-3.13 (m, 2H), 3.24-3.43 (m, 3H), 4.90 (q,  $J = 5.6$  Hz, 1H), 6.32 (d,  $J = 7.2$ , 1H), 6.96 (s, 1H), 7.07 (t,  $J = 7.6$ , 1H), 7.15 (t,  $J = 7.2$ , 1H), 7.30 (d, 8.1 Hz, 1H), 7.52 (d,  $J = 7.8$  Hz, 1H), 8.57 (s, 1H); <sup>13</sup>C NMR (CDCl<sub>3</sub>)  $\delta$  25.1, 27.1, 28.6, 34.4, 36.0, 38.4, 40.2, 53.4, 56.4, 109.4, 111.5, 118.4, 119.6, 122.1, 123.3, 127.7, 136.1, 174.1, 175.3



### Tryptophan-functionalized AuNPs (TRP-AuNP)

To a solution of 2.6 nm citrate-stabilized gold nanoparticles (10 mL), prepared from literature procedures,<sup>131</sup> was added 1 mL TRP-conj solution (0.015 M in 20 mM pH 7.4 HEPES buffer) and stirred for 1 d at room temperature. Removal of unbound tryptophan-conjugate was accomplished by filtration of the product mixture solution through a Millipore Centriplus YM-30 size-exclusion filter. The nanoparticles were washed with 0.2 M aq. NaOH and filtered again. Final nanoparticle solutions were obtained by dissolving the filtered nanoparticles in an appropriate amount of phosphate buffer (50 mM, pH = 7.0). Functionalization was confirmed by UV-VIS and fluorescence spectroscopy.

### 8.8.4 mPCN-Esters

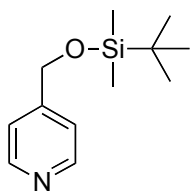


#### *N*,4-dimethyl-2-pyridinecarbonitrile (mPCN Model Compound)

4-methyl-2-pyridinecarbonitrile (0.25 g, 2.1 mmol) is dissolved in acetone (25 mL) to which trimethyloxonium tetrafluoroborate (0.62 g,



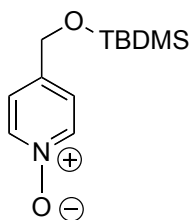
4.2 mmol) is added. The mixture is stirred at room temperature overnight. TLC (1/1 EtOAc/hexanes) after 17 h showed no visible amount of starting material. The solvent is removed *in vacuo* and the red residue is recrystallized from hot dichloromethane/acetone (3/1) to afford colorless crystals (0.27 g, 59%). **Mp** 146 °C; **<sup>1</sup>H NMR** (CD<sub>3</sub>CN) δ 2.68 (s, 3H), 4.39 (s, 3H), 8.07 (d, *J* = 5.9 Hz, 1H), 8.34 (d, *J* = 1.1 Hz, 1H), 8.72 (d, *J* = 6.3 Hz, 1H); **<sup>13</sup>C NMR** (CD<sub>3</sub>CN) δ 22.3, 48.9, 111.5, 127.6, 132.9, 135.7, 149.0, 162.5; **IR** (neat) 3069, 1634, 1584, 1523, 1460, 1302, 1270, 1203, 1031, 853, 727; **HRMS (ESI+)** calculated for [C<sub>8</sub>H<sub>9</sub>N<sub>2</sub>]<sup>+</sup> 133.0760, found 133.0764



**4-[(*tert*-Butyldimethylsilyloxy)methyl]pyridine (i)**

Imidazole (14.0 g, 206.2 mmol) is dissolved in a minimal amount of anhydrous DMF/DCM (9/1). *tert*-Butyldimethylsilyl chloride (24.9 g, 164.9 mmol) is added slowly and the mixture is allowed to stir for 10 minutes under nitrogen atmosphere. 4-Pyridylcarbinol (15.0 g, 137.5 mmol) dissolved in a minimal amount of solvent is added slowly and the mixture is allowed to stir overnight at room temperature. After 13 h, TLC (1/1 EtOAc/hexanes) showed no visible amount of starting material. The solvent is removed by vacuum distillation and 200 mL millipore water is added. Subsequent extraction with EtOAc/hexanes (1/1, 2x 200 mL) and concentration *in vacuo* yields the product as a light yellow oil (30.23g, 99 %). The product was not purified further, as it appears pure by <sup>1</sup>H NMR. **TLC** *R<sub>f</sub>* = 0.6 (EtOAc/hexanes, 1/1); **<sup>1</sup>H NMR** (CDCl<sub>3</sub>) δ 0.12 (s, 6H), 0.96 (s, 9H), 4.74 (s, 2H), 7.24 (d, *J* = 5.9 Hz, 2H), 8.54 (dd, *J* = 4.5 Hz, *J* = 1.6 Hz, 2H); **<sup>13</sup>C NMR** (CDCl<sub>3</sub>) δ -5.4, 18.4, 25.9, 63.5, 120.6,

149.6, 150.5; **HRMS (ESI+)** calculated for  $[C_{12}H_{22}NOSi]^+$  224.1480 (M+H)<sup>+</sup>, found 224.1471. <sup>1</sup>H NMR data are in agreement with previously reported spectra.<sup>145</sup>



**4-[(*tert*-Butyldimethylsilyloxy)methyl]pyridine *N*-oxide (*ii*)**

Compound *i* (32.0 g, 143.4 mmol) is dissolved in anhydrous DCM (250 mL). 70% mCPBA (45.95 g, 186.4 mmol) is added slowly and the mixture is stirred at room temperature for 24 h. TLC (1/1,

EtOAc/hexanes) after 24 h showed no visible amount of starting material. The solution is washed with 1 M NaOH (1x500 mL), separated, and dried over anhydrous Na<sub>2</sub>SO<sub>4</sub>.

Evaporation of the solvent yields a white amorphous solid (26.1 g, 76%) which was used without further purification. **TLC** *R*<sub>f</sub> = 0.1 (EtOAc/hexanes, 1/1); **<sup>1</sup>H NMR** (CDCl<sub>3</sub>) δ

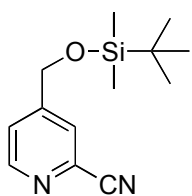
0.12 (s, 6H), 0.95 (s, 9H), 4.71 (s, 2H), 7.24 (d, *J* = 7.0 Hz, 2H), 8.18 (d, *J* = 7.0 Hz, 2H);

**<sup>13</sup>C NMR** (CDCl<sub>3</sub>) δ -5.4, 18.3, 25.8, 62.8, 123.1, 138.9, 141.0; **IR** (neat) 3102, 2955,

2930, 1856, 1488, 1472, 1444, 1372, 1251, 1210, 1170, 1104, 1067, 1007, 890, 833, 760,

698, 664 cm<sup>-1</sup>; **HRMS (ESI+)** calculated for  $[C_{12}H_{22}NO_2Si]^+$  240.1433 (M+H)<sup>+</sup>, found

240.1420. <sup>1</sup>H NMR data are in agreement with previously reported spectra.<sup>145</sup>

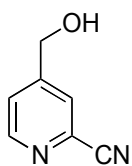


**4-((*tert*-butyldimethylsilyloxy)methyl)picolinonitrile (*iii*)**

Compound *ii* (25.6 g, 107.2 mmol) is dissolved in anhydrous distilled triethylamine (300 mL). Trimethylsilyl cyanide (31.9 g, 321.7 mmol) is added and the mixture is refluxed overnight. TLC (1/1, EtOAc/hexanes) of the reaction mixture after 17 h showed no visible sign of the starting material. The solvent is evaporated and water (250 mL) was added to the residue. The crude product mixture is

extracted with EtOAc (2 x 500 mL) and the solvent removed to yield a dark brown oil.

The product is purified by flash column chromatography (hexanes/EtOAc, 9/1) to yield a brown oil (20.2 g, 76 %). **TLC**  $R_f$  = 0.2 (hexanes/EtOAc, 9/1);  **$^1\text{H}$  NMR** ( $\text{CDCl}_3$ )  $\delta$  0.14 (s, 6H), 0.96 (s, 9H), 4.79 (s, 2H), 7.48 (dq,  $J$  = 5.0 Hz,  $J$  = 0.9 Hz, 1H), 7.69 (m,  $J$  = 0.8 Hz, 1H), 8.65 (dd,  $J$  = 5.1 Hz,  $J$  = 0.6 Hz, 1H);  **$^{13}\text{C}$  NMR** ( $\text{CDCl}_3$ )  $\delta$  -5.4, 18.3, 25.8, 62.8, 117.5, 123.7, 125.5, 133.9, 150.8, 152.5; **IR** (neat) 2955, 2931, 2858, 2238, 1600, 1561, 1471, 1407, 1363, 1256, 1141, 1108, 1007, 992, 939, 901, 835, 778, 671; **HRMS** (**ESI** $^+$ ) calculated for  $[\text{C}_{13}\text{H}_{21}\text{N}_2\text{OSi}]^+$  249.1426 ( $\text{M}+\text{H}$ ) $^+$ , found 249.1423.  $^1\text{H}$  NMR data are in agreement with previously reported spectra.<sup>145</sup>



**4-(hydroxymethyl)picolinonitrile (iv)**

Compound **iii** (15.0 g, 60.5 mmol) is dissolved in methanol (100 mL). 2 N  $\text{H}_2\text{SO}_4$  (30 mL) is added slowly and the mixture is stirred at room

temperature for 1 h. **TLC** (1/1 EtOAc/hexanes) after 1 h shows no visible sign of the starting material. The solvent is evaporated and water (250 mL) is added to the residue.

The crude product is extracted with EtOAc (1x 250 mL) and the solvent removed to yield a yellow solid. The compound is dissolved in EtOAc/hexanes (1/1) and passed through silica to yield a white crystalline solid (6.0 g, 74 %). **TLC**  $R_f$  = 0.2 (EtOAc/hexanes, 1/1); **Mp** 111-112  $^\circ\text{C}$ ;  **$^1\text{H}$  NMR** ( $\text{CDCl}_3$ )  $\delta$  2.18 (bs, 1H), 4.83 (s, 2H), 7.53 (dq,  $J$  = 5.1 Hz,  $J$  = 0.9 Hz, 1H), 7.74 (m,  $J$  = 0.8, 1H), 8.68 (dd,  $J$  = 5.0 Hz,  $J$  = 0.6, 1H);  **$^{13}\text{C}$  NMR** ( $\text{CDCl}_3$ )  $\delta$  62.5, 117.3, 124.1, 125.8, 134.0, 151.0, 151.8; **IR** (neat) 3292, 2927, 2839, 2361, 2239, 1604, 1559, 1470, 1446, 1405, 1323, 1285, 1257, 1258, 1154, 1096, 1072,

996, 912, 894, 855, 837, 628, 608; **HRMS (ESI+)** calculated for  $[C_7H_7N_2O]^+$  135.0558 (M+H)<sup>+</sup>, found 135.0549

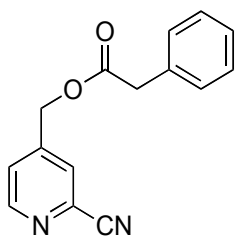
### General procedure for synthesis of 4-(hydroxymethyl)picolinonitrile (PCN) esters (**v**)

The esters were prepared by modification of previously reported procedures.<sup>109</sup>

Compound **iv** (20 mmol) was dissolved in a minimal amount of benzene/acetonitrile.

Triethylamine (36 mmol) was added and the mixture was stirred for several minutes. The respective acid chloride (32 mmol) is added slowly and the mixture is allowed to stir at room temperature for several hours until TLC shows the absence of starting material.

The solvent is evaporated and benzene is added (250 mL). The mixture is washed with water (1 x 250 mL), the organic layer is separated, concentrated, and dried. Purification and characterization of individual esters are described below.

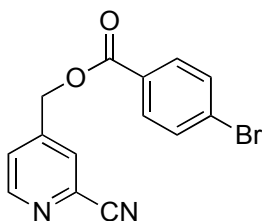


#### PCN-(phenylacetate) (**v-4**)

Compound **v-4** is prepared using the general method above with phenylacetyl chloride. TLC (1/1 EtOAc/hexanes) after 3 h shows no visible sign of starting material. The product is purified by flash

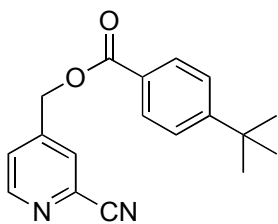
column chromatography (3/1 hexanes/EtOAc) to yield a yellow oil (93%). **TLC**  $R_f$  = 0.8 (EtOAc/hexanes, 1/1); **<sup>1</sup>H NMR** (CDCl<sub>3</sub>)  $\delta$  3.74 (s, 2H), 5.17 (s, 2H), 7.28-7.39 (m, 6H), 7.49 (m,  $J$  = 0.7 Hz, 1H), 8.64 (d,  $J$  = 5.1 Hz, 1H); **<sup>13</sup>C NMR** (CDCl<sub>3</sub>)  $\delta$  41.2, 63.4, 117.0, 124.7, 126.3, 127.6, 128.8, 129.2, 133.2, 134.2, 146.8, 151.2, 170.8; **IR** (neat) 3076, 3056, 2955, 2239, 1727, 1602, 1474, 1454, 1415, 1365, 1300, 1238, 1119, 1042,

991, 905, 876, 855, 758, 739, 645, 602; **HRMS (ESI+)** calculated for  $[C_{15}H_{13}N_2O_2]^+$  253.0977 (M+H)<sup>+</sup>, found 253.0985



**PCN-(4-bromobenzoate) (v-5)**

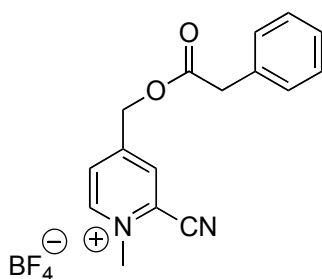
Compound **v-5** is prepared using the general method above with 4-bromobenzoyl chloride. TLC (1/1 EtOAc/hexanes) after 3 h shows no visible sign of starting material. The product is purified by flash column chromatography (4/1 hexanes/EtOAc) to yield a beige powder (99%). **TLC**  $R_f$  = 0.7 (EtOAc/hexanes, 1/1); **Mp** 106-107 °C; **<sup>1</sup>H NMR** (CDCl<sub>3</sub>) δ 5.42 (s, 2H), 7.56 (dt,  $J$  = 5.1 Hz,  $J$  = 0.7 Hz, 1H), 7.64 (dt,  $J$  = 8.6 Hz,  $J$  = 1.8 Hz, 2H), 7.75 (d,  $J$  = 0.6 Hz, 1H), 7.95 (dt,  $J$  = 8.6 Hz,  $J$  = 1.9 Hz, 2H), 8.74 (dd,  $J$  = 4.9 Hz,  $J$  = 0.6), 1H); **<sup>13</sup>C NMR** (CDCl<sub>3</sub>) δ 63.9, 117.0, 125.0, 126.5, 127.8, 129.1, 131.3, 132.1, 134.4, 146.7, 151.4, 165.2; **IR** (neat) 3068, 2556, 2242, 1785, 1720, 1679, 1587, 1556, 1484, 1431, 1397, 1374, 1321, 1270, 1228, 1174, 1155, 1107, 1084, 1068, 1003, 942, 862, 842, 754, 681; **HRMS (ESI+)** calculated for  $[C_{14}H_{10}BrN_2O_2]^+$  316.9926 (M+H)<sup>+</sup>, found 316.9936



**PCN-(4-tert-butylbenzoate) (v-6)**

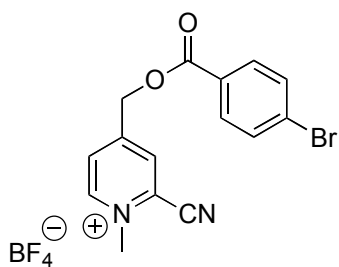
Compound **v-6** is prepared using the general method above with 4-tert-butylbenzoyl chloride. TLC (1/1 EtOAc/hexanes) after 3 h shows no visible sign of starting material. The product is purified by flash column chromatography (85/15 hexanes/EtOAc) to yield a beige powder (94%). **TLC**  $R_f$  = 0.2 (EtOAc/hexanes, 1/1); **Mp** 94-95 °C; **<sup>1</sup>H NMR** (CDCl<sub>3</sub>) δ 1.36 (s, 9 H), 5.42 (s, 2H), 7.51 (dt,  $J$  = 8.6 Hz,  $J$  = 1.8 Hz, 2H), 7.54 (dt,  $J$  = 5.2 Hz,  $J$  = 0.7 Hz, 1H),

7.74 (d,  $J = 0.6$  Hz, 1H), 8.03 (dt,  $J = 8.6$  Hz,  $J = 1.8$  Hz, 2H), 8.72 (d,  $J = 5.2$  Hz, 1H);  $^{13}\text{C}$  NMR ( $\text{CDCl}_3$ )  $\delta$  31.1, 35.2, 63.4, 117.1, 124.8, 125.7, 126.1, 126.4, 129.7, 134.4, 147.3, 151.3, 157.7, 165.9; **IR** (neat) 3061, 2964, 2874, 2233, 1719, 1605, 1572, 1464, 1439, 1410, 1363, 1319, 1270, 1214, 1190, 1150, 1120, 1105, 1019, 993, 944, 916, 865, 841, 829, 775, 724, 707, 637; **HRMS (ESI+)** calculated for  $[\text{C}_{18}\text{H}_{19}\text{N}_2\text{O}_2]^+$  295.1447 ( $\text{M}+\text{H}$ ) $^+$ , found 295.1436



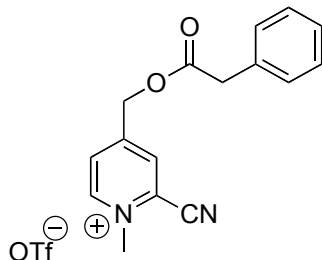
**mPCN-(phenylacetate) tetrafluoroborate salt (4BF4)**

Compound **v-4** (2.1 g, 8.3 mmol) is dissolved in dry acetonitrile (25 mL). To the solution is added trimethyloxonium tetrafluoroborate (2.5 g, 16.6 mmol) and the mixture is stirred at room temperature for two hours. TLC (1/1 EtOAc/hexanes) after 2 h shows no visible sign of starting material. The solvent is evaporated off and the residue is recrystallized from hot pentane/acetone (9/1) to yield off white crystals (0.3 g, 10%). **Mp** 104-106 °C;  $^1\text{H}$  NMR ( $\text{CD}_3\text{CN}$ )  $\delta$  3.85 (s, 2H), 4.43 (s, 3H), 5.41 (s, 2H), 7.33-7.38 (m, 5H), 8.15 (d,  $J = 6.2$  Hz, 1H), 8.36 (d,  $J = 1.3$  Hz, 1H), 8.84 (d,  $J = 6.4$  Hz, 1H);  $^{13}\text{C}$  NMR ( $\text{CDCl}_3$ )  $\delta$  41.1, 49.3, 63.9, 111.3, 128.3, 128.5, 129.6, 129.7, 130.6, 132.1, 134.9, 149.8, 159.4, 171.9; **IR** (neat) 3074, 1747, 1634, 1581, 1521, 1499, 1455, 1427, 1385, 1344, 1324, 1287, 1215, 1161, 1090, 1058, 908, 847, 703, 746, 709, 607; **HRMS (ESI+)** calculated for  $[\text{C}_{16}\text{H}_{15}\text{N}_2\text{O}_2]^+$  267.1128, found 267.1124



**mPCN- (4-bromobenzoate) tetrafluoroborate salt (5BF<sub>4</sub>)**

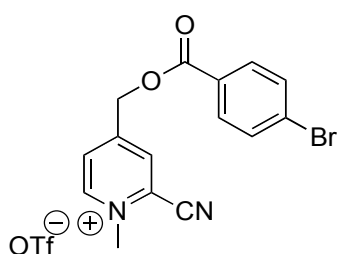
To a solution of compound **v-5** (5.0 g, 15.8 mmol) in acetone (100 mL) is added trimethyloxonium tetrafluoroborate (4.7 g, 31.6 mmol). The mixture is allowed to stir at room temperature overnight. A white precipitate forms within the first few minutes of stirring. TLC (1/1 EtOAc/hexanes) after 24 h shows no visible sign of starting material. The white precipitate is filtered off, washed with cold methanol, and dried (4.8 g, 73 %). **Mp** 236-238 °C; <sup>1</sup>H NMR (CD<sub>3</sub>CN) δ 4.46 (s, 3H), 5.64 (s, 2H), 7.74 (dt, *J* = 8.6 Hz, *J* = 1.9 Hz, 2H), 8.03 (dt, *J* = 8.6 Hz, *J* = 1.9 Hz, 2H), 8.30 (d, *J* = 6.3 Hz, 1H), 8.56 (d, *J* = 1.6 Hz, 1H), 8.89 (d, *J* = 6.4 Hz, 1H); <sup>13</sup>C NMR (CDCl<sub>3</sub>) δ 49.4, 64.5, 111.3, 128.6, 129.1, 129.5, 129.8, 132.3, 132.6, 133.1, 149.9, 159.1, 165.9; **IR** (neat) 3114, 2361, 1785, 1723, 1637, 1587, 1521, 1486, 1450, 1427, 1398, 1324, 1277, 1257, 1194, 1178, 1108, 1055, 1005, 860, 842, 756, 721, 704, 683, 627; **HRMS (ESI<sup>+</sup>)** calculated for [C<sub>15</sub>H<sub>12</sub>BrN<sub>2</sub>O<sub>2</sub>]<sup>+</sup> 331.0077, found 331.0065



**mPCN-(phenylacetate) trifluoromethane sulfonate salt (4OTf)**

To a solution of compound **v-4** (2.8 g, 11.0 mmol) in dry dichloromethane (50 mL) is added methyl trifluoromethane sulfonate (2.9 g, 16.5 mmol). The mixture is allowed to stir at room temperature under nitrogen atmosphere for 3 h. A white precipitate forms within a few minutes of stirring. TLC (1/1 EtOAc/hexanes) after 3 h shows no visible sign of starting material. The solvent is evaporated *in vacuo* and the residue recrystallized from hot ethanol to afford a white flaky crystalline solid (3.5 g, 77%). **Mp** 108-110 °C; <sup>1</sup>H

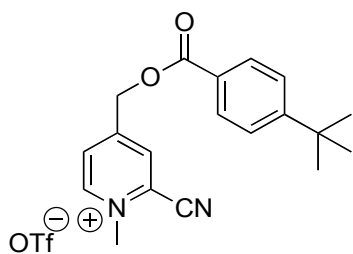
**NMR** (CD<sub>3</sub>CN)  $\delta$  3.85 (s, 2H), 4.43 (s, 3H), 5.41 (s, 2H), 7.35 (m, 5H), 8.14 (d,  $J$  = 6.2 Hz, 1H), 8.37 (s, 1H), 8.84 (d,  $J$  = 6.4 Hz, 1H); **<sup>13</sup>C NMR** (CDCl<sub>3</sub>)  $\delta$  41.1, 49.3, 63.9, 111.3, 128.4, 128.6, 129.6, 129.7, 130.6, 132.1, 134.9, 149.8, 159.5, 171.9; **IR** (neat) 3061, 1746, 1638, 1585, 1526, 1500, 1455, 1440, 1412, 1379, 1345, 1255, 1215, 1141, 1076, 1028, 1048, 958, 919, 833, 786, 750, 713, 635; **HRMS (ESI+)** calculated for [C<sub>16</sub>H<sub>15</sub>N<sub>2</sub>O<sub>2</sub>]<sup>+</sup> 267.1128, found 267.1126



**mPCN-(4-bromobenzoate) trifluoromethane sulfonate salt (5OTf)**

To a solution of compound **v-5** (6.3 g, 19.9 mmol) in dry dichloromethane (100 mL) is added methyl trifluoromethane sulfonate (4.3 g, 25.9 mmol). The mixture is allowed to stir at room temperature overnight. A white precipitate forms within a few minutes of stirring. TLC (1/1 EtOAc/hexanes) after 24 h shows no visible sign of starting material. The solvent is evaporated *in vacuo* and the residue recrystallized from hot ethanol to afford off-white flaky crystals (7.7 g, 80%). **Mp** 160-162 °C; **<sup>1</sup>H NMR** (CD<sub>3</sub>CN)  $\delta$  4.46 (s, 3H), 5.64 (s, 2H), 7.75 (dt,  $J$  = 8.6 Hz,  $J$  = 1.9 Hz, 2H), 8.04 (dt,  $J$  = 8.6 Hz,  $J$  = 1.9 Hz, 2H), 8.29 (d,  $J$  = 6.1 Hz, 1H), 8.56 (s, 1H), 8.89 (d,  $J$  = 6.4 Hz, 1H); **<sup>13</sup>C NMR** (CDCl<sub>3</sub>)  $\delta$  49.4, 64.5, 111.3, 128.6, 129.1, 129.5, 129.8, 132.3, 132.6, 133.1, 149.9, 159.1, 165.9; **IR** (neat) 3064, 1720, 1637, 1588, 1523, 1486, 1433, 1399, 1326, 1262, 1224, 1192, 1173, 1147, 1104, 1066, 1030, 1009, 958, 848, 758, 721, 705, 684, 637; **HRMS (ESI+)** calculated for [C<sub>15</sub>H<sub>12</sub>BrN<sub>2</sub>O<sub>2</sub>]<sup>+</sup> 331.0077, found 331.0069





**mPCN-(4-*tert*-butylbenzoate) trifluoromethane sulfonate salt (6OTf)**

To a solution of compound **v-6** (2.0 g, 6.8 mmol) in dry dichloromethane (50 mL) is added methyl trifluoromethane sulfonate (1.5 g, 8.8 mmol). The mixture is allowed to stir

at room temperature overnight. A white precipitate forms within a few hours of stirring.

TLC (1/1 EtOAc/hexanes) after 24 h shows no visible sign of starting material. The

solvent is evaporated *in vacuo* and the residue recrystallized from hot ethanol to afford

white needle-like crystals (2.1 g, 68%). **Mp** 223-224 °C; **<sup>1</sup>H NMR** (CD<sub>3</sub>CN) δ 1.36 (s,

9H), 4.45 (s, 3H), 5.63 (s, 2H), 7.61 (dd, *J* = 6.8 Hz, *J* = 1.7 Hz, 2H), 8.08 (dd, *J* = 6.8

Hz, *J* = 1.6 Hz, 2H), 8.30 (d, *J* = 6.3 Hz, 1H), 8.56 (s, 1H), 8.88 (d, *J* = 6.4 Hz, 1H); **<sup>13</sup>C**

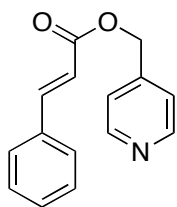
**NMR** (CDCl<sub>3</sub>) δ 31.3, 35.9, 49.4, 64.2, 111.3, 126.9, 127.2, 128.6, 129.8, 130.8, 132.3,

149.9, 158.8, 159.5, 166.4; **IR** (neat) 3054, 2973, 1718, 1630, 1610, 1580, 1524, 1439,

1411, 1372, 1317, 1274, 1253, 1227, 1190, 1169, 1145, 1119, 1030, 922, 851, 774, 757,

718, 706, 638; **HRMS (ESI+)** calculated for [C<sub>19</sub>H<sub>21</sub>N<sub>2</sub>O<sub>2</sub>]<sup>+</sup> 309.1598, found 309.1602

### 8.8.5 *N*-Methylpicolinium *trans*-cinnamate bromide (NAP-tCA)



**Picolyl *trans*-cinnamate**

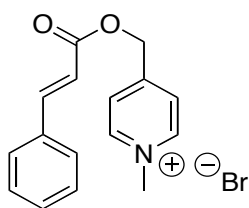
Picolyl *trans*-cinnamate was prepared according to literature

procedures.<sup>109</sup> **<sup>1</sup>H NMR** (CDCl<sub>3</sub>) δ 5.27 (s, 2H), 6.53 (d, *J* = 16.0 Hz,

1H), 7.31 (d, *J* = 5.8 Hz, 2H), 7.40-7.41 (m, 3H), 7.54-7.56 (m, 2H), 7.78 (d, *J* = 16.0 Hz,

1H), 8.63 (d, *J* = 6.1 Hz, 2H); **<sup>13</sup>C NMR** (CD<sub>3</sub>CN) δ 65.1, 118.5, 122.8, 129.3, 130.0,

131.6, 135.3, 146.3, 146.7, 150.9, 167.2  $^1\text{H}$  and  $^{13}\text{C}$  spectra are in agreement with previously reported spectra.

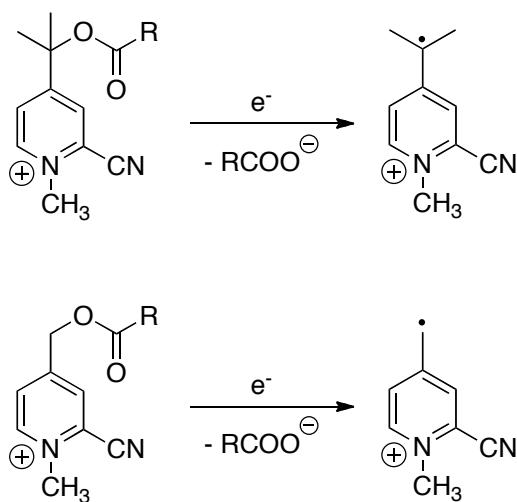


***N*-methylpicolinium *trans*-cinnamate bromide (NAP-tCA)**

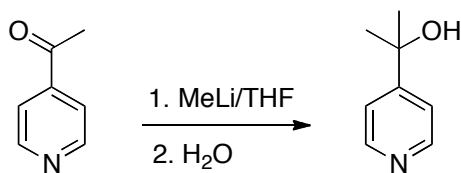
A solution of picolyl *trans*-cinnamate (1.0 g, 4.18 mmol) in dry, distilled acetonitrile (10 mL) was prepared in an oven-dried round bottom flask. The round-bottom flask was equipped with a dry ice condenser filled with isopropanol and dry ice. 2 M bromomethane in *tert*-butylmethyl ether (Aldrich, 6.3 mL, 12.54 mmol) is added to the flask by syringe and the solution is heated to reflux and stirred for 3 h. TLC (1/1 EtOAc/hexanes) after 3 h shows no visible sign of starting material. Ethyl acetate is added to precipitate the crude product. Subsequent recrystallization from ether/chloroform/ethanol (7/2/1) affords white needle-like crystals (1.19 g, 85 %). **Mp** 138-140 °C;  $^1\text{H}$  NMR ( $\text{CD}_3\text{CN}$ )  $\delta$  4.31 (s, 3H), 5.50 (s, 2H), 6.68 (d,  $J$  = 16.0 Hz, 1H), 7.46-7.47 (m, 3H), 7.68-7.70 (m, 2H), 7.84 (d,  $J$  = 16.1 Hz, 1H), 8.00 (d,  $J$  = 6.4 Hz, 2H), 8.68 (d,  $J$  = 6.7 Hz, 2H);  $^{13}\text{C}$  NMR ( $\text{CD}_3\text{CN}$ )  $\delta$  48.9, 64.3, 117.9, 126.1, 129.5, 130.1, 131.9, 135.2, 146.4, 147.1, 157.6, 166.9  $^1\text{H}$  and  $^{13}\text{C}$  NMR data are in agreement with previously published spectra.<sup>109</sup>

## Appendix A: Improvements for Substituted NAP Systems

The mPCN deprotection system discussed in Chapter 5 suffered from rapid deprotonation of an mPCN group benzylic proton when mPCN-esters were not present in acidic media. A possible remedy to this situation was explored. Substitution of the benzylic protons with alkyl groups is expected to eliminate the problem and significantly improve stability and compatibility with a variety of environments. In addition to avoiding the acid-base complications, this change is expected to benefit deprotection release efficiencies. Upon one-electron reduction and carboxylate release, the dialkyl-substituted mPCN group is likely to form a more stable tertiary benzylic radical as a biproduct rather than the primary benzylic radical formed with the NAP and mPCN groups. (Scheme A-1) Thus, efficiencies of the bond breaking reaction are expected to be enhanced. Toward this end, we attempted to prepare the cyano-substituted



**Scheme A-1: mPCN-ester deprotection versus benzylic dimethyl substituted mPCN-ester deprotection**



**Scheme A-2: Synthesis of dimethyl-substituted 4-pyridylcarbinol**

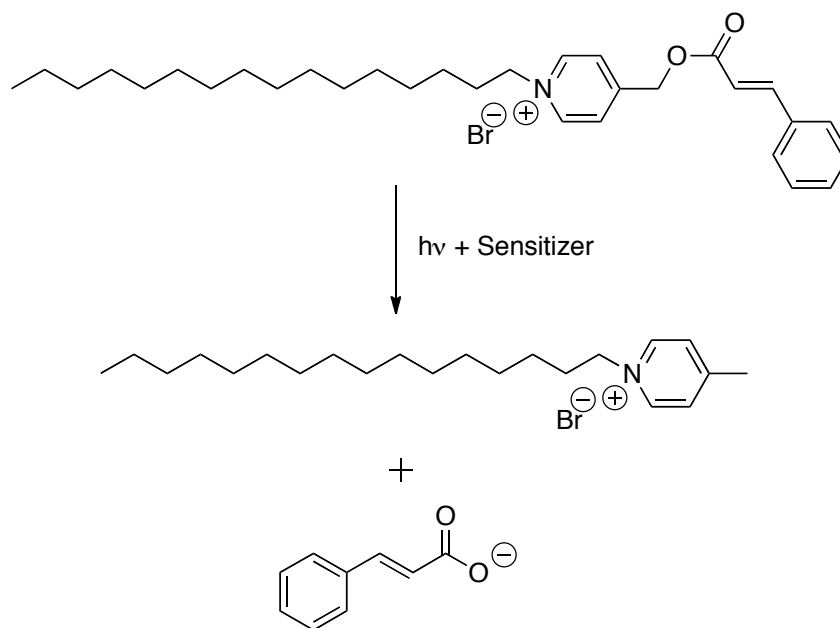
4-pyridylcarbinol precursor with methyl groups substituted for the two benzylic protons. (Scheme A-2) This compound was prepared in moderate yields. However, attempts to adapt the previously used synthesis that introduces the cyano-substituent (Scheme 5-2) to the current compound were met with considerable difficulties. Reactions to introduce a TBDMS or TMS group onto the alcohol functionality resulted in negligible yields of the protected product. It is likely that the increased steric bulk around the hydroxyl group from the added methyl groups inhibits nucleophilic attack on the silylating reagents. This may foreshadow difficulties in the acid chloride coupling esterification step later in the compound synthesis. Attempts to bypass the hydroxyl-protection and proceed directly to the oxidation step with mCPBA also resulted in negligible yields of the desired product. Thus, the synthesis of the dimethyl-substituted mPCN-esters remains a challenge, but the successful modification of the mPCN groups would offer the potential to significantly improve the compatibility and efficiency of this deprotection system.

## **Appendix B: Alternatives for Light-induced Viscosity Changes**

Aside from the previously described NAP-tCA/CTAB system, several systems for photoinduced viscosity transitions were explored utilizing NAP-release. Some of the design considerations, preliminary results, and challenges experienced with these systems will be briefly discussed here.

### **Linked Surfactant-NAP-Additive**

In the previously described experiments, the fate of the NAP group after photorelease is unclear. Since it is aqueous soluble and has a positive charge, it is possible for it to be free in solution or it may prefer to associate with the CTAB/H<sub>2</sub>O interface which may complicate the formation of a stable interpenetrating wormlike micelle network. Since pyridinium-based surfactants also demonstrated the ability to form a gel upon addition of certain carboxylate additives, we considered incorporating the surfactant directly into the NAP group. Alkylation of the pyridine nitrogen in the last synthetic step with a hexadecyl chain would be a facile transformation. Subsequently, upon one electron reduction, the released NAP group would function as the surfactant and the carboxylate would be free to align with the pyridinium group. (Scheme B-1) This would ensure that the optimal 1:1 ratio of surfactant:additive is met while minimizing the amount of potentially problematic byproducts. The starting compound was prepared, but was sparingly soluble in water thus halting any potential photolysis experiments.



**Scheme B-1: Release of tCA and pyridinium surfactant**

### Nanoparticle-supported Gelation Additive Release

Experiments with early candidate systems to photochemically induce a viscosity change often resulted in solubility challenges or the use of components that inhibit the formation of stable gels. The presence of hydrophilic moieties such as hydroxyl or carboxylate groups on non-gelation-inducing additives seemed to have a negative effect on gelation. Unfortunately, the sensitizer required for deprotection would likely incorporate these groups in order to be aqueous soluble. In the search for a useable sensitizer, we reasoned that it would be possible to use gold nanoparticles as sensitizers as the large size would have little effect on smaller-scale self-assembly; the wormlike micelles should grow around the nanoparticles. Control experiments that combined TRP-AuNP with equimolar CTAB/tCA confirmed the formation of stable gels. (Figure B-1)

Furthermore, we reasoned that functionalizing the nanoparticle surface with a certain amount of solubilizing tryptophan-conjugate ligands, for solubility, together with a NAP-protected gelation additive would allow photorelease while sequestering the NAP byproduct. With these benefits in mind, the synthesis of the additive ligand for

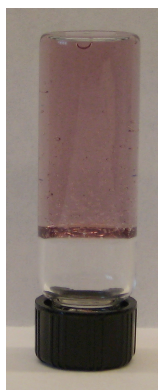
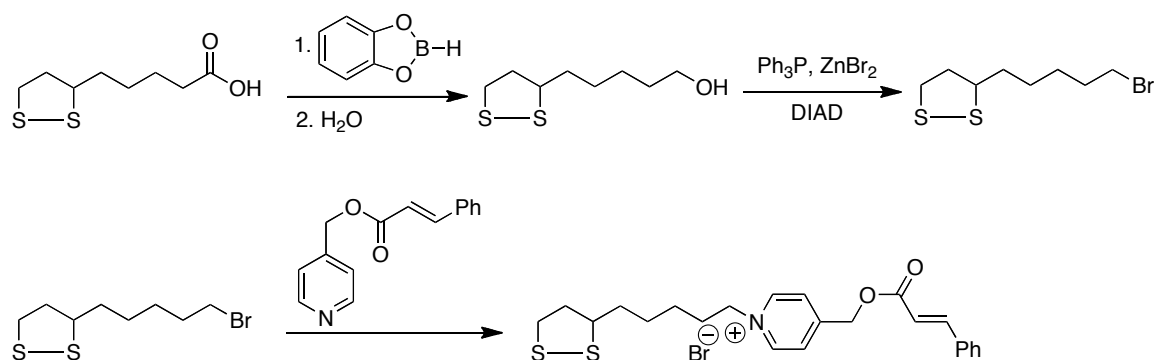
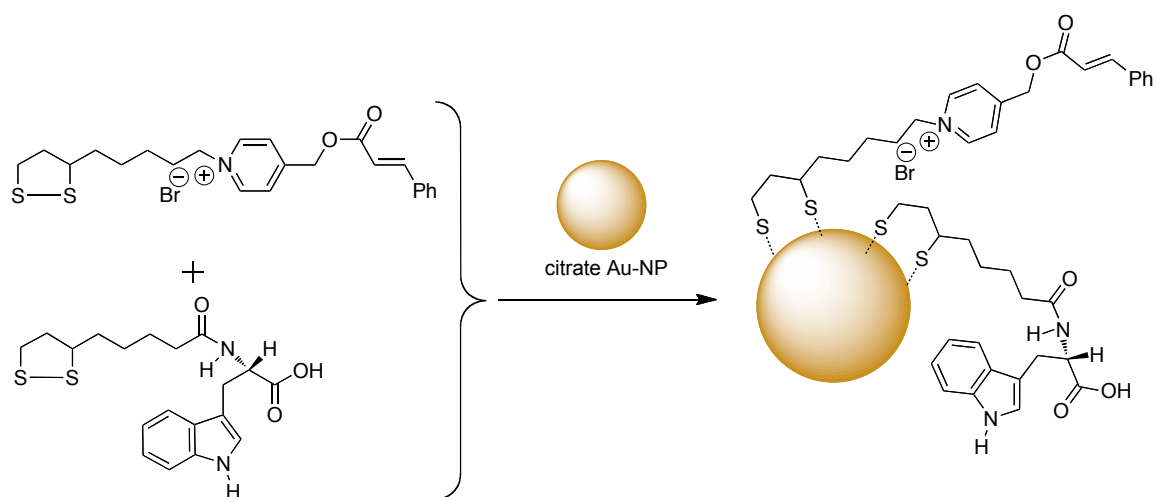


**Figure B-1: TRP-AuNP prepared in 50 mM aqueous CTAB/tCA (1/1)**

nanoparticle functionalization was undertaken. (Scheme B-2) The synthesis of the thioctic bromide linker has been previously reported.<sup>185</sup> Incorporation of this AuNP linking moiety onto the NAP group can be accomplished by alkylating the picoline nitrogen in place of the previously used methylation reaction. The final compound has been prepared and characterized but remains to be incorporated onto gold nanoparticles and tested for



**Scheme B-2: Synthesis of NAP-tCA ligand for gold nanoparticle functionalization**

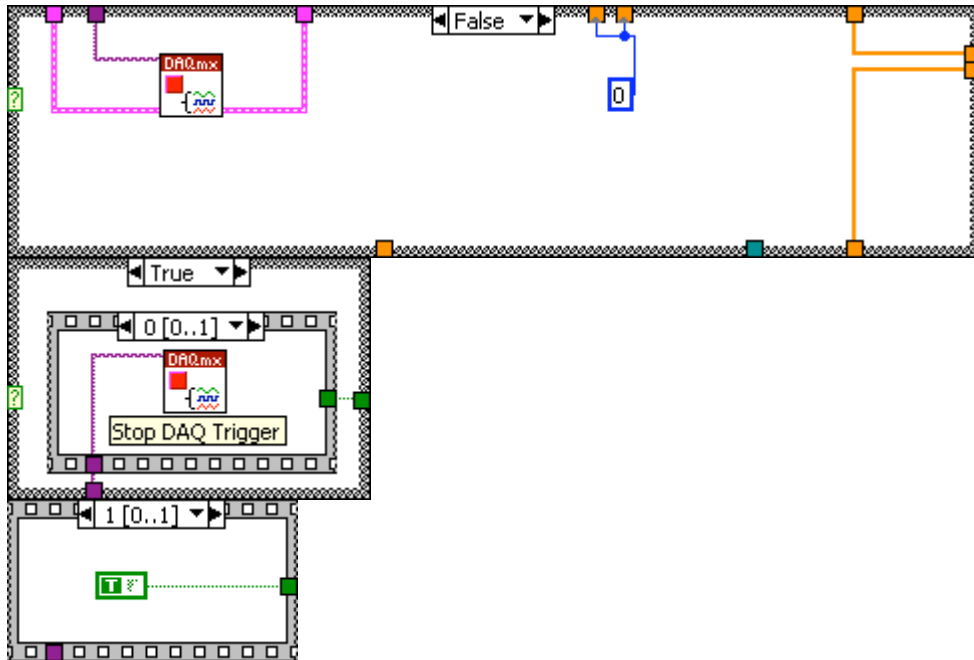


**Scheme B-3: NAP-tCA and TRP-conj functionalized gold nanoparticles for gelation additive release**

photorelease. (Scheme B-3) AuNPs with a sufficiently large diameter must be chosen such that a significant amount of the NAP-ligand and tryptophan conjugate ligands will be located on the surface of each nanoparticle.







#### List of SubVIs and Express VIs with Configuration Information



##### **CV\_DAQ Startup.vi**

E:\Users\Brian\Documents\UMCP Research\CV LabView Program\v1.0\CV\_DAQ Startup.vi



##### **DAQmx Start Task.vi**

C:\Program Files\National Instruments\LabVIEW 8.0\vi.lib\DAQmx\configure\task.llb\DAQmx Start Task.vi



##### **DAQmx Stop Task.vi**

C:\Program Files\National Instruments\LabVIEW 8.0\vi.lib\DAQmx\configure\task.llb\DAQmx Stop Task.vi



##### **CV\_DAQ2.vi**

E:\Users\Brian\Documents\UMCP Research\CV LabView Program\v1.0\CV\_DAQ2.vi



##### **CV\_Voltage Data to Current Data.vi**

E:\Users\Brian\Documents\UMCP Research\CV LabView Program\v1.0\CV\_Voltage Data to Current Data.vi



##### **CV\_Build Plot Data2.vi**

E:\Users\Brian\Documents\UMCP Research\CV LabView Program\v1.0\CV\_Build Plot Data2.vi



##### **Merge Errors.vi**

C:\Program Files\National Instruments\LabVIEW 8.0\vi.lib\Utility\error.llb\Merge Errors.vi



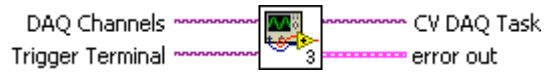
##### **Simple Error Handler.vi**

C:\Program Files\National Instruments\LabVIEW 8.0\vi.lib\Utility\error.llb\Simple Error Handler.vi

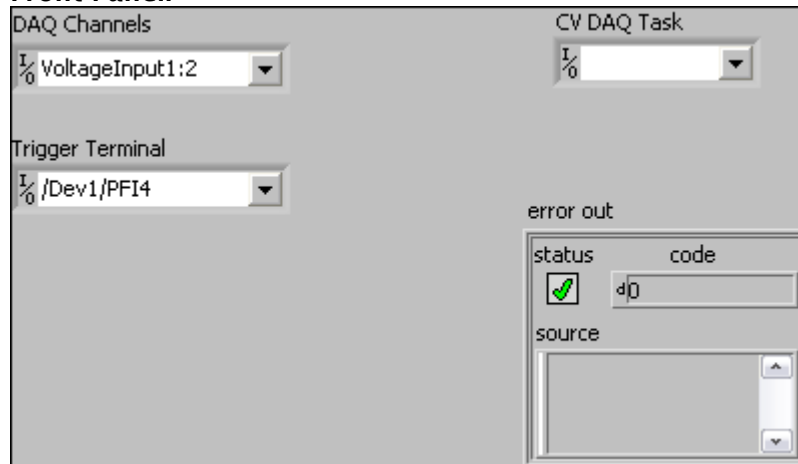
## Startup VI

### CV\_DAQ Startup.vi

#### Connector Pane:



#### Front Panel:



**DAQ Channels**

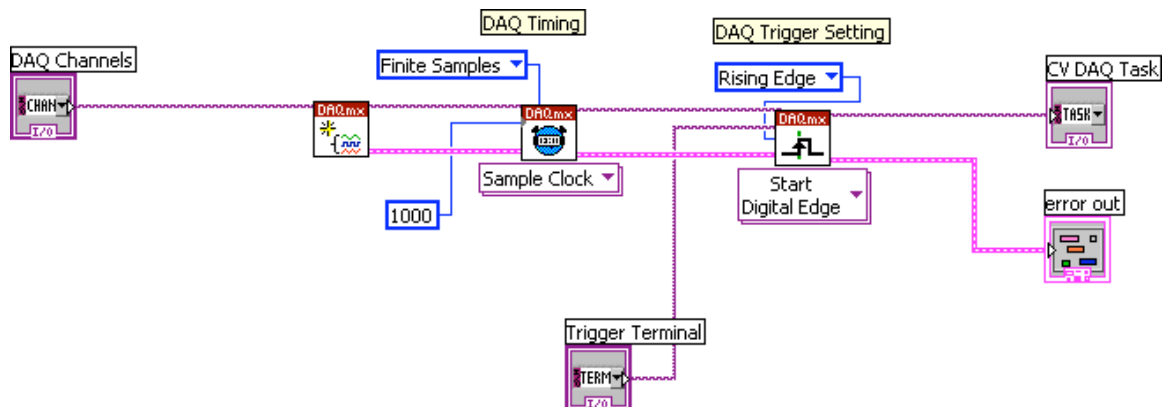
**Trigger Terminal**

**CV DAQ Task**

**error out** error out passes error or warning information out of a VI to be used by other VIs.

Right-click the **error out** indicator on the front panel and select **Explain Error** or **Explain Warning** from the shortcut menu for more information about the error.

#### Block Diagram:



**SubVIs:**



**DAQmx Create Task.vi**

C:\Program Files\National Instruments\LabVIEW  
8.0\vi.lib\DAQmx\create\task.llb\DAQmx Create Task.vi



**DAQmx Timing.vi**

C:\Program Files\National Instruments\LabVIEW  
8.0\vi.lib\DAQmx\configure\timing.llb\DAQmx Timing.vi



**DAQmx Timing (Sample Clock).vi**

C:\Program Files\National Instruments\LabVIEW  
8.0\vi.lib\DAQmx\configure\timing.llb\DAQmx Timing (Sample Clock).vi



**DAQmx Trigger.vi**

C:\Program Files\National Instruments\LabVIEW  
8.0\vi.lib\DAQmx\configure\trigger.llb\DAQmx Trigger.vi



**DAQmx Start Trigger (Digital Edge).vi**

C:\Program Files\National Instruments\LabVIEW  
8.0\vi.lib\DAQmx\configure\trigger.llb\DAQmx Start Trigger (Digital Edge).vi

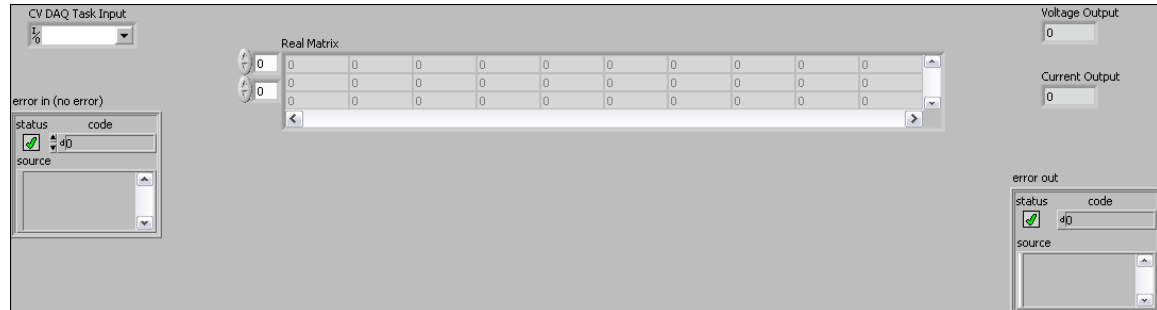
## Data Acquisition

### CV\_DAQ2.vi


#### Connector Pane:



#### Front Panel



#### Controls and Indicators


 **error in (no error)** **error in** can accept error information wired from VIs previously called. Use this information to decide if any functionality should be bypassed in the event of errors from other VIs.

Right-click the **error in** control on the front panel and select **Explain Error** or **Explain Warning** from the shortcut menu for more information about the error.

 **CV DAQ Task Input**

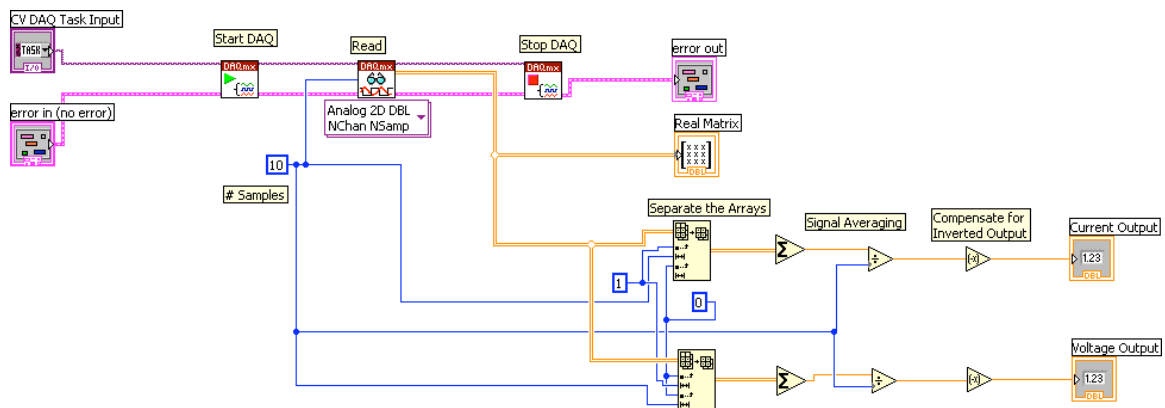
 **Voltage Output**

 **Current Output**

 **error out** **error out** passes error or warning information out of a VI to be used by other VIs.

Right-click the **error out** indicator on the front panel and select **Explain Error** or **Explain Warning** from the shortcut menu for more information about the error.

## Block Diagram:



## List of SubVIs and Express VIs with Configuration Information:



### NI\_Matrx.lvlib:RealMatrix.ctl

C:\Program Files\National Instruments\LabVIEW  
8.0\vi.lib\Analysis\Matrix\Datatypes\RealMatrix.ctl



### DAQmx Start Task.vi

C:\Program Files\National Instruments\LabVIEW  
8.0\vi.lib\DAQmx\configure\task.lib\DAQmx Start Task.vi



### DAQmx Read.vi

C:\Program Files\National Instruments\LabVIEW  
8.0\vi.lib\DAQmx\read.lib\DAQmx Read.vi



### DAQmx Read (Analog 2D DBL NChan NSamp).vi

C:\Program Files\National Instruments\LabVIEW  
8.0\vi.lib\DAQmx\read.lib\DAQmx Read (Analog 2D DBL NChan NSamp).vi



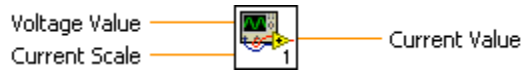
### DAQmx Stop Task.vi

C:\Program Files\National Instruments\LabVIEW  
8.0\vi.lib\DAQmx\configure\task.lib\DAQmx Stop Task.vi

## Convert Voltage Data to Current Data

### CV\_Voltage Data to Current Data.vi

#### Connector Pane:



#### Front Panel



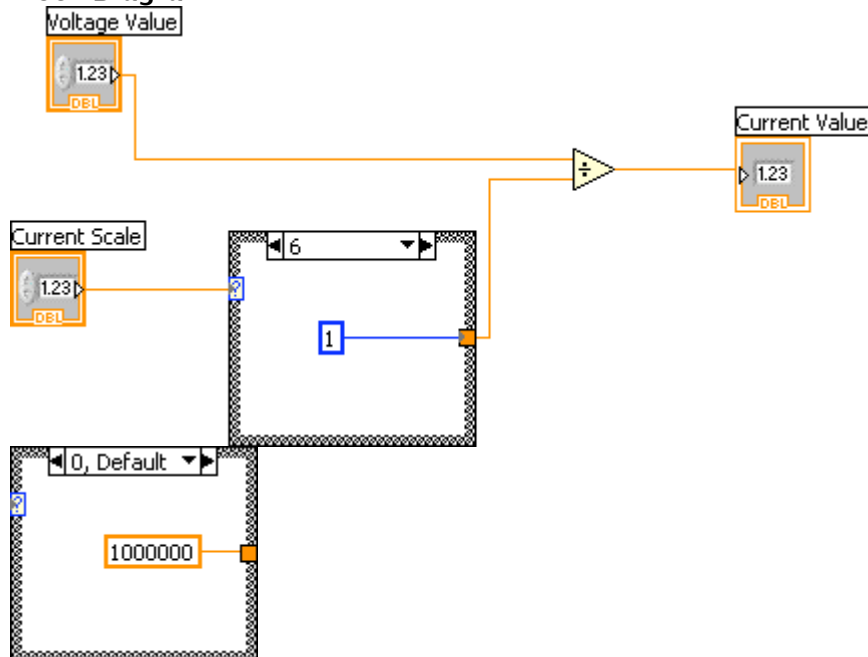
#### Controls and Indicators

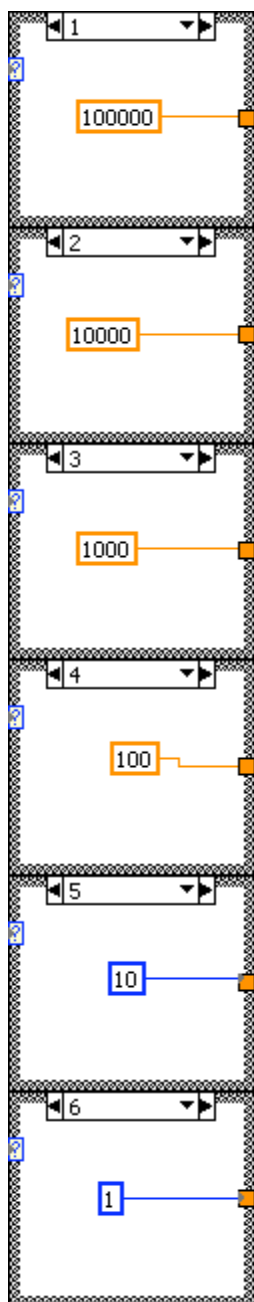
Voltage Value

Current Scale

Current Value

#### Block Diagram



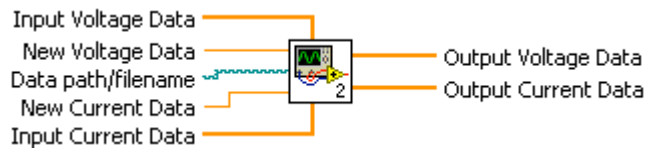




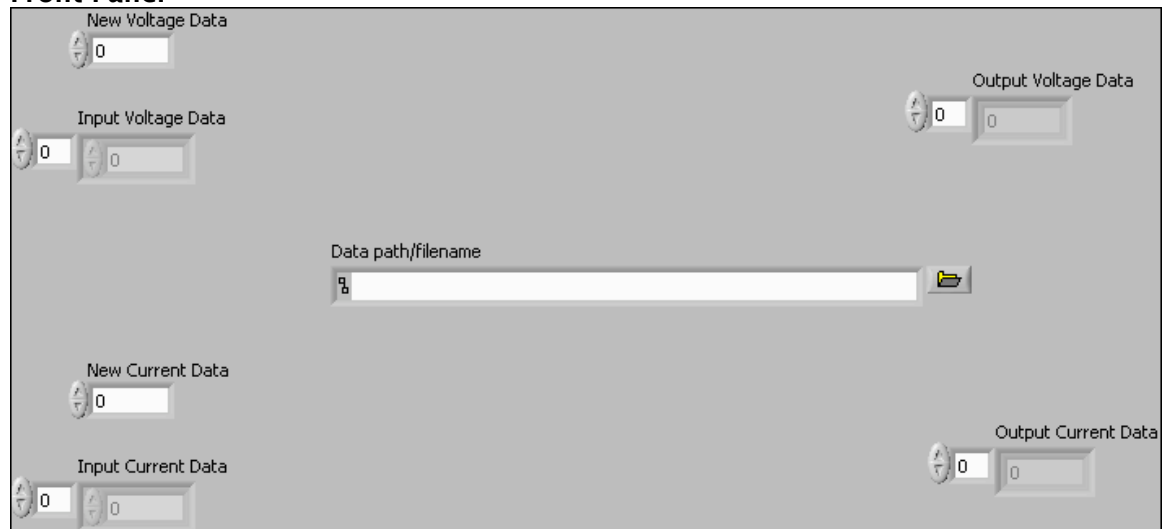
## **Build Plot Data**

### **CV\_Build Plot Data2.vi**












#### **Connector Pane:**



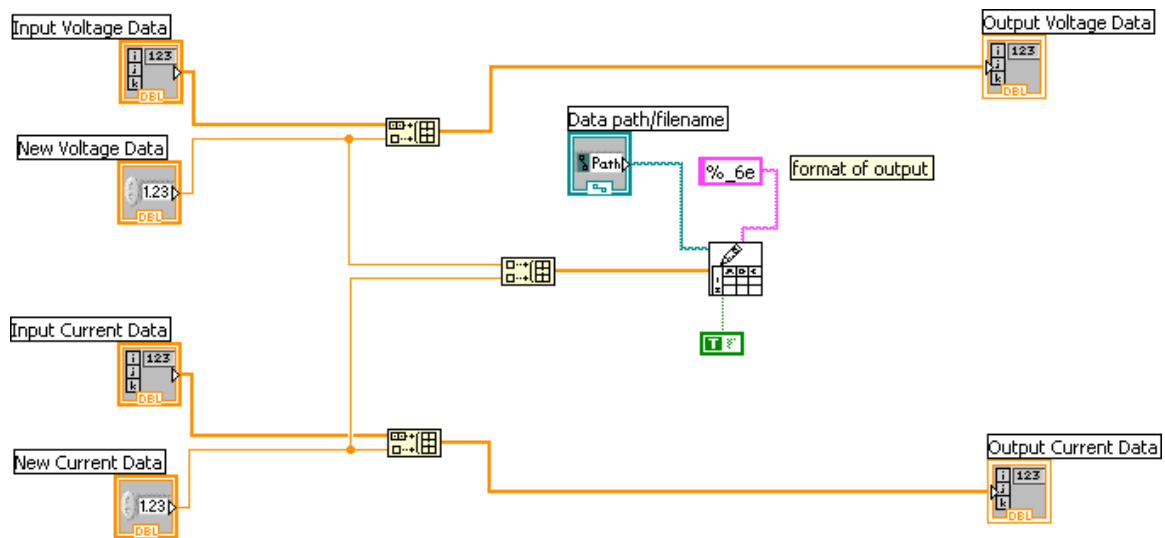
#### **Front Panel**



#### **Controls and Indicators**

-  **New Voltage Data**
-  **New Current Data**
-  **Data path/filename**
-  **Input Voltage Data**
  -  **Numeric**
-  **Input Current Data**
  -  **Numeric**
-  **Output Voltage Data**
  -  **Numeric**
-  **Output Current Data**
  -  **Numeric**

### Block Diagram:



### List of SubVIs and Express VIs with Configuration Information:



#### Write To Spreadsheet File.vi

C:\Program Files\National Instruments\LabVIEW 8.0\vi.lib\Utility\file.lib\Write To Spreadsheet File.vi

## References

- (1) Wuts, P. G. M.; Greene, T. W. *Greene's Protective Groups in Organic Synthesis*; 4th ed.; John Wiley & Sons, Inc.: Hoboken, NJ, 2007.
- (2) Pelliccioli Anna, P.; Wirz, J. *Photochem. Photobiol. Sci.* **2002**, *1*, 441-58.
- (3) Bochet, C. G. *J. Chem. Soc.-Perkin Trans. I* **2002**, 125-142.
- (4) Givens, R. S.; Kotala, M. B.; Lee, J.-I. *Dyn. Stud. Biol.* **2005**, 95-129.
- (5) Mayer, G.; Heckel, A. *Angew. Chem., Int. Ed.* **2006**, *45*, 4900-4921.
- (6) Ellis-Davies, G. C. R. *Nat. Methods* **2007**, *4*, 619-628.
- (7) Bochet, C. G. *Pure Appl. Chem.* **2006**, *78*, 241-247.
- (8) Givens, R.; Goeldner, M. *Dynamic Studies in Biology: Phototriggers, Photoswitches, and Caged Biomolecules*; Wiley-VCH: Weinheim, 2005.
- (9) Barltrop, J. A.; Schofield, P. *Tetrahedron Lett.* **1962**, 697-699.
- (10) Barltrop, J. A.; Schofield, P. *J. Chem. Soc.* **1965**, 4758-65.
- (11) Barltrop, J. A.; Plant, P. J.; Schofield, P. *Chem. Commun.* **1966**, 822-3.
- (12) Zhu, Q. Q.; Schnabel, W.; Schupp, H. *J. Photochem.* **1987**, *39*, 317-332.
- (13) Walker, J. W.; Reid, G. P.; McCray, J. A.; Trentham, D. R. *J. Am. Chem. Soc.* **1988**, *110*, 7170-7177.
- (14) Barth, A.; Corrie, J. E. T.; Gradwell, M. J.; Maeda, Y.; Mantele, W.; Meier, T.; Trentham, D. R. *J. Am. Chem. Soc.* **1997**, *119*, 4149-4159.
- (15) Barth, A.; Hauser, K.; Maentele, W.; Corrie, J. E. T.; Trentham, D. R. *J. Am. Chem. Soc.* **1995**, *117*, 10311-16.
- (16) Il'ichev, Y. V.; Schwoerer, M. A.; Wirz, J. *J. Am. Chem. Soc.* **2004**, *126*, 4581-4595.
- (17) Bamford, C. H.; Norrish, R. G. W. *J. Chem Soc. Abstr.* **1935**, 1504-11.
- (18) Patchornik, A.; Amit, B.; Woodward, R. B. *J. Am. Chem. Soc.* **1970**, *92*, 6333-6335.

- (19) Ajayaghosh, A.; Pillai, V. N. R. *Tetrahedron* **1988**, *44*, 6661-6.
- (20) Cameron, J. F.; Frechet, J. M. J. *J. Am. Chem. Soc.* **1991**, *113*, 4303-13.
- (21) McGall, G. H.; Barone, A. D.; Diggelmann, M.; Fodor, S. P. A.; Gentalen, E.; Ngo, N. *J. Am. Chem. Soc.* **1997**, *119*, 5081-5090.
- (22) Pease, A. C.; Solas, D.; Sullivan, E. J.; Cronin, M. T.; Holmes, C. P.; Fodor, S. P. A. *Proc. Natl. Acad. Sci. U.S.A.* **1994**, *91*, 5022-6.
- (23) Buehler, S.; Lagoja, I.; Giegrich, H.; Stengele, K.-P.; Pfeleiderer, W. *Helv. Chim. Acta* **2004**, *87*, 620-659.
- (24) Hasan, A.; Stengele, K. P.; Giegrich, H.; Cornwell, P.; Isham, K. R.; Sachleben, R. A.; Pfeleiderer, W.; Foote, R. S. *Tetrahedron* **1997**, *53*, 4247-4264.
- (25) Walbert, S.; Pfeleiderer, W.; Steiner, U. E. *Helv. Chim. Acta* **2001**, *84*, 1601-1611.
- (26) Bochet, C. G. *Tetrahedron Lett.* **2000**, *41*, 6341-6346.
- (27) Aujard, I.; Benbrahim, C.; Gouget, M.; Ruel, O.; Baudin, J.-B.; Neveu, P.; Jullien, L. *Chem.--Eur. J.* **2006**, *12*, 6865-6879.
- (28) Kaplan, J. H.; Forbush, B.; Hoffman, J. F. *Biochemistry* **1978**, *17*, 1929-1935.
- (29) Ellis-Davies, G. C. R.; Kaplan, J. H. *Proc. Natl. Acad. Sci. U.S.A.* **1994**, *91*, 187-91.
- (30) Ellis-Davies, G. C.; Kaplan, J. H.; Barsotti, R. J. *Biophys J* **1996**, *70*, 1006-16.
- (31) Adams, S. R.; Kao, J. P. Y.; Gryniewicz, G.; Minta, A.; Tsien, R. Y. *J. Am. Chem. Soc.* **1988**, *110*, 3212-3220.
- (32) Adams, S. R.; Kao, J. P. Y.; Tsien, R. Y. *J. Am. Chem. Soc.* **1989**, *111*, 7957-68.
- (33) Dussy, A.; Meyer, C.; Quennet, E.; Bickle, T. A.; Giese, B.; Marx, A. *ChemBioChem* **2002**, *3*, 54-60.
- (34) Ordoukhanian, P.; Taylor, J.-S. *J. Am. Chem. Soc.* **1995**, *117*, 9570-1.
- (35) Fodor, S. P. A.; Read, J. L.; Pirrung, M. C.; Stryer, L.; Lu, A. T.; Solas, D. *Science (Washington, DC, United States)* **1991**, *251*, 767-73.
- (36) Hansen, K. C.; Rock, R. S.; Larsen, R. W.; Chan, S. I. *J. Am. Chem. Soc.* **2000**, *122*, 11567-11568.

- (37) Cameron, J. F.; Frechet, J. M. J. *J. Org. Chem.* **1990**, *55*, 5919-22.
- (38) Rock, R. S.; Chan, S. I. *J. Org. Chem.* **1996**, *61*, 1526-1529.
- (39) Pirrung, M. C.; Bradley, J. C. *J. Org. Chem.* **1995**, *60*, 1116-1117.
- (40) Pirrung, M. C.; Fallon, L.; Lever, D. C.; Shuey, S. W. *J. Org. Chem.* **1996**, *61*, 2129-2136.
- (41) Givens, R. S.; Matuszewski, B. *J. Am. Chem. Soc.* **1984**, *106*, 6860-6861.
- (42) Sheehan, J. C.; Wilson, R. M.; Oxford, A. W. *J. Am. Chem. Soc.* **1971**, *93*, 7222-7228.
- (43) Sheehan, J. C.; Umezawa, K. *J. Org. Chem.* **1973**, *38*, 3771-3774.
- (44) Rock, R. S.; Chan, S. I. *J. Am. Chem. Soc.* **1998**, *120*, 10766-10767.
- (45) Sheehan, J. C.; Wilson, R. M. *J. Am. Chem. Soc.* **1964**, *86*, 5277-81.
- (46) Shi, Y. J.; Corrie, J. E. T.; Wan, P. *J. Org. Chem.* **1997**, *62*, 8278-8279.
- (47) Boudebous, H.; Kosmrlj, B.; Sket, B.; Wirz, J. *J. Phys. Chem. A* **2007**, *111*, 2811-3.
- (48) Givens, R. S.; Athey, P. S.; Kueper, L. W.; Matuszewski, B.; Xue, J. Y. *J. Am. Chem. Soc.* **1992**, *114*, 8708-8710.
- (49) Givens, R. S.; Kueper, L. W. *Chem. Rev.* **1993**, *93*, 55-66.
- (50) Gee, K. R.; Kueper, L. W.; Barnes, J.; Dudley, G.; Givens, R. S. *J. Org. Chem.* **1996**, *61*, 1228-1233.
- (51) Pirrung, M. C.; Bradley, J.-C. *J. Org. Chem.* **1995**, *60*, 6270-6.
- (52) Givens, R. S.; Jung, A.; Park, C. H.; Weber, J.; Bartlett, W. *J. Am. Chem. Soc.* **1997**, *119*, 8369-8370.
- (53) Anderson, J. C.; Reese, C. B. *Tetrahedron Lett.* **1962**, 1-4.
- (54) Givens, R. S.; Athey, P. S.; Matuszewski, B.; Kueper, L. W.; Xue, J. Y.; Fister, T. *J. Am. Chem. Soc.* **1993**, *115*, 6001-6012.
- (55) Givens, R. S.; Park, C. H. *Tetrahedron Lett.* **1996**, *37*, 6259-6262.
- (56) Banerjee, A.; Falvey, D. E. *J. Am. Chem. Soc.* **1998**, *120*, 2965-2966.

- (57) Ma, C.; Kwok, W. M.; Chan, W. S.; Zuo, P.; Kan, J. T. W.; Toy, P. H.; Phillips, D. L. *J. Am. Chem. Soc.* **2005**, *127*, 1463-1472.
- (58) Ma, C.; Kwok, W. M.; Chan, W. S.; Du, Y.; Kan, J. T. W.; Toy, P. H.; Phillips, D. L. *J. Am. Chem. Soc.* **2006**, *128*, 2558-2570.
- (59) Givens, R. S.; Heger, D.; Hellrung, B.; Kamdzhilov, Y.; Mac, M.; Conrad, P. G., II; Cope, E.; Lee, J. I.; Mata-Segreda, J. F.; Schowen, R. L.; Wirz, J. *J. Am. Chem. Soc.* **2008**, *130*, 3307-3309.
- (60) Stensrud, K.; Noh, J.; Kandler, K.; Wirz, J.; Heger, D.; Givens, R. S. *J. Org. Chem.* **2009**, *74*, 5219-5227.
- (61) Conrad, P. G.; Givens, R. S.; Weber, J. F. W.; Kandler, K. *Org. Lett.* **2000**, *2*, 1545-1547.
- (62) Park, C. H.; Givens, R. S. *J. Am. Chem. Soc.* **1997**, *119*, 2453-2463.
- (63) Stensrud, K. F.; Heger, D.; Sebej, P.; Wirz, J.; Givens, R. S. *Photochem. Photobiol. Sci.* **2008**, *7*, 614-624.
- (64) Givens, R. S.; Weber, J. F. W.; Conrad, P. G., II; Orosz, G.; Donahue, S. L.; Thayer, S. A. *J. Am. Chem. Soc.* **2000**, *122*, 2687-2697.
- (65) Furuta, T. In *Phototriggers, Photoswitches and Caged Biomolecules*; Givens, R., Goeldner, M., Eds.; WileyVCH: Weinheim, 2005.
- (66) Furuta, T.; Torigai, H.; Sugimoto, M.; Iwamura, M. *J. Org. Chem.* **1995**, *60*, 3953-3956.
- (67) Furuta, T.; Momotake, A.; Sugimoto, M.; Hatayama, M.; Torigai, H.; Iwamura, M. *Biochem. Biophys. Res. Commun.* **1996**, *228*, 193-198.
- (68) Furuta, T.; Wang, S. S. H.; Dantzker, J. L.; Dore, T. M.; Bybee, W. J.; Callaway, E. M.; Denk, W.; Tsien, R. Y. *Proc. Natl. Acad. Sci. U.S.A.* **1999**, *96*, 1193-1200.
- (69) Schade, B.; Hagen, V.; Schmidt, R.; Herbrich, R.; Krause, E.; Eckardt, T.; Bendig, J. *J. Org. Chem.* **1999**, *64*, 9109-9117.
- (70) Lin, W.; Lawrence, D. S. *J. Org. Chem.* **2002**, *67*, 2723-2726.
- (71) Lu, M.; Fedoryak, O. D.; Moister, B. R.; Dore, T. M. *Org. Lett.* **2003**, *5*, 2119-2122.

- (72) Suzuki, A. Z.; Watanabe, T.; Kawamoto, M.; Nishiyama, K.; Yamashita, H.; Ishii, M.; Iwamura, M.; Furuta, T. *Org. Lett.* **2003**, *5*, 4867-4870.
- (73) Geissler, D.; Antonenko, Y. N.; Schmidt, R.; Keller, S.; Krylova, O. O.; Wiesner, B.; Bendig, J.; Pohl, P.; Hagen, V. *Angew. Chem., Int. Ed.* **2005**, *44*, 1195-1198.
- (74) Hagen, V.; Bendig, J.; Frings, S.; Wiesner, B.; Schade, B.; Helm, S.; Lorenz, D.; Kaupp, U. B. *J. Photochem. Photobiol., B* **1999**, *53*, 91-102.
- (75) Schonleber, R. O.; Bendig, J.; Hagen, V.; Giese, B. *Bioorg. Med. Chem.* **2002**, *10*, 97-101.
- (76) Geissler, D.; Kresse, W.; Wiesner, B.; Bendig, J.; Kettenmann, H.; Hagen, V. *ChemBioChem* **2003**, *4*, 162-170.
- (77) Hagen, V.; Bendig, J.; Frings, S.; Eckardt, T.; Helm, S.; Reuter, D.; Kaupp, U. B. *Angew. Chem., Int. Ed.* **2001**, *40*, 1046-1048.
- (78) Noguchi, M.; Skwarczynski, M.; Prakash, H.; Hirota, S.; Kimura, T.; Hayashi, Y.; Kiso, Y. *Bioorg. Med. Chem.* **2008**, *16*, 5389-5397.
- (79) Schelhaas, M.; Waldmann, H. *Angew. Chem., Int. Ed.* **1996**, *35*, 2056-2083.
- (80) Bochet, C. G. *Angew. Chem., Int. Ed.* **2001**, *40*, 2071-2073.
- (81) Blanc, A.; Bochet, C. G. *J. Org. Chem.* **2002**, *67*, 5567-5577.
- (82) Blanc, A.; Bochet, C. G. *J. Am. Chem. Soc.* **2004**, *126*, 7174-7175.
- (83) Blanc, A.; Bochet, C. G. *Org. Lett.* **2007**, *9*, 2649-2651.
- (84) Kessler, M.; Glatthar, R.; Giese, B.; Bochet, C. G. *Org. Lett.* **2003**, *5*, 1179-1181.
- (85) Corrie, J. E. T.; Trentham, D. R. *J. Chem. Soc.-Perkin Trans. I* **1992**, 2409-2417.
- (86) Roth, H. D. *Top. Curr. Chem.* **1990**, *156*, 1-19.
- (87) Gould, I. R.; Farid, S. *Acc. Chem. Res.* **1996**, *29*, 522-528.
- (88) Kavarnos, G. J.; Turro, N. J. *Chem. Rev.* **1986**, *86*, 401-49.
- (89) Weller, A. *Pure Appl. Chem.* **1968**, *16*, 115-23.
- (90) Marcus, R. A. *J. Chem. Phys.* **1956**, *24*, 966-78.
- (91) Marcus, R. A. *J. Phys. Chem.* **1963**, *67*, 853-7.

- (92) Marcus, R. A.; Eyring, H. *Annu. Rev. Phys. Chem.* **1964**, *15*, 155-96.
- (93) Marcus, R. A. *J. Chem. Phys.* **1965**, *43*, 3477-89.
- (94) Rehm, D.; Weller, A. *Isr. J. Chem.* **1970**, *8*, 259-71.
- (95) Miller, J. R.; Beitz, J. V.; Huddleston, R. K. *J. Am. Chem. Soc.* **1984**, *106*, 5057-68.
- (96) Miller, J. R.; Calcaterra, L. T.; Closs, G. L. *J. Am. Chem. Soc.* **1984**, *106*, 3047-9.
- (97) Gould, I. R.; Ege, D.; Mattes, S. L.; Farid, S. *J. Am. Chem. Soc.* **1987**, *109*, 3794-6.
- (98) Gould, I. R.; Ege, D.; Moser, J. E.; Farid, S. *J. Am. Chem. Soc.* **1990**, *112*, 4290-301.
- (99) Hamada, T.; Nishida, A.; Yonemitsu, O. *J. Am. Chem. Soc.* **1986**, *108*, 140-145.
- (100) Hamada, T.; Nishida, A.; Yonemitsu, O. *Tetrahedron Lett.* **1989**, *30*, 4241-4.
- (101) Nishida, A.; Hamada, T.; Yonemitsu, O. *J. Org. Chem.* **1988**, *53*, 3386-3387.
- (102) Binkley, R. W.; Koholic, D. J. *J. Org. Chem.* **1989**, *54*, 3577-81.
- (103) Bruncko, M.; Crich, D. *J. Org. Chem.* **1994**, *59*, 4239-4249.
- (104) Urjasz, W.; Celewicz, L. *J. Phys. Org. Chem.* **1998**, *11*, 618-621.
- (105) Papageorgiou, G.; Corrie, J. E. T. *Tetrahedron* **1999**, *55*, 237-254.
- (106) Banerjee, A.; Falvey, D. E. *J. Org. Chem.* **1997**, *62*, 6245-6251.
- (107) Banerjee, A.; Lee, K.; Yu, Q.; Fang, A. G.; Falvey, D. E. *Tetrahedron Lett.* **1998**, *39*, 4635-4638.
- (108) Lee, K.; Falvey, D. E. *J. Am. Chem. Soc.* **2000**, *122*, 9361-9366.
- (109) Sundararajan, C.; Falvey, D. E. *J. Org. Chem.* **2004**, *69*, 5547-5554.
- (110) Sundararajan, C.; Falvey, D. E. *Org. Lett.* **2005**, *7*, 2631-2634.
- (111) Sundararajan, C.; Falvey, D. E. *J. Am. Chem. Soc.* **2005**, *127*, 8000-8001.
- (112) Sundararajan, C.; Falvey, D. E. *Photochem. Photobiol. Sci.* **2006**, *5*, 116-121.



- (113) Young, G. T.; Garner, R. *J. Chem. Soc., C* **1971**, 50-3.
- (114) Camble, R.; Garner, R.; Young, G. T. *Nature (London, U.K.)* **1968**, 217, 247-8.
- (115) Rizo, J.; Albericio, F.; Romero, G.; Garcia-Echeverria, C.; Claret, J.; Muller, C.; Giralt, E.; Pedroso, E. *J. Org. Chem.* **1988**, 53, 5386-9.
- (116) Murov, S. L.; Carmichael, I.; Hug, G. L. *Handbook of Photochemistry, Second ed.*; 2nd Edition ed.; marcel Dekker Inc.: NewYork, 1993.
- (117) Falvey, D. E.; Sundararajan, C. *Photochem. Photobiol. Sci.* **2004**, 3, 831-838.
- (118) Sahyun, M. R. V.; Sharma, D. K. *Chem. Phys. Lett.* **1992**, 189, 571-6.
- (119) Specht, D. P.; Martic, P. A.; Farid, S. *Tetrahedron* **1982**, 38, 1203-11.
- (120) Williams, J. L. R.; Specht, D. P.; Farid, S. *Polym. Eng. Sci.* **1983**, 23, 1022-4.
- (121) Shida, T. *Electronic Absorption Spectra of Radical Ions*; Elsevier: New York, 1988.
- (122) Daniel, M.-C.; Astruc, D. *Chem. Rev.* **2004**, 104, 293-346.
- (123) Mie, G. *Annalen der Physik* **1908**, 25, 377-445.
- (124) Mulvaney, P. *Langmuir* **1996**, 12, 788-800.
- (125) Lee, D.; Donkers, R. L.; Wang, G.; Harper, A. S.; Murray, R. W. *J. Am. Chem. Soc.* **2004**, 126, 6193-6199.
- (126) Hostetler, M. J.; Wingate, J. E.; Zhong, C.-J.; Harris, J. E.; Vachet, R. W.; Clark, M. R.; Londono, J. D.; Green, S. J.; Stokes, J. J.; Wignall, G. D.; Glish, G. L.; Porter, M. D.; Evans, N. D.; Murray, R. W. *Langmuir* **1998**, 14, 17-30.
- (127) Brust, M.; Kiely, C. J. *Colloids Surf., A* **2002**, 202, 175-186.
- (128) Turkevich, J.; Stevenson, P. C.; Hillier, J. *Discuss. Faraday Soc.* **1951**, No. 11, 55-75.
- (129) Kimling, J.; Maier, M.; Okenve, B.; Kotaidis, V.; Ballot, H.; Plech, A. *J. Phys. Chem. B* **2006**, 110, 15700-15707.
- (130) Frens, G. *Nat. Phys. Sci.* **1973**, 241, 20-2.
- (131) Brown, K. R.; Walter, D. G.; Natan, M. J. *Chem. Mater.* **2000**, 12, 306-313.

- (132) Slot, J. W.; Geuze, H. J. *J Cell Biol* **1981**, *90*, 533-6.
- (133) Park, J.-H.; DeShong, P. Unpublished Work, **2007**.
- (134) Balzani, V.; Barigelletti, F.; De Cola, L. *Top. Curr. Chem.* **1990**, *158*, 31-71.
- (135) Balzani, V.; Juris, A.; Venturi, M.; Campagna, S.; Serroni, S. *Chem. Rev. (Washington, D. C.)* **1996**, *96*, 759-833.
- (136) O'Regan, B.; Graetzel, M. *Nature (London, U.K.)* **1991**, *353*, 737-40.
- (137) Nazeeruddin, M. K.; Gratzel, M. *Structure and Bonding (Berlin, Germany)* **2007**, *123*, 113-175.
- (138) Meyer, T. J. *Acc. Chem. Res.* **1989**, *22*, 163-70.
- (139) Hara, K. *Springer Ser. Mater. Sci.* **2009**, *111*, 217-250.
- (140) Tinker, L. L.; McDaniel, N. D.; Bernhard, S. *J. Mater. Chem.* **2009**, *19*, 3328-3337.
- (141) Meyer, T. J. *Pure Appl. Chem.* **1986**, *58*, 1193-206.
- (142) Kalyanasundaram, K. *Coord. Chem. Rev.* **1982**, *46*, 159-244.
- (143) Kalyanasundaram, K. *Photochemistry of polypyridine and porphyrin complexes*; Academic Press: London, UK, 1992.
- (144) Campagna, S.; Puntoriero, F.; Nastasi, F.; Bergamini, G.; Balzani, V. *Top. Curr. Chem.* **2007**, *280*, 117-214.
- (145) El Hadri, A.; Leclerc, G. *J. Heterocycl. Chem.* **1993**, *30*, 631-5.
- (146) Kitamura, N.; Kim, H. B.; Okano, S.; Tazuke, S. *J. Phys. Chem.* **1989**, *93*, 5750-6.
- (147) Ruiz, G.; Rodriguez-Nieto, F.; Wolcan, E.; Feliz, M. R. *J. Photochem. Photobiol., A* **1997**, *107*, 47-54.
- (148) Rivarola, C. R.; Bertolotti, S. G.; Previtali, C. M. *Photochem. Photobiol.* **2006**, *82*, 213-218.
- (149) Mulazzani, Q. G.; Emmi, S.; Fuoichi, P. G.; Hoffman, M. Z.; Venturi, M. *J. Am. Chem. Soc.* **1978**, *100*, 981-3.

- (150) Gaspar, A.; Piyasena, M. E.; Daroczi, L.; Gomez, F. A. *Microfluid. Nanofluid.* **2008**, *4*, 525-531.
- (151) Rankin, P. J.; Ginder, J. M.; Klingenberg, D. J. *Curr. Opin. Colloid Interface Sci.* **1998**, *3*, 373-381.
- (152) Tsuchiya, K.; Orihara, Y.; Kondo, Y.; Yoshino, N.; Ohkubo, T.; Sakai, H.; Abe, M. *J. Am. Chem. Soc.* **2004**, *126*, 12282-12283.
- (153) Eastoe, J.; Vesperinas, A. *Soft Matter* **2005**, *1*, 338-347.
- (154) Wolff, T.; Schmidt, F.; Von Buenau, G. *J. Photochem. Photobiol., A* **1989**, *48*, 435-46.
- (155) Lee, C. T., Jr.; Smith, K. A.; Hatton, T. A. *Macromolecules* **2004**, *37*, 5397-5405.
- (156) Sakai, H.; Orihara, Y.; Kodashima, H.; Matsumura, A.; Ohkubo, T.; Tsuchiya, K.; Abe, M. *J. Am. Chem. Soc.* **2005**, *127*, 13454-13455.
- (157) Eastoe, J.; Dominguez, M. S.; Wyatt, P.; Beeby, A.; Heenan, R. K. *Langmuir* **2002**, *18*, 7837-7844.
- (158) Paulusse, J. M. J.; Sijbesma, R. P. *Angew. Chem., Int. Ed.* **2006**, *45*, 2334-2337.
- (159) Sauer-Budge, A. F.; Mirer, P.; Chatterjee, A.; Klapperich, C. M.; Chargin, D.; Sharon, A. *Lab Chip* **2009**, *9*, 2803-2810.
- (160) Satarkar, N. S.; Zhang, W.; Eitel, R. E.; Hilt, J. Z. *Lab Chip* **2009**, *9*, 1773-1779.
- (161) Sershen, S. R.; Mensing, G. A.; Ng, M.; Halas, N. J.; Beebe, D. J.; West, J. L. *Adv. Mater. (Weinheim, Ger.)* **2005**, *17*, 1366-1368.
- (162) Nagarajan, R. In *Structure-Performance Relationships in Surfactants*; Esumi, K., Ueno, M., Eds.; Marcel Dekker, Inc.: New York, 2003.
- (163) Estroff, L. A.; Hamilton, A. D. *Chem. Rev. (Washington, DC, U. S.)* **2004**, *104*, 1201-1217.
- (164) Schnur, J. M. *Science (Washington, DC, United States)* **1993**, *262*, 1669-76.
- (165) Israelachvili, J. N. *Intermolecular and Surface Forces*; Academic Press: New York, 1991.
- (166) Cates, M. E.; Candau, S. J. *J. Phys.: Condens. Matter* **1990**, *2*, 6869-92.
- (167) Shikata, T.; Hirata, H.; Kotaka, T. *Langmuir* **1987**, *3*, 1081-6.

- (168) Lin, Z.; Cai, J. J.; Scriven, L. E.; Davis, H. T. *J. Phys. Chem.* **1994**, *98*, 5984-93.
- (169) Shikata, T.; Hirata, H.; Kotaka, T. *Langmuir* **1989**, *5*, 398-405.
- (170) Trickett, K.; Eastoe, J. *Adv. Colloid Interface Sci.* **2008**, *144*, 66-74.
- (171) Tung, S.-H.; Huang, Y.-E.; Raghavan, S. R. *J. Am. Chem. Soc.* **2006**, *128*, 5751-5756.
- (172) Tung, S.-H.; Huang, Y.-E.; Raghavan, S. R. *Soft Matter* **2008**, *4*, 1086-1093.
- (173) Davies, T. S.; Ketner, A. M.; Raghavan, S. R. *J. Am. Chem. Soc.* **2006**, *128*, 6669-6675.
- (174) Frounfelker, B. D.; Kalur, G. C.; Cipriano, B. H.; Danino, D.; Raghavan, S. R. *Langmuir* **2009**, *25*, 167-172.
- (175) Wolff, T.; Klaussner, B. *Adv. Colloid Interface Sci.* **1995**, *59*, 31-94.
- (176) Eastoe, J.; Sanchez-Dominguez, M.; Wyatt, P.; Heenan, R. K. *Chem. Commun. (Cambridge, U. K.)* **2004**, 2608-2609.
- (177) Tomatsu, I.; Hashidzume, A.; Harada, A. *Macromolecules* **2005**, *38*, 5223-5227.
- (178) Eastoe, J. *Prog. Colloid Polym. Sci.* **2006**, *133*, 106-110.
- (179) Eastoe, J.; Vesperinas, A.; Donnewirth, A.-C.; Wyatt, P.; Grillo, I.; Heenan, R. K.; Davis, S. *Langmuir* **2006**, *22*, 851-853.
- (180) Eastoe, J.; Zou, A.; Espidel, Y.; Glatter, O.; Grillo, I. *Soft Matter* **2008**, *4*, 1215-1218.
- (181) Yu, X.; Wolff, T. *Langmuir* **2003**, *19*, 9672-9679.
- (182) Ketner, A. M.; Kumar, R.; Davies, T. S.; Elder, P. W.; Raghavan, S. R. *J. Am. Chem. Soc.* **2007**, *129*, 1553-1559.
- (183) Kumar, R.; Raghavan, S. R. *Soft Matter* **2009**, *5*, 797-803.
- (184) Baglioni, P.; Braccalenti, E.; Carretti, E.; Germani, R.; Goracci, L.; Savelli, G.; Tiecco, M. *Langmuir* **2009**, *25*, 5467-5475.
- (185) Saah, M.; Wu, W.-M.; Eberst, K.; Marvanyos, E.; Bodor, N. *J. Pharm. Sci.* **1996**, *85*, 496-504.